On the Structure and Properties of S-Nitrosated Cysteine Models: A Computational Study

Dmitry Khomyakov
Marquette University

ON THE STRUCTURE AND PROPERTIES OF S-NITROSATED CYSTEINE MODELS: A COMPUTATIONAL STUDY

by

Dmitry G. Khomyakov, B.Sc., M.Sc.

A Dissertation submitted to the Faculty of the Graduate School,
Marquette University,
in Partial Fulfillment of the Requirements for
the Degree of Doctor of Philosophy

Milwaukee, Wisconsin
May 2017

ABSTRACT
ON THE STRUCTURE AND PROPERTIES OF
S-NITROSATED CYSTEINE MODELS: A COMPUTATIONAL STUDY

Dmitry G. Khomyakov, B.Sc., M.Sc.

Marquette University, 2017

S-Nitrosation of cysteine (Cys) residues, a covalent modification of its S atom by NO group, is a major post-translational modification of proteins. Despite the importance of S-nitrosoproteins in numerous physiological processes, lability of the S-nitrosothiol (-SNO) group hinders the research progress. In this work, computational chemistry methods were applied to S-nitrosated cysteine (CysNO) models to gain a deeper insight into its structure and properties.

First, we obtained the most accurate at the moment computational estimation of the molecular structure and properties of CH_3SNO model molecule using Feller-Peterson-Dixon (FPD) *ab initio* protocol. The S–N bond length in *cis*-CH_3SNO is calculated as 1.814 Å, and its dissociation energy (BDE) is 32.4 kcal/mol. We found that although the vibrational frequency of the S–N stretch is unusually low for a covalent bond (398 cm^{-1}), the S–N bond has a remarkably harmonic character. After the benchmarking of the density functional theory (DFT) methods against the FPD reference, we recommend MPW2PLYP and MPW2PLYPD double hybrid functionals for calculation of the geometric properties, vibrational frequencies and isomerization barriers of S-nitrosothiols, and PBE0 (PBE0-GD3) hybrid functional for the S–N BDEs.

Further, we evaluated the influence of charged amino acid residues and steric constraints on the conformational dynamics of CysNO, using an α-helix model and a DJ-1 (PARK7) protein using hybrid quantum mechanics/molecular mechanics (QM/MM) approach. We found that while the rotational barrier around the S–N bond is ca. 13 kcal/mol in free CysNO, it can vary between 10 and 24 kcal/mol in the protein environment due to the effect of neighboring charged amino acids.

Finally, to address a long-standing problem of the CysNO identification in proteins, we computationally designed a novel CysNO labeling reaction, (3+2) dipolar cycloaddition between the -SNO group activated by N-coordinated Lewis acid and a strain-activated alkene. We show that the most effective labeling reagent should covalently link both crucial reaction components—the Lewis acid and the dipolarophile—into one molecule, to lower the entropic penalty and corresponding reaction barrier.

TABLE OF CONTENTS

LIST OF ABBREVIATIONS

RSNO – S-nitrosothiol

CysNO – S-nitrosocysteine

PDB – Protein Data Bank

Cys (C) – Cysteine

Lys (K) – Lysine

Arg (R) – Arginine

His (H) – Histidine

Asp (D) – Aspartic Acid

Glu (E) – Glutamic Acid

MMTK – Molecular Modeling Toolkit

DFT- Density Functional Theory

PCM – Polarizable Continuum Model

HF – Hartree-Fock

FPD – Feller-Peterson-Dixon approach

ONIOM – extrapolation algorithm in Gaussian program package

QM – Quantim Mechanics

MM – Molecular Mechanics

MD – Molecular Dynamics

FF – Force Field

TS – Transition State

PES - Potential Energy Surface

LA - Lewis Acid

IRC - Intrinsic Reaction Coordinate analysis

NBO - Natural Bond Orbitals

NRT - Natural Resonance Theory

NB - Norbornadiene

AdSNO - Adamantil SNO

BCF - Tris(pentafluorophenyl)borane

LIST OF TABLES AND FIGURES

Chapter I. Introduction

A. Current Problems in S-Nitrosoproteomics

Proteins are involved in virtually all physiological processes of human body: indeed, the human genome encodes more than 20000 proteins, according to the Uniprot database.[8] Formation of proteins, their function and lifespan are tightly regulated under normal physiological conditions. One of the ways used by the nature to regulate the structure and functions of proteinsf, as well as to increase chemical diversity beyond the 20 naturally occurring amino acids, is chemical modification of protein residues, also known as posttranslational modifications (PTMs).[9] A recent study,[10] aimed at supplying the scientific community with constantly updated proteome-wide statistics of most abundant PTMs from the Swiss-Prot database,[11] demonstrated that phosphorylation, acetylation and N-linked glycosylation are the most frequent types of chemical residue modifications in proteins.

A vast body of research regards the role of reversible protein phosphorylation, or addition/removal of a phosphate fragment to/from serine, threonine, tyrosine or histidine residues, in human physiology.[12-14] One of the most important implications of tightly controlled reversible protein phosphorylation is to regulate (activate or deactivate) the function of enzymes.[15] Some of the examples of physiological regulation via reversible phosphorylation of proteins include (but not limited to) insulin signaling,[16] protein-protein recognition,[17] and cellular death

through apoptosis.[18]

Similarly to phosphorylation of serine, threonine, tyrosine or histidine, a growing number of studies indicate that more than 3000 proteins undergo cysteine (Cys) residue modification via reversible S-nitrosation, leading to the formation of S-nitrosoproteins[1,19-21] (Figure 1 A). Figure 1 B depicts major pathways of S-nitrosothiol (RSNO) formation *in vivo*.[2] Remarkably, all but one of those pathways (namely the trans-S-nitrosation pathway) include nitric oxide (NO) as a reagent. NO is a well-known endogenously produced signaling molecule in biology,[22-25] and plays a major role in regulation of physiological functions in human body.

The resulting S-nitrosoproteins are involved in a multitude of key biological processes across all branches of the tree of life,[26-28] from immune response in plants to neurotransmission in humans. Despite the fact that all Cys residues in proteins can be potential targets of S-nitrosaion, not all of them undergo this transformation. For example, an RNA-binding domain of heterogeneous nuclear ribonucleoprotein M contains four Cys residues (Cys652, Cys675, Cys693, Cys708), but only the Cys675 residue was experimentally detected to be S-nitrosated *in vivo*[3] (Figure 2). Thus, S-nitrosation and denitrosation occurs in a tightly controlled manner, whereas disregulated S-nitrosation is linked to the development of a number of pathological conditions[1,29] (Table 1). The mechanisms of such control on a molecular level are not yet fully understood.

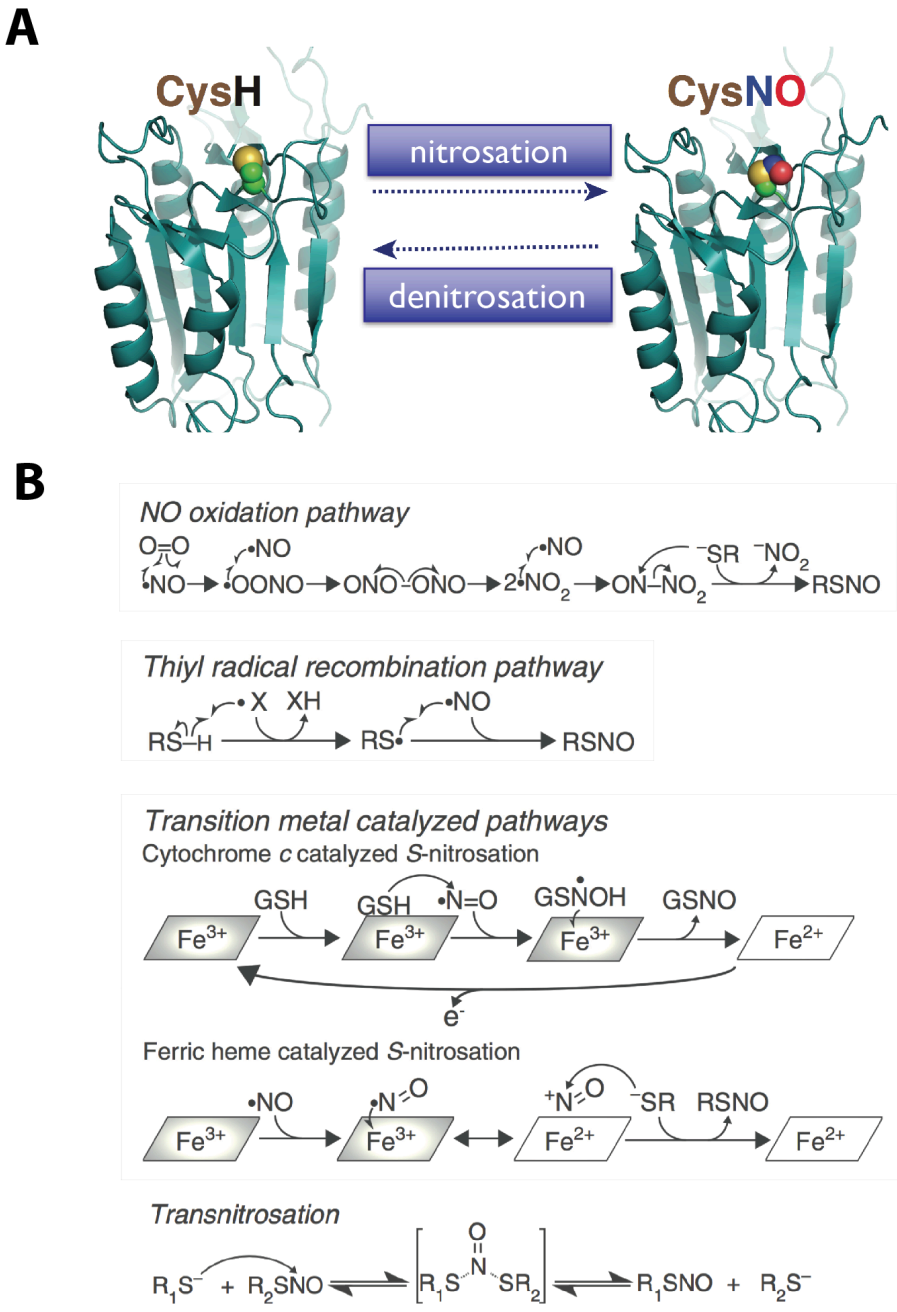

Figure 1. S-Nitrosation and denirosation of Cys residue in peoteins (A); physiological pathways of RSNO formation in vivo (B) - adapted from[2].

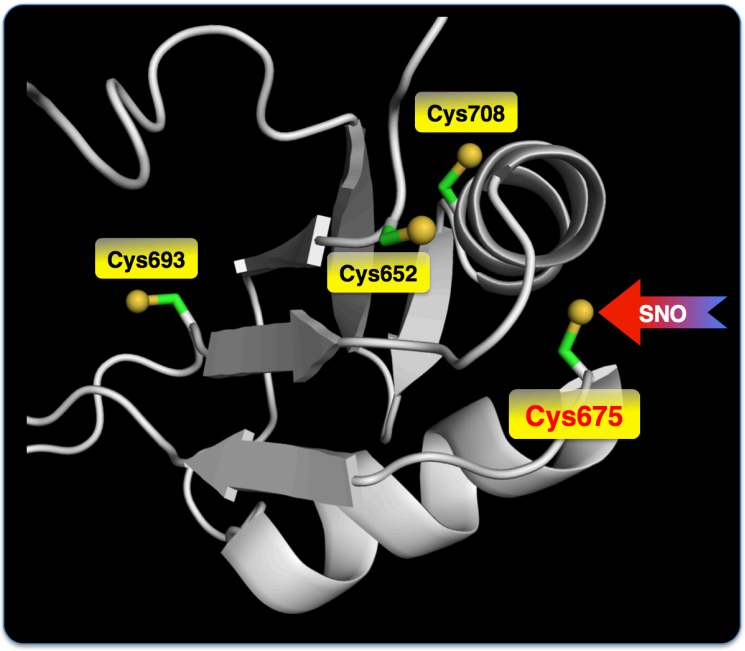

Figure 2. An example of specificity of S-nitrosation in proteins: four Cys residues of RNA-binding domain of heterogeneous nuclear ribonucleoprotein M[3].

Table 1. Pathological conditions caused by the disregulated S-nitrosation in proteins[1].

Neurological	Alzheimer disease
	Parkinson disease
	Stroke
Cardiovascular	Heart failure
	Preeclampsia
	Arterial hypertension
	Septic shock
	Diabetes (type I, type II)
Hematological	Banked blood storage defect
	Sickle cell anemia
Pulmonary	Asthma
	Cystic fibrosis
	Lung inflammation
Cancer	Liver cancer
	Tumor radiosensitivity

One of the recent examples of S-nitrosated proteins, involved in the development of crucial health problems, is protein deglycase DJ-1, also known as Parkinson disease (PD) protein 7.[30,31] Neurodegenerative diseases pose a major health problem in modern society with quickly aging population. For example, the PD has an impact on daily lives of more than one million people in the United States.[32] A recent hypothesis from S. Lipton group (Department of Neurosciences, UCSD) suggested that one of the physiological functions of DJ-1 is to protect the neurons under oxidative conditions, and to prevent neuronal cell death. A disruption of this function may lead to the accelerated degeneration of dopamine-generating cells in human brain, and progression of the PD.[19,33,34] The S-nitrosation of Cys106 in DJ-1 protein was subsequently linked to the neuroprotective function. Therefore, a deeper insight into the structure and properties of evidently physiologically relevant CysNO residue in DJ-1 is, therefore, required.

Considering S-nitrosproteins as the prominent targets for pharmacological interventions,[35] several challenges limit the progress in this field. Firstly, despite clear need for more structural and reactivity data on S-nitrosoproteins, their experimental studies are complicated due to the inherent instability of the SNO fragment.[36] Chemically, the side chain of S-nitrosated Cys residue belongs to the class of compounds called S-nitrosothiols. RSNOs only recently gained significant attention of the scientific community, mostly due to their involvement in a multitude of physiological mechanisms.[1,37,38] A number of physiologically relevant S-nitrosothiols, as well as their typical lifetimes *in vivo*, are shown on Figure 3. It is clear that in the most cases, the stability of RSNOs is on par with stability of organic

peroxides.[39] Several factors can lead to even faster decomposition of RSNOs (Figure 4), such as temperature, light, and the presence of metal ions.[5,36,40,41]

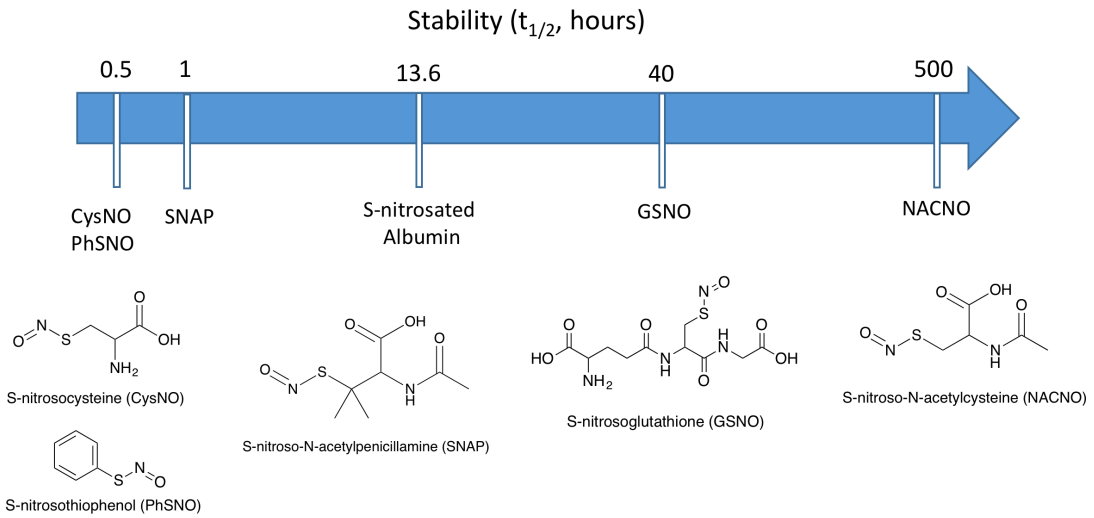

Figure 3. Structures and stabilities of selected biologically relevant RSNOs[4,5].

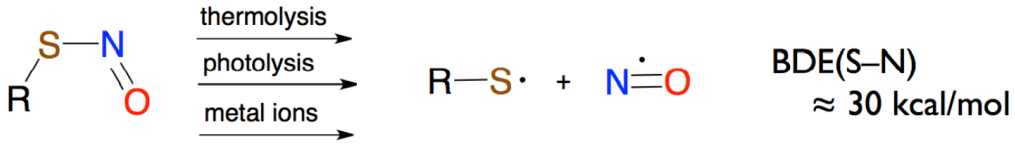

Figure 4. Common factors, involved in decomposition of RSNOs.

Secondly, the number of thoroughly characterized S-nitrosoproteins is rather limited. As of January 2017, only a few X-ray structures of S-nitrosated proteins are available in the RCSB protein data bank[42] (see section III A), and two S-nitrosoproteomes with *thousands* of proteins have been published.[3,43] Therefore, the ability to shed light on the structure and individually assess the reactivity of the CysNO residues in those proteins will be of a high demand for the future studies of pharmacologically targeted proteins. Thirdly, the current techniques to locate

CysNO residues in protein molecules are cumbersome and error-prone, due to the lack of simple and robust procedure to identify the SNO group.

Considering the difficulties that experimental biochemistry is often facing, computational (bio)chemistry can offer a compelling way to gain a deeper insight into the structure and properties of the molecules of interest. Thus, computational tools have become an ordinary part of the drug discovery routine and development of new materials.[44,45] Some of the chemical properties, like bond dissociation energies, or reaction barriers, can be estimated within the margins of chemical accuracy (1 kcal/mol) at a reasonable computational cost.[46,47] Remarkably, the acknowledged success of modern computer-based tools was highlighted by the Nobel Prize in Chemistry (1998), awarded to Walter Kohn "for his development of the density-functional theory" and John A. Pople "for his development of computational methods in quantum chemistry". Another Nobel Prize in Chemistry, awarded in 2013 to Martin Karplus, Michael Levitt and Arieh Warshel, regarded "the development of multiscale models for complex chemical systems".

In the case of S-nitrosoproteins, computational (bio)chemistry allows one to readily access the structure and properties of any CysNO residue, and estimate the effect of the protein environment. For example, recent computational papers[6,48-51] from the Timerghazin group shed light onto a few aspects of the complex electronic structure of RSNOs. The main goal of the present work is to further explore the properties and capabilities of computer simulated models of the CysNO residues, to aid the future experimental studies on S-nitrosoproteins and inspire the development of prominent pharmaceutical agents.

B. Computational Approach

In the rapidly developing field of computational chemistry, capable of producing useful insights in combination with the experiment, a number of challenges are still present. To be a robust quantitative tool, reasonable balance between accuracy and computational cost is required. In computational thermochemistry, 'chemical accuracy' is commonly defined as a maximum difference from the exact value, evaluated by experiment, of 1 kcal/mol.[52,53] Indeed, under biological conditions, a change in reaction barrier height of 1.4 kcal/mol will result in one order of magnitude change of the reaction rate, according to the Arrhenius equation. In recent literature,[46,47] 'chemical accuracy' was roughly associated with ±0.005 Å and ±15 cm^{-1} fidelity in corresponding bond lengths and vibrational frequencies.

Current implementations of *ab initio* electronic structure methods are capable of achieving chemical accuracy, but only for small molecules (with 5-6 non-hydrogen atoms). For most *ab initio* methods, a steep dependence of computational time on the number of electrons in larger molecules[52,53] makes them unusable for any real-world application. For example, a coupled cluster theory method CCSD(T) with single, double and perturbative triple excitations,[54,55] often considered as the 'gold standard' of computational chemistry, scales as n^3N^4 with regard to required CPU time (where n is the number of occupied orbitals and N is the number of virtual orbitals). This approximately translates into M^7 (M is the total number of the basis

functions) size dependence, making those calculations possible only for small molecules (up to 7 non-hydrogen atoms).

In this work, we use the Feller-Peterson-Dixon (FPD)[46,47] procedure to calculate the reference data for cis-MeSNO, trans-MeSNO and the transition state of their interconversion. The FPD protocol was developed to obtain accurate thermochemical and spectroscopic data, without invoking empirical corrections. It is a flexible, multi-step approach, to address major sources of errors in electronic structure calculations. The main building block of FPD is frozen-core coupled cluster method CCSD(T) with extrapolation to the complete basis set (CBS) limit, CCSD(T)/CBS. Explicitly correlated (F12) coupled-cluster methods such as CCSD(T)-F12 demonstrate much faster convergence toward the CBS limit, and allow much more efficient evaluation of the CBS-extrapolated electronic energy. To this E_{elec}(CBS) value, a number of corrections are added:

- ΔCV, core-valence correction, which accounts for the contributions to electronic energy due to correlation of the outer-core electrons;
- ΔSR, scalar-relativistic correction, which approximates the contribution to the electronic energy due to scalar-relativistic effect;
- ΔSO, spin-orbit correction, accounting for the effect of spin-orbit coupling;
- ΔHO, high-order correction, evaluating the electron correlation beyond CCSD(T) level, usually limited to quadruple excitations correction, ΔQ;
- ΔZPE, or the effect of zero-point vibrational energy (when necessary, can incorporate the effect of anharmonicity of bond vibrations).

The expression for the zero-point corrected total energy on the FPD scheme can thus be written:[46,47]

$$E_{0\,\mathrm{FPD}} = E_{\mathrm{elec}}(\mathrm{CBS}) + \Delta\mathrm{CV} + \Delta\mathrm{SR} + \Delta\mathrm{SO} + \Delta\mathrm{HO} + \Delta\mathrm{ZPE}.$$

One of the core differences between FPD approach and much more widely used 'off the shelf' composite methods available in the popular software packages such as Gaussian 09,[56] is the flexibility of FPD building blocks, contrary to the fixed recipe of composite methods. For example, the Gaussian-series G3[57] method, available in Gaussian 09 code, always utilizes the following steps regardless of the nature of the molecule:

- Preliminary geometry optimization and calculation of vibrational frequencies at the HF/6-31G(d) level;
- More accurate geometry optimization at the MP2(Full)/6-31G(d) level (this molecular geometry will be used in all following steps);
- Single-point energy calculation at the QCISD(T,E4T)/6-31G(d) level;
- Single-point energy calculations at the MP4/6-31G(d) and MP4/6–31G(2df,p) levels;
- Single-point energy calculation at the MP2(Full)/GTLarge level;
- Applying an empirical ‘High Level’ correction, fitted to experimental data.

On the other hand, the FPD scheme can be easily modified to better adjust for the nature of the specific chemical system. Therefore, limited computational resources can be managed more efficiently, with more effort directed towards the problematic areas. Recent developments in the electronic structure theory are easily implemented in FPD, for example more cost-effective explicitly correlated coupled

cluster methods CCSD(T)-F12x[58,59] are now used to estimate CCSD(T)/CBS limit instead of traditional slow-converging CCSD(T) method. The FPD scheme also addresses one of the possible sources of errors in a number of widely used composite methods (G3B3, G4, CBS-QB3, W1 and W2), which are based on the DFT methods to perform the initial geometry optimization. Finally, the FPD protocol is free from any empirical corrections obtained by fitting against experimental training sets. This makes the FPD approach an ideal candidate to generate the set of reference data, that can be further used in benchmarking more approximate DFT methods.

C. Overview and Goals of the project

In this work, we applied modern computational chemistry tools to investigate the structure and properties of CysNO residues in proteins. Different computational models of CysNO are used to reproduce the key features of the CysNO. Relatively small CH_3SNO molecule was used as a benchmarking case to test the performance of DFT methods in comparison to the accurate FPD results, as well as served as a CysNO model in development of the novel labeling reactions. The CysNO residue, embedded in an α-helix or a protein, revealed the possibilities of the protein environment to control its properties via steric effects and coordination of the charged residues to the -SNO group. Overall, the present thesis consists of the following parts:

- Chapter II is devoted to the high-level *ab initio* modeling of the structure and properties of the CH_3SNO molecule, the smallest RSNO with C–S bond, similar to the one in a protein CysNO. A generated set of data is used to benchmark the performance of selected DFT methods.

- Chapter III includes electronic structure calculations of two larger CysNO models: α-helix and DJ-1 protein, and highlights the importance of protein environment on regulating the structure and properties of the SNO group.

- Chapter IV covers the proposed novel reactivity of CysNO on the example of CH_3SNO (3+2) cycloaddition and S–N bond insertion reactions with model reagents, as well as the prominent pathways to direct this reactivity via Lewis acid coordination.

Main goals of the project include testing the abilities and limitations of modern readily available computational chemistry tools, applied to the CysNO models; providing a better set of reference data on the CH_3SNO molecule; studying how the protein environment can control the structure and conformational dynamics of CysNO; and exploring how the directed change of electronic structure of CysNO can help to create a more efficient reactions for S-nitrosation detection in proteins.

Chapter II: An Accurate *Ab Initio* Investigation of Structure and Properties of MeSNO

A. Introduction

S-Nitrosothiols, or RSNOs, attract significant attention in the biomedical and biochemical literature in recent time. This growing interest, and the constant flow of new publications,[43,60,61] can be easily rationalized. RSNOs are can be formed and decomposed *in vivo*,[62,63] and play an important role in the nitric oxide biological functions. Especially important in mammalian[1,64,65] and plant physiology[26,66] is the process of post-translational S-nitrosation of the cysteine residues (Cys) in proteins, leading to the formation of S-nitrosated CysNO. Thousands of proteins have been already reported to undergo S-nitrosation,[43] but the detailed mechanism of this reaction remains unclear, and moreover, the fate of newly formed CysNO is difficult to predict. Usually, RSNOs are sensitive to light, presence of the metal ions, and have low thermal stability.[5,40] In the protein environment, a number of studies[19,37] suggest that CysNO can participate in tightly controlled enzymatic trans-*S*-nitrosation reactions, the mechanism of which is open to question. Considering those facts, a reliable computational model of CysNO is highly desired.

Additional challenges represent the complexity of the electronic structure of RSNOs, which are proven to be a difficult object to study with the computational chemistry tools. The HSNO molecule, due to its small size, is among the most rigorously studied RSNOs with the use of high-level *ab initio* calculations.[49,67-70] As shown on the example of HSNO,[67,71] reliable information about its properties can be either obtained through a laborious and computationally demanding *ab initio*

calculations, or via the use of thoroughly tested density functional theory (DFT) methods. Recently, we performed a benchmarking study of the most popular DFT methods, using the HSNO model.[71] Methyl thionitrite MeSNO may represent a better model of S-nitrosated Cys residues in proteins than the HSNO molecule. Accurate estimation of the MeSNO thermochemical parameters is, therefore, of a high demand.

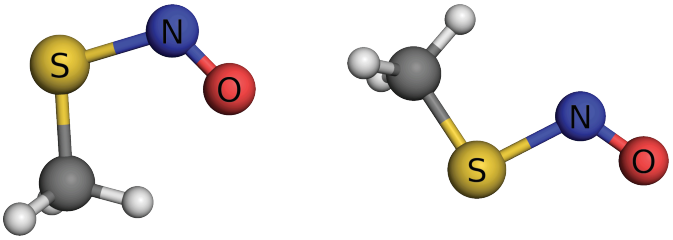

cis-MeSNO trans-MeSNO

In 2012,[72] Koppenol proposed a thermochemical scheme to derive a bond dissociation energy of S-nitrosocysteine, based on the theoretical value of the gas phase S–N bond dissociation energy in CH_3CH_2SNO (32.4 kcal/mol at the CBS-QB3 level of theory[36]). In the literature, a number of studies report S–N BDE in MeSNO, using different levels of theory (Table 2).

Table 2. S–N bond lengths and S–N BDEs in cis-MeSNO.

Method	S–N bond length, Å	S–N BDE, kcal/mol	Reference
B3LYP/6 31G(d)	1.865	29.6	[73]
CBS-4M	1.732	34.4	[73]
CBS-Q	1.850	33.7	[73]
G3	1.775	31.5	[73]
B3LYP/6-311G(2df,p)	-	29.7	[73]
RMP2/6-311++G(d,p)	-	22.5	[73]
MP2/6-31+G(d)	1.760	28.1	[74]
MP2(full)/6-31+G(d)	1.761	28.0	[75]
CBS-QB3	-	32.4	[36]

Nevertheless, none of those studies used accurate *ab initio* methods with no empirical corrections, due to the prohibitively high cost of such calculations during the previous years. Thankfully, due to the constant development of the electronic structure theory, as well as computational chemistry software, highly accurate *ab initio* calculations are now feasible for the MeSNO molecule. In this work, we present the first computational study of MeSNO molecule with the Feller-Peterson-Dixon (FPD) approach,[46,47] that provides near-chemical accuracy for the thermochemical parameters and vibrational frequencies.

B. Computational Details

All *ab initio* electronic structure calculations were performed using Molpro 2015.1[76] and MRCC/CFOUR[77] program packages, with computational resources offered by Marquette University (Pere cluster) and via XSEDE allocation under 'Computational Modeling of Biologically Important S–Nitrosothiol Reactions' project TG-CHE140079.

1. Geometry optimization

Full geometry optimizations of cis-MeSNO, trans-MeSNO, and MeSNO cis-trans isomerization transition state (TS) were performed using frozen-core explicitly-correlated coupled cluster method with single, double and perturbative triple excitations CCSD(T)-F12a,[58,59] in combination with F12-optimized basis sets of Peterson et al. cc-pVnZ-F12 (n = D, T, Q; will be referred to in text as VDZ-F12, VTZ-F12 and VQZ-F12, respectively).[79] For such calculations, corresponding VnZ-F12/OPTRI basis sets are used by default in Molpro 2015.1 to construct the complementary auxiliary orbital basis (CABS).[76] The nature of all stationary points (except the ones calculated with CCSD(T)-F12a/VQZ-F12 method) was confirmed by calculating the Hessian matrix of second-order derivatives of the energy with respect to atomic coordinates, and corresponding eigenvalues (vibrational frequencies). Absence of imaginary frequencies indicated a minimum, and presence of one imaginary frequency indicated a transition state.

The two-point complete basis set (CBS) extrapolation scheme

$$E(n) = E_{CBS} + \frac{B}{n^3}, \quad (1)$$

where *n* is the cardinal number, which indicates the maximum angular momentum function in the basis set,[80] based on CCSD(T)-F12a/VTZ-F12 and CCSD(T)-F12a/VQZ-F12 data, was used to estimate the CCSD(T)-F12a/CBS limit for the geometry parameters of MeSNO structures, the foundation of the FPD scheme.

The corrections for the perturbative quadruple excitations or Δ(Q), due to their extreme computational cost, were calculated only to the S–N bond distances, as the difference in geometric parameters of fully optimized structure at CCSD(T) level, and partially optimized structure at CCSDT(Q) level. We used MIDI![81] and cc-pV(D+d)Z basis sets[82] from EMSL basis set exchange database, to optimize MeSNO conformations with Molpro at CCSD(T) level, and then used optimized structures to relax only the S–N bond in internal coordinates with CCSDT(Q) in MRCC/CFOUR codes, leaving other geometric parameters frozen. Core-valence corrections ΔCV to the geometric parameters were estimated as the difference between the structures, obtained at CCSD(T)-F12a level with weighted CV basis set cc-pCVTZ-F12[83] with full-electron correlation (except the 1s-electrons for the S atom), and the frozen-core ones. Scalar-relativistic corrections ΔSR were calculated at CCSD(T)/cc-pVQZ-DK level by the Douglas-Kroll-Hess method[84,85] in Molpro.

2. Energy calculations

We used customized variations of the FPD scheme to calculate an accurate S–N BDE in MeSNO, the energy difference between cis- and trans-MeSNO

conformations, and the activation barrier of cis-trans isomerization.

The S–N BDE scheme included the following. CCSD(T)-F12a/CBS values were calculated using two-point Schwenke-style extrapolation formula:[86]

$$E_{\mathrm{CBS}}^{\mathrm{corr}} = (E_{\mathrm{large}}^{\mathrm{corr}} - E_{\mathrm{small}}^{\mathrm{corr}})F + E_{\mathrm{small}}^{\mathrm{corr}}, \qquad (2)$$

with separate CBS extrapolation of the CCSD-F12a and (T) components of the electronic energy. Corresponding *F* coefficients for the VTZ-F12/VQZ-F12 pair of basis sets are used from Ref.[87] This approach is better suited to calculate the energetic parameters, because it can exploit the fact that the explicitly correlated CCSD-F12a component of the electronic energy converges significantly faster to the CBS limit with increasing basis set size, than the (T) component, that does not benefit from explicit correlation treatment.

The Δ(Q) corrections for NO· and MeS· radicals were calculated as single-point calculations with MIDI! and cc-pV(D+d) basis sets, whereas the S–N distance in MeSNO was optimized at the CCSDT(Q) level.

ΔCV and ΔSR corrections were calculated with full geometry optimization of both *cis*- and *trans*- MeSNO conformations and the radical fragments (see 'Geometry optimization' section above). Spin-orbit coupling correction for MeS· radical, ΔSO, was calculated with the Breit-Pauli operator,[88] with multireference configuration interaction (MRCI) method[89,90] with aug-cc-pV(Q+d)Z basis set,[91] as implemented in Molpro. Zero-point vibrational energy (ZPE) was calculated at the CCSD(T)-F12a/CBS level, with two-point extrapolation scheme[80] based on CCSD(T)-F12a/VTZ-F12 and CCSD(T)-F12a/VQZ-F12 data. The anharmonic contribution to ΔZPE was calculated in Gaussian 09[56] with second-order perturbative theory

(PT2),[92] using DFT methods MPW2PLYPD[93] (double-hybrid functional) and PBE0[94] (global hybrid functional) with def2-TZVPPD basis set by Weigend and Ahlrichs[95].

The solvent effect on the S–N BDE was studied with polarizable continuum model PCM,[96] with parameters for water (ε=78.3553) and diethylether (ε=4.24). We used previously tested[71] DFT methods with def2-TZVPPD basis set in Gaussian 09, namely B3LYP,[97,98] PBE0,[94] PBE0-GD3[99], PBE0-1/3,[100] wB97XD,[101] B2PLYP,[102] B2PLYPD,[102] MPW2PLYP[93] and MPW2PLYPD, [93] to obtain an average solvent effect for water and diethylether cases. The FPD scheme to calculate relative stability of cis-MeSNO and trans-MeSNO conformers and $\Delta E^{\neq}$ of cis-trans isomerization reaction used same building blocks, except ΔSO.

3. Calculation of vibrational frequencies

To calculate the accurate vibrational frequencies of cis-MeSNO and trans-MeSNO conformers, we used a modified FPD scheme. The harmonic frequencies, calculated with CCSD(T)-F12a/VTZ-F12 and CCSD(T)-F12a/VQZ-F12, were further extrapolated to the CCSD(T)-F12a/CBS limit using a two-point scheme(Equation 1).[80] Anharmonic corrections were calculated with fully automatic second-order perturbation theory (PT2) [92], implemented in Gaussian 09, with double-hybrid DFT method MPW2PLYPD[93], as well as dispersion-corrected PBE0-GD3[103] using the def2-TZVPPD basis set by Weigend and Ahlrichs.[95]

4. Energy profile along the S–N bond

To study the energy profile along the S–N bond, CCSD(T)-F12a/VQZ-F12 optimized geometries of cis-MeSNO, trans-MeSNO and the isomerization TS were

used as starting points. In internal coordinates, only the S–N bond length was varied, leaving the rest of the structure frozen. CCSD, distinguishable coupled cluster DCSD[104,105] and CCSD(T) calculations were performed in Molpro code, CCSDT and CCSDT(Q) - in MRCC/CFOUR; cc-pV(D+d) basis set was used for all methods. To produce the reference FPD S–N bond energy profile of cis-MeSNO, we used CCSD(T)-F12a/VQZ-F12 optimized structure, and performed a series of single-point calculations to obtain the core CCSD(T)-F12a/CBS energies. All further FPD corrections (Δ(Q), ΔCV and ΔSR) were also done as single-point calculations (see 'Geometry Optimization' section for detailed methods and basis sets information).

5. Benchmarking of DFT methods

DFT calculations were performed with Gaussian 09 code[56], with 'UltraFine' settings for the integration grid (99 radial shells, 590 angular points per shell). The list of benchmarked methods includes B3LYP,[97,98] PBE0,[94] PBE0-GD3,[99] PBE0-1/3,[100] wB97XD,[101] B2PLYP, [102] B2PLYPD,[102] MPW2PLYP[93] and MPW2PLYPD,[93] combined with the def2-SV(P)+d and def2-TZVPPD basis sets by Weigend and Ahlrichs[95]. The modified FPD scheme has the same building blocks as described in the previous sections, but lacks ΔSR and ΔSO contributions, which are not available for the implementation in Gaussian DFT. We limited the frequencies calculations to harmonic values only, due to lack of *ab initio* anharmonic data on MeSNO.

C. Results and Discussion

1. Structure of MeSNO

In recent studies,[49,67] accurate FPD-based schemes were applied to investigate the structure and properties of the simplest S-nitrosothiol, HSNO (thionitrous acid). Further improvement of the FPD scheme by applying the explicitly correlated coupled cluster theory[58,59] allowed a dramatic improvement in computational efficiency in the key building block of this modular scheme, frozen-core CCSD(T)/CBS evaluation of the geometric parameters and electronic energy, of HSNO and its protonated and de-protonated forms.[71]

Sensitivity of the RSNO structure to the applied level of theory is the main issue in the accurate electronic structure calculations of RSNOs.[67,106] For example, S–N bond length in the more stable trans-HSNO converges slowly with the increase of the basis set size from AVDZ (1.903 Å) to AV5Z (1.841 Å) at the same CCSD(T) level of theory, as shown in Ref.[67] Further use of CCSD(T)/CBS extrapolation formula[107,108] revealed the S–N bond length limit in trans-HSNO as 1.837 Å.[49] Recently,[71] we used explicitly correlated CCSD(T)-F12a method to drastically increase computational efficiency of ab initio calculations: in trans-HSNO, even a small double-zeta basis set VDZ-F12, comparable in size to AVDZ, produced a S–N bond lenght, reasonably close to CCSD(T)/CBS limit of 1.838 Å. These developments are applied in the present work to MeSNO, which is significantly more taxing from the computational viewpoint.

Cis-MeSNO and *trans*-MeSNO conformations, analogously to previously

studied cis-HSNO and trans-HSNO,[49,67] were studied in this work. Geometric parameters of cis-MeSNO and trans-MeSNO, optimized with FPD approach, are shown in Tables 3 and 4, correspondingly.

Table 3. Cis-MeSNO, ab initio geometrical properties

Method	*r*(S–N), Å	*r*(N–O), Å	*r*(C–S), Å	∠SNO, °	∠CSN, °
CCSD(T)-F12a/VDZ-F12	1.797	1.193	1.791	117.44	102.16
CCSD(T)-F12a/VTZ-F12	1.796	1.192	1.792	117.41	102.22
CCSD(T)-F12a/VQZ-F12	1.795	1.191	1.792	117.42	102.28
CBS(T-Q)	1.794	1.191	1.791	117.42	102.33
Δ(Q)1(MIDI!)	0.016	-	-	-	-
Δ(Q)2(cc-pV(D+d)Z)	0.023	-	-	-	-
ΔCV(cc-pCVTZ-F12)	-0.007	-0.002	-0.004	0.08	0.10
ΔSR(cc-pVQZ-DK)	0.005	-0.001	0.002	-0.06	-0.12
CBS(T-Q)+ΔQ2+ΔCV+ΔSR	1.814	1.189	1.789	117.45	102.31

Table 4. Trans-MeSNO, ab initio geometrical properties

Method	*r*(S–N), Å	*r*(N–O), Å	*r*(C–S), Å	∠SNO, °	∠CSN, °
CCSD(T)-F12a/VDZ-F12	1.802	1.189	1.798	115.63	94.82
CCSD(T)-F12a/VTZ-F12	1.801	1.189	1.798	115.64	94.90
CCSD(T)-F12a/VQZ-F12	1.800	1.188	1.798	115.62	94.95
CBS(T-Q)	1.799	1.188	1.797	115.62	94.98
Δ(Q)1(MIDI!)	0.020	-	-	-	-
Δ(Q)2(cc-pV(D+d)Z)	0.026	-	-	-	-
ΔCV(cc-pCVTZ-F12)	-0.005	-0.002	-0.005	0.001	0.10
ΔSR(cc-pVQZ-DK)	0.004	-0.001	0.002	-0.06	-0.10
CBS(T-Q)+ΔQ2+ΔCV+ΔSR	1.824	1.186	1.795	115.56	94.98

Here, we used CCSD(T)-F12a method in combination with VnZ-F12 basis sets (n = D, T, Q), optimized for explicitly correlated wavefunctions, to perform geometry optimization of MeSNO conformers. Similarly to the HSNO,[71] we anticipated a significant acceleration in geometry convergence to the CBS limit with basis set increase. In fact, the most computationally efficient CCSD(T)-F12a/VDZ-F12 method in the current work overestimated the S–N bond length in trans-MeSNO and cis-MeSNO only by 0.003 Å from the corresponding CBS values (Figure 5). At CCSD(T)-F12a/CBS level, the S–N bonds in MeSNO are noticeably shorter (1.794 Å for cis-MeSNO, 1.799 Å for trans-MeSNO) than in HSNO (1.821 Å for cis-HSNO, 1.837 Å for trans-HSNO with CCSD(T)/CBS[49]).

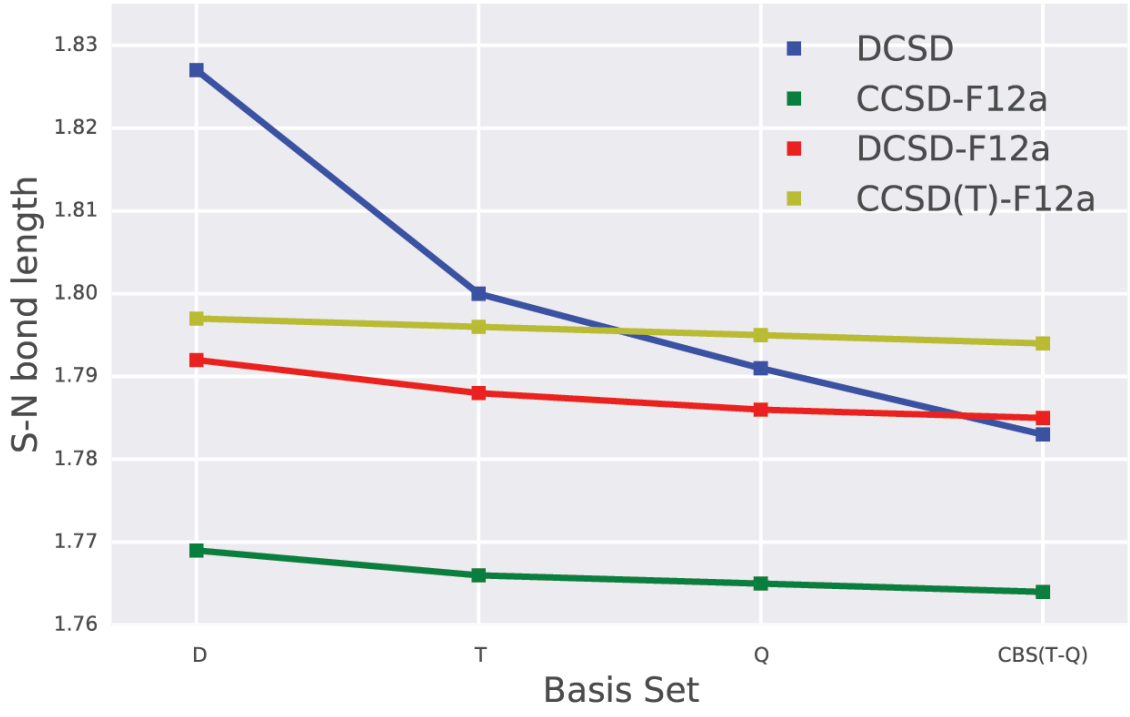

Figure 5. S–N bond length (Å) dependence on the size of the basis set in cis-MeSNO.

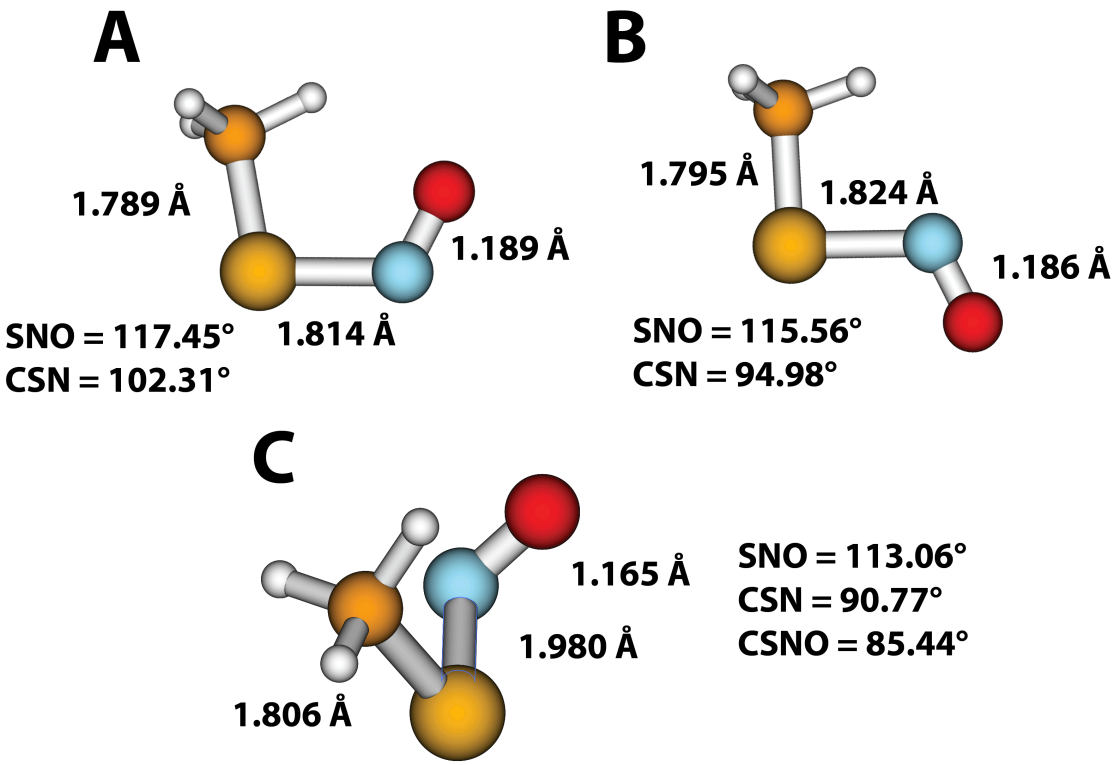

Figure 6. Recommended ab initio geometrical properties of cis-MeSNO (A), trans-MeSNO (B), and MeSNO cis-trans isomerization TS (C). Values are based on CCSD(T)-F12a/CBS(T-Q) geometries, enhanced by corrections for CCSDT(Q) S–N bond change ΔQ, core-valence ΔCV and scalar-relativistic ΔSR geometry corrections

The N–O bonds in HSNO and MeSNO are less sensitive to the basis set size even with the conventional CCSD(T) method, and converge almost instantly to the CBS limit with CCSD(T)/F12a. For example, in HSNO, the CCSD(T)/AVTZ value (1.183 Å) reasonably approximates the CCSD(T)/CBS limit (1.180 Å). In MeSNO, even the smallest basis set VDZ-F12 provides an acceptable N–O bond value of 1.193 Å, with corresponding CBS limit of 1.191 Å. In MeSNO conformers, C–S bonds and all valence angles similarly demonstrate low sensitivity to the applied level of theory. Calculated at CCSD(T)-F12a/VDZ-F12 level C–S bond length value mathes the one calculated with the extrapolated CCSD(T)-F12a/CBS scheme: 1.791 Å.

Remaining contributions to geometrical parameters of *cis*-MeSNO and *trans*-MeSNO from other components in the FPD approach are also shown in Tables 3 and 4. The 0.023 Å post-CCSD(T)/CBS correction to the S–N bond length in *cis*-MeSNO (0.026 Å in *trans*-MeSNO) arose from the accounting for perturbative quadruple corrections in the coupled cluster theory, CCSDT(Q). Due to the extremely high cost of the CCSDT(Q) calculations, we only performed limited optimization of the S–N bond in cis-MeSNO and trans-MeSNO, while keeping all other geometry variables frozen. Generally shorter in comparison with HSNO, the S–N bond in MeSNO also appears to be less sensitive to the level of excitation in the coupled cluster theory: S–N bond elongation due to Δ(Q) effect in cis-HSNO is 0.034 Å, 0.033 Å in trans-HSNO.[49]

Previously,[67,71] we demonstrated weak dependence of Δ(T) and Δ(Q) contributions to the HSNO parameters on the basis set size, such as S–N bond lengths, S–N homolytic BDEs, relative stability of cis-HSNO and trans-HSNO. In this work, we also observe that the Δ(Q) contribition to the S–N bond length in MeSNO, calculated with smaller MIDI! and larger cc-pV(D+d) basis sets, are in good agreement with each other (0.016 Å and 0.023 Å in cis-MeSNO, 0.020 Å and 0.026 Å in trans-MeSNO). Core-valence and scalar-relativistic effects in FPD scheme oppose each other in predicting accurate S–N bond length in cis-MeSNO and trans-MeSNO. ΔCV in cis-MeSNO shortens the S–N bond by 0.007 Å, and ΔSR elongates it by 0.005 Å (-0.005 Å and 0.004 Å in trans-MeSNO).

2. Stability of cis-MeSNO and trans-MeSNO

The tendency of RSNOs to adapt planar conformations of the SNO fragment is evident from experimental[109-111] and theoretical[67,112] investigations. Hindered rotation around an elongated S–N bond has become one of the hallmarks of the SNO group, revealing its complex electronic structure[112]. The simplest S-nitrosothiol, HSNO, has been repeatedly shown to be more stable in the trans-conformation.[49,67-70]

In the case of MeSNO, the possibility of cis-trans isomerism was proposed as early as in 1961 by Phillippe,[113] while measuring the IR spectra of MeSNO in the gas phase. He compared the methylnitrite (MeONO), which can exist in cis- and trans-forms, and thionitrite molecules, based on the same number of atoms, symmetry and bonding pattern. Later, in 1968, Christensen et al.[114] observed cis-trans conformational change in MeSNO in low-temperature proton NMR experiment. Muller and Huber,[115] in a later work conformed cis-trans isomerism of MeSNO with the low-temperature argon matrix isolation technique and FTIR.

Here, we report FPD energy components of the relative stability of cis-MeSNO and trans-MeSNO (Table 5). To evaluate an accurate CCSD(T)-F12a/CBS limit of electronic energy, we used Schwenke-style 2-point scheme (T, Q)[86,87] with separate convergence treatment of the explicitly correlated CCSD-F12a and conventional (T) components. As the result, both conformations have close electronic energies; cis-MeSNO has intrinsic stability advantage of 1.15 kcal/mol over trans-HSNO at CCSD(T)-F12a/CBS level. Conversely, recent data on HSNO[49]

with CCSD(T)/CBS (T, Q) indicate 0.91 kcal/mol stability advantage of trans-HSNO.

Further augmentation of the FPD scheme only marginally affected the results: ΔZPE (harmonic) and ΔCV increased the relative stability of cis-MeSNO by 0.04 and 0.01 kcal/mol, correspondingly. In HSNO, ΔZPE and ΔCV similarly contributed to the increased stability of trans-HSNO by 0.10 and and 0.01 kcal/mol.[49] Contribution of perturbative quadruple excitations in coupled cluster theory, Δ(Q), in case of MeSNO neutralized mentioned above additional stabilization of cis-conformation (-0.06 kcal/mol). In HSNO, Δ(Q) contribution is similar, -0.10 kcal/mol.[49] Scalar-relativistic correction, ΔSR, had no effect on relative stability of HSNO and MeSNO conformations.

Table 5. Ab Initio relative stability of cis-MeSNO and trans-MeSNO

Computational Method	ΔE(cis-trans), kcal/mol
CCSD-F12a/CBS(T-Q, Schwenke)	0.74
CCSD(T)-F12a/CBS(T-Q, Schwenke)	1.15
ΔZPE (CCSD(T)-F12a/CBS(T-Q), Harmonic)	0.04
ΔCV (cc-pCVTZ-F12)	0.01
ΔSR (cc-pVQZ-DK)	0.00
Δ(Q)1 (S–N bond fixed, MIDI!)	-0.04
Δ(Q)2 (S–N bond fixed, cc-pV(D+d)Z)	-0.03
Δ(Q)3 (S–N bond relaxed, cc-pV(D+d)Z)	-0.06
Reference (CCSD(T)-F12a/CBS(T-Q)+ +ΔZPE+ΔAnharmonic+ΔCV+ΔSR+Δ(Q)3)	1.15

Table 6. DFT solvent corrections

Method (with def2-TZVPPD basis set)	ΔSolvent (PCM, water), kcal/mol	ΔSolvent (PCM, diethylether), kcal/mol
B3LYP	0.01	0.00
PBE0	-0.02	-0.02
PBE0-GD3	-0.01	-0.01
PBE0-1/3	-0.05	-0.04
ωB97XD	-0.07	-0.05

B2PLYP	-0.01	-0.01
B2PLYPD	0.00	0.00
MPW2PLYP	-0.03	-0.03
MPW2PLYPD	-0.03	-0.02
Average	-0.02	-0.02

Evaluation of solvent influence on the relative stability of cis-MeSNO and trans-MeSNO at DFT/PCM level of theory exposed its limited sensitivity to both presence and nature of the solvent (trans-MeSNO stability was increased by 0.02 kcal/mol on average in water and diethylether, see Table 6). Thereby, we recommend a value of 1.15 kcal/mol as the measure of stability of cis-conformation of MeSNO over trans-MeSNO in gas phase, 1.13 kcal/mol in solution. For comparison, in Ref.[115], authors were able to experimentally assign ΔG^0_{298} (*cis-trans*) as 1.34±0.19 kcal/mol, using the matrix isolation technique.

3. Conformational dynamics of MeSNO

Isomerization reaction between two planar conformations of RSNOs (cis- and trans-conformations), an intrinsic feature of the partially double S–N bond, is discussed in experimental[115,116] and computational[49] studies. Here, we use an FPD approach to locate and characterize the transition state of MeSNO cis-trans isomerization. Table 7 contains corresponding FPD geometrical and energetic parameters of such a transition state. As we can see, a significantly elongated S–N bond, as well as a near-square CSNO dihedral angle, are the two most distinct features of the TS structure.

Table 7. MeSNO cis-trans isomerization TS, ab initio geometrical properties

Method	*r*(S–N), Å	*r*(N–O), Å	*r*(C–S), Å	∠SNO, °	∠CSN, °	∠CSNO, °
CCSD(T)-F12a/VDZ-F12	1.956	1.169	1.808	113.08	90.71	85.63
CCSD(T)-F12a/VTZ-F12	1.957	1.168	1.809	113.06	90.69	85.49
CCSD(T)-F12a/VQZ-F12	1.956	1.168	1.809	113.07	90.79	85.43
CBS(T-Q)	1.955	1.167	1.809	113.07	90.85	85.39
ΔQ1(MIDI!)	0.016	-	-	-	-	-
ΔQ2(cc-pV(D+d)Z)	0.026	-	-	-	-	-
ΔCV(cc-pCVTZ-F12)	-0.007	-0.002	-0.004	0.02	0.10	-0.01
ΔSR(cc-pVQZ-DK)	0.006	-0.001	0.002	-0.03	-0.18	0.06
CBS(T-Q)+ΔQ2+ΔCV+ΔSR	1.980	1.165	1.806	113.06	90.77	85.44

Indeed, the calculated S–N bond length in the transition state at the CCSD(T)-F12a/CBS level is noticeably elongated compared to the most stable conformation, cis-MeSNO, by 0.161 Å (1.955 Å vs. 1.794 Å). Similarly, S–N bond elongation during isomerization reaction of HSNO[49,71] at the CCSD(T)/CBS level[49] is 0.175 Å, and 0.174

Å at CCSD(T)-F12a/VQZ-F12 level.[71] More rigid S–N bond in MeSNO, as it will be shown later, led to consequent increase of the activation barrier height in comparison to HSNO.

Another major contribution in the FPD approach is the effect of quadruple excitations in coupled cluster theory, Δ(Q). With all basis sets (MIDI! and cc-pV(D+d)Z), the further elongation of the S–N bond is observed (by 0.016 Å with MIDI!, and 0.026 Å by cc-pV(D+d)Z). Core-valence effect ΔCV and scalar-relativistic effect ΔSR are comparable in magnitude (~0.01 Å) and nearly compensate each other. In this work, we recommend 1.980 Å as the reference value of the S–N bond in MeSNO isomerization transition state. The CSNO dihedral angle in isomerization TS converges comparatively faster on the basis set size at CCSD(T) level, for HSNO and MeSNO. With all corrections applied, recommended value for MeSNO is 85.44°, noticeably smaller than 88.02° in HSNO.[49]

The activation barrier of cis-trans MeSNO interconversion was calculated as 12.65 kcal/mol in the gas phase using FPD approach (Table 8). Preceding evaluation of cis-trans isomerization of HSNO yielded noticeably lower value of the activation barrier, 9.52 kcal/mol.[49] Increased MeSNO isomerization barrier is likely has an electronic origin, due to more efficient stabilization of planar conformations by the CH_3 substituent compared to H. More detailed analysis of these effects will be reported elsewhere. In the final FPD value of the activation energy, the major counteracting contributors to the fundamental CCSD(T)-F12a/CBS value are ΔZPE and Δ(Q) effects: ΔZPE lowers activation energy by 0.55 kcal/mol whereas Δ(Q) increases it by 0.56 kcal/mol. In HSNO,[49] ΔZPE more significantly lowered the

barrier by 0.83 kcal/mol, and Δ(Q) contribution remained at similar to MeSNO value of 0.54 kcal/mol. ΔCV and ΔSR effects were less significant, and also nearly neutralized each outer in MeSNO and HSNO cases. Polar and non-polar solvents, as shown in Table 9, pull the activation barrier in different directions: polar solvent (water) on average increases the barrier by 0.57 kcal/mol, whereas a less polar solvent (diethylether) decreases the barrier by 0.12 kcal/mol. For comparison, Arulsamy et al.[111] evaluated the conformational dynamics of CH_3CH_2SNO and $(CH_3)_3SNO$ with low-temperature ^{15}N NMR technique, and obtained 11.1 and 10.7 kcal/mol rotational barrier heights, respectively.

Table 8. Ab Initio activation energy of cis-trans MeSNO isomerization

Computational Method	$\Delta E^{\neq}$(cis-trans), kcal/mol
CCSD-F12a/CBS(T-Q, Schwenke)	11.93
CCSD(T)-F12a/CBS(T-Q, Schwenke)	12.61
ΔZPE (CCSD(T)-F12a/ CBS(T-Q), Harmonic)	-0.55
ΔCV (cc-pCVTZ-F12)	0.10
ΔSR (cc-pVQZ-DK)	-0.07
ΔQ1 (S–N bond fixed, MIDI!)	0.46
ΔQ2 (S–N bond fixed, cc-pV(D+d)Z)	0.47
ΔQ3 (S–N bond relaxed, cc-pV(D+d)Z)	0.56
Reference (CCSD(T)-F12a/CBS(T-Q)+ +ΔZPE+ΔCV+ΔSR+ΔQ3)	12.65

Table 9. DFT solvent corrections

Method (with def2-TZVPPD basis set)	ΔSolvent (PCM, water), kcal/mol	ΔSolvent (PCM, diethylether), kcal/mol
B3LYP	0.51	-0.17
PBE0	0.51	-0.14
PBE0-GD3	0.55	-0.14
PBE0-1/3	0.61	-0.10
ωB97XD	0.61	-0.10
B2PLYPD	0.52	-0.15
MPW2PLYP	0.60	-0.10

MPW2PLYPD	0.61	-0.09
Average	0.57	-0.12

4. S–N BDE in MeSNO

An unusually long and weak S–N bond in RSNOs is the key reason of lability of these species in biochemistry. Primary and secondary RSNOs are reported to have half-lives from seconds to minutes,[117] which poses additional challenges for the experimental assessment, which increases the importance of accurate theoretical predictions. Here, we use an FPD approach to evaluate S–N BDE in MeSNO, in the gas phase and in solution. Components of the recommended FPD BDE value are listed in Table 10. The CCSD(T)-F12a/CBS value of MeSNO S–N BDE is 34.20 kcal/mol, noticeably higher than S–N BDE in HSNO at a comparable level of theory[67] (31.72 kcal/mol, CCSD(T)/CBS). Accounting for the harmonic ΔZPE significantly lowers the BDE by 2.79 kcal/mol for MeSNO, and 2.71 kcal/mol for HSNO.[67] Second largest component of S–N BDE, Δ(Q) effect, partially neutralizes ΔZPE increment (by 1.33 kcal/mol for MeSNO, and approx. 1.0 kcal/mol for HSNO). We also included into consideration the anharmonicity of bond vibrations for MeSNO, which adds an extra 0.38 kcal/mol to the BDE. The ΔSR contribution in MeSNO and HSNO, next in the order of importance, reduces S–N BDE by 0.41 and 0.35 kcal/mol, correspondingly. The least significant ΔCV contributions decreases S–N BDE of MeSNO by 0.02 kcal/mol, but increases it for HSNO by 0.05 kcal/mol.

Table 10. Ab Initio S–N BDE in cis-MeSNO

Computational Method	D_0(S–N), kcal/mol
CCSD-F12a/CBS(T-Q, Schwenke)	27.63
CCSD(T)-F12a/CBS(T-Q, Schwenke)	34.20
ΔZPE (CCSD(T)-F12a/CBS Harmonic)	-2.79
ΔAnharmonic, MPW2PLYPD/def2-TZVPPD	0.38
ΔCV (cc-pCVTZ-F12)	-0.02

ΔSR (cc-pVQZ-DK)	-0.41
ΔSO (MRCI/AVQZ)	-0.18
ΔQ1 (S–N bond fixed, MIDI!)	0.95
ΔQ2 (S–N bond fixed, cc-pV(D+d)Z)	0.99
ΔQ3 (S–N bond relaxed, cc-pV(D+d)Z)	1.33
Reference (CCSD(T)-F12a/CBS(T-Q)+ +ΔZPE+ΔAnharmonic+ΔCV+ΔSR+ΔSO+ΔQ3)	32.4

Interestingly, we observed an example of an interplay between a Jahn-Teller effect and the relativistic spin-orbit coupling effect in case of MeS· radical. The more symmetrical (C_{3v} point group) structure of MeS· radical is less stable than MeS· structure with lower symmetry point group (C_s), according to the Jahn–Teller theorem. MeS radical in C_{3v} form has spatially degenerate electronic ground state (Figure 7), and undergoes geometry distortion that removes that degeneracy.

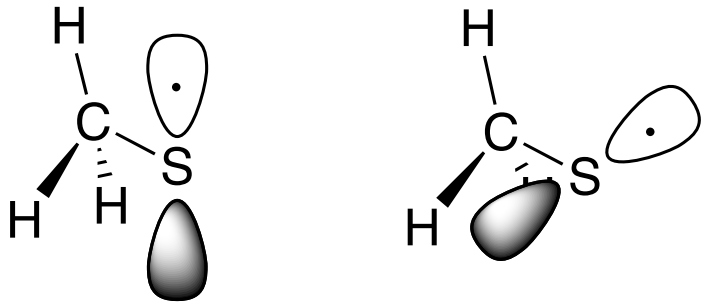

Figure 7. Degenerate 2A' and 2A"electronic states of MeS• radical (C_{3v} symmetry).

In the C_{3v} MeS· geometry, all C–H bonds are equivalent, but in the C_s-symmetry structure one of them is elongated (Figure 8). At the CCSD(T)-F12a/VQZ-F12 level of theory, this distortion leads to 0.26 kcal/mol stabilization. Less symmetric MeS· radical structure was also free from imaginary frequencies. The energy gap between non-degenerate ^{2}A' and ^{2}A" states in C_s-symmetry MeS· radical is 1.54 kcal/mol at MRCI/aug-cc-pV(Q+d)Z level.

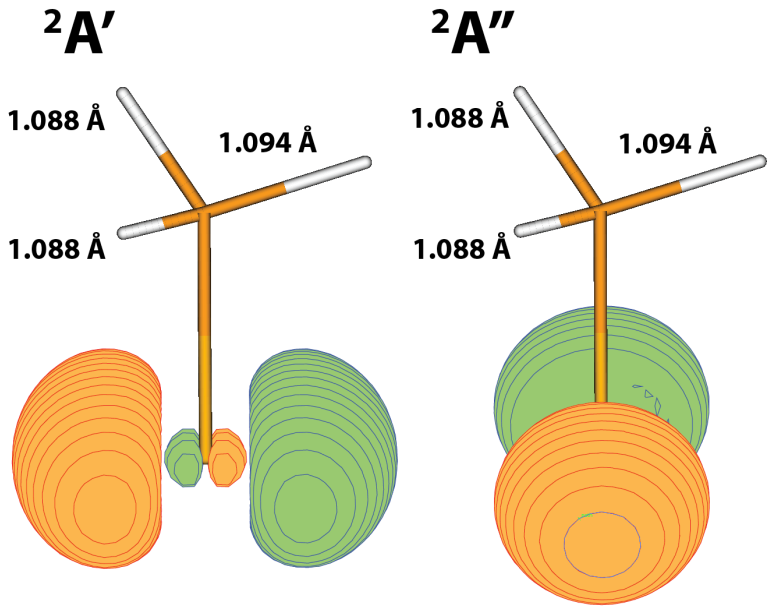

Figure 8. Non-degenerate 2A' and 2A"electronic states of MeS• radical after Jahn-Teller distortion (Cs symmetry). C–H bond distances are calculated at the CCSD(T)-F12a/VQZ-F12a level of theory.

Spin-orbit coupling effect is usually most important for the open-shell species, and increases with the increase of the nuclear mass (therefore, MeS· radical is expected to have a non-zero ΔSO value). In case of HSNO, for the linear HS· radical two $^2\Pi$ states and one $^2\Sigma$ state were included in the SO calculation, which resulted in 0.48 kcal/mol stabilizaion of HS· radical.[67] In MeSNO, SO stabilization of MeS· radical is only 0.18 kcal/mol, calculated with MRCI/aug-cc-pV(Q+d)Z using CCSD(T)-F12a/VQZ-F12 geometry.

To estimate the solvent effect on MeSNO BDE, we used polarized-continuum DFT calculations (Table 11). As the result, we observed further decrease of the S–N BDE, by 0.17 kcal/mol in water and by 0.15 kcal/mol in diethylether. Therefore, we recommend the S–N BDE value for MeSNO as 32.4 kcal/mol in gas phase, 32.2

kcal/mol in solution. The latest FPD value of S–N BDE for HSNO in gas phase is 29.4 kcal/mol, 3 kcal/mol lower than in MeSNO[49]. Bartberger et al.[36] previously reported calculated S–N BDEs ≈30 kcal/mol in (using the CBS-QB3 methodology[119]) a number of physiologically relevant RSNOs, and pointed out that thermal stability of aliphatic RSNOs should be similar to organic peroxides.

Table 11. DFT solvent corrections to S–N BDE in cis-MeSNO

Method (with def2-TZVPPD basis set)	ΔSolvent (PCM, water), kcal/mol	ΔSolvent (PCM, diethylether), kcal/mol
B3LYP	-0.22	-0.19
PBE0	-0.22	-0.18
PBE0-GD3	-0.21	-0.17
PBE0-1/3	-0.13	-0.12
ωB97XD	-0.14	-0.13
B2PLYP	-0.20	-0.18
B2PLYPD	-0.19	-0.17
MPW2PLYP	-0.12	-0.12
MPW2PLYPD	-0.11	-0.12
Average	-0.17	-0.15

5. MeSNO Vibrational Frequencies

MeSNO was first characterized in the gas phase by IR spectroscopy as early as in 1961 by Philippe.[113] At the time, only a few fundamental frequencies in the spectrum were assigned, and the S–N and N–O vibration frequencies were identified as 655 cm^{-1} and 1534 cm^{-1}, correspondingly. Judging by the absence of doubled IR bands in the spectrum, which is typical for cis- and trans conformations of nitrous acid and methylnitrite, he suggested that MeSNO exists only in cis-conformation in the gas phase.

Later, in 1968, Christensen at al.[114] found an evidence of conformational isomerism in MeSNO using proton NMR at -60°C. In the IR spectra, they were able to tentatively assign S–N–O bending at 375 cm^{-1} frequency, S–N stretching at 734 cm^{-1}, and N–O stretching at 1530 cm^{-1}.

In 1984, Muller and Huber[115] used FT-IR in argon matrix at 12 K, and reported the IR spectra of both cis-MeSNO and trans-MeSNO conformations. According to this study, prior attempts to find both conformations at the room temperature failed due to low natural abundance of the less stable trans-MeSNO, approx. 10%. The reported difference in the position of the N–O band for trans- and cis-MeSNO is 21 cm^{-1} (1548 cm^{-1} for trans-MeSNO, 1527 cm^{-1} for cis-MeSNO), while the S–N vibrational frequency was identified as 376 cm^{-1} in cis-MeSNO, 371 cm^{-1} in trans-MeSNO.

Here, we present an accurate vibrational frequencies and zero-point vibrational energies (ZPEs) of cis- and trans-MeSNO conformers, using coupled

cluster and DFT methodology. The list of calculated and experimental[115] vibrational modes, as well as ZPEs of cis-MeSNO are shown in Table 12, for trans-MeSNO - in Table 14. We adopted computationally feasible FPD approach to calculate the vibrational frequencies. First, harmonic modes were calculated using CCSD(T)-F12a/VnZ (n = D, T, Q) methodology, and then extrapolated to the CBS limit via a 2-point extrapolation scheme (T ,Q). Even at the simplest level of theory (explicitly-correlated CCSD(T)-F12a/VDZ-F12), vibrational frequencies were already near the CBS limit. The ZPE values for cis-MeSNO and trans-MeSNO with CCSD(T)-F12a/VDZ-F12 is higher than the CCSD(T)-F12a/CBS limit only by 0.1 kcal/mol.

To account for the anharmonic correction, we used a double-hybrid DFT method MPW2PLYPD with def2-TZVPPD basis set, implemented in Gaussian 09 program package.[56] As mentioned in Ref.[47], the anharmonic contribution can be evaluated by lower levels of theory, as a correction to corresponding accurate and expensive ab initio harmonic value. It has been suggested to use at least CCSD(T)/cc-pVQZ or similar in accuracy harmonic frequencies, and supplement them with the anharmonic corrections, calculated with the MP2/aug-cc-pVDZ approximation.[47] Anharmonic *ab initio* frequency calculations require multiple evaluations of the Hessian matrix, and although we were previously able to perform anharmonic coupled cluster calculations,[71] they are not yet computationally feasible for a larger MeSNO molecule.

The final predicted values of vibrational frequencies of cis-MeSNO and trans-MeSNO, as well as their ZPEs, are listed in Tables 12 and 14, correspondingly. Tables 13 and 15 demonstrate harmonic and anharmonic vibrational frequencies of MeSNO

conformers (Table 13- cis-MeSNO, Table 15 - trans-MeSNO) using DFT methods in Gaussian 09, namely double-hybrid MPW2PLYPD and dispersion-corrected PBE0-GD3.

Table 12. Cis-MeSNO vibrational frequencies

Mode	CCSD(T)-F12a/VDZ-F12	CCSD(T)-F12a/VTZ-F12	CCSD(T)-F12a/VQZ-F12	CCSD(T)-F12a/CBS(T-Q)	Anharmonic correction (MPW2PLYPD/def2-TZVPPD)	Final FPD value	Expt.[75]
1 A"	92.0	88.4	86.2	84.6	-39.6	45.1	-
2 A'	281.2	281.0	280.5	280.1	-10.0	270.1	268.0
3 A"	290.2	290.8	290.9	291.0	-4.8	286.2	-
4 A' (S–N)	400.6	399.1	399.5	399.7	-1.5	398.2	376.0
5 A'	663.3	662.4	662.4	662.4	-9.5	652.9	649.0
6 A'	756.4	754.0	754.2	754.3	-16.4	737.9	731.5
7 A'	964.0	963.2	962.8	962.5	-22.8	939.7	-
8 A"	973.4	970.9	970.8	970.8	-12.8	958.0	940.0
9 A'	1340.2	1335.6	1334.8	1334.3	-35.2	1299.1	1298.0
10 A"	1480.4	1475.4	1476.4	1477.2	-41.3	1436.0	1428.5
11 A'	1485.3	1480.3	1480.6	1480.8	-44.7	1436.1	1455.0
12 A' (N–O)	1571.5	1572.2	1573.9	1575.1	-33.2	1541.9	1527.0
13 A'	3032.1	3027.8	3028.2	3028.4	-96.8	2931.6	2910.0
14 A'	3128.9	3126.1	3126.8	3127.3	-137.3	2990.0	2928.0
15 A"	3163.6	3160.8	3158.7	3157.2	-145.3	3011.9	2932.0
ZPE, kcal/mol	28.1	28.0	28.0	28.0	-0.9	27.1	-

Table 13. DFT vibrational frequencies for cis-MeSNO (with def2-TZVPPD basis set)

Mode	MPW2PLYPD, Harmonic	MPW2PLYPD, Anharmonic	PBE0-GD3, Harmonic	PBE0-GD3, Anharmonic	Expt.[75]
1 A"	101.6	62.0	105.7	76.4	-
2 A'	266.3	256.4	264.6	259.4	268.0
3 A"	303.1	298.3	311.1	305.7	-
4 A' (S–N)	388.4	386.9	424.1	421.2	376.0
5 A'	666.8	657.3	677.1	667.9	649.0
6 A'	744.8	728.4	759.9	742.8	731.5
7 A'	969.9	947.1	953.2	937.9	-
8 A"	974.9	962.2	958.2	939.9	940.0
9 A'	1346.5	1311.4	1321.9	1293.2	1298.0
10 A"	1484.0	1442.8	1456.5	1417.0	1428.5
11 A'	1488.2	1443.5	1461.6	1420.5	1455.0
12 A' (N–O)	1578.3	1545.1	1666.5	1639.5	1527.0
13 A'	3043.8	2947.0	3031.7	2926.3	2910.0
14 A'	3141.4	3004.1	3129.6	2994.3	2928.0
15 A"	3176.4	3031.1	3164.7	3021.3	2932.0
ZPE, kcal/mol	28.1	27.2	28.1	27.3	-

Table 14. Trans-MeSNO vibrational frequencies

Mode	CCSD(T)-F12a/VDZ-F12	CCSD(T)-F12a/VTZ-F12	CCSD(T)-F12a/VQZ-F12	CCSD(T)-F12a/CBS (T-Q)	Anharm. correction (MPW2PLYPD/def2-TZVPPD)	Final FPD value	Expt.[75]
1 A"	121.7	119.7	119.6	119.5	-17.3	102.2	-
2 A'	227.9	227.7	227.6	227.5	-6.9	220.6	234.5
3 A"	236.1	235.7	235.6	235.6	-11.1	224.5	-
4 A' (S–N)	394.2	393.5	393.9	394.2	-7.6	386.5	371.0
5 A'	670.3	669.3	669.5	669.6	-9.5	660.1	651.0
6 A'	753.2	751.0	751.5	751.8	-14.7	737.1	736.5
7 A'	972.6	971.0	994.1	1011.0	-16.3	994.7	-
8 A"	996.5	994.4	970.8	953.5	-17.8	935.7	971.5
9 A'	1358.5	1353.5	1353.0	1352.6	-32.9	1319.7	1314.0
10 A"	1471.9	1468.5	1468.4	1468.3	-41.7	1426.6	1441.0
11 A'	1498.3	1493.1	1493.9	1494.5	-42.4	1452.1	1456.0
12 A' (N–O)	1590.7	1590.9	1592.4	1593.5	-31.8	1561.8	1548.0
13 A'	3049.3	3044.7	3045.6	3046.2	-98.2	2948.0	2909.0
14 A'	3142.9	3140.1	3141.4	3142.3	-138.9	3003.4	2928.5
15 A"	3162.2	3159.9	3154.5	3150.6	-144.2	3006.4	2931.5
ZPE, kcal/mol	28.1	28.0	28.0	28.0	-0.9	27.1	-

Table 15. DFT vibrational frequencies for trans-MeSNO (with def2-TZVPPD basis set)

Mode	MPW2PLYPD, Harmonic	MPW2PLYPD, Anharmonic	PBE0-GD3, Harmonic	PBE0-GD3, Anharmonic	Expt.[75]
1 A"	129.5	112.1	131.4	112.5	-
2 A'	235.0	228.1	237.8	230.7	234.5
3 A"	239.0	227.9	242.4	224.6	-
4 A' (S–N)	384.5	376.9	409.5	402.9	371.0
5 A'	671.5	662.0	683.6	674.8	651.0
6 A'	742.2	727.5	758.8	744.6	736.5
7 A'	980.3	964.0	959.5	945.6	-
8 A"	1000.2	982.3	984.3	965.4	971.5
9 A'	1366.3	1333.4	1339.0	1309.6	1314.0
10 A"	1476.5	1434.8	1449.4	1406.5	1441.0
11 A'	1502.2	1459.8	1475.3	1432.8	1456.0
12 A' (N–O)	1604.3	1572.5	1698.3	1670.1	1548.0
13 A'	3063.0	2964.8	3051.0	2943.9	2909.0
14 A'	3157.1	3018.2	3145.2	3008.6	2928.5
15 A"	3176.9	3032.6	3164.5	3023.4	2931.5
ZPE, kcal/mol	28.2	27.3	28.2	27.3	-

We compared our final theoretical values for vibrational frequencies with the experimental data of Muller and Huber.[115] The majority of bands are in good agreement, including the S–N and N–O vibrations. The experimental and calculated frequencies of the S–N bond stretch are below 400 cm^{-1} for cis-MeSNO (398.2 cm^{-1} calculated, 376.0 cm^{-1} experimental) and trans-MeSNO (386.5 cm^{-1} calculated, 371.0 cm^{-1} experimental). The N–O vibrations used in Ref.[115] to distinguish between the cis- and trans-conformations of MeSNO, are also in good agreement (1541.9 cm^{-1} calculated, 1527 cm^{-1} measured for cis-MeSNO; 1561.8 cm^{-1} calculated, 1548.0 cm^{-1} measured for trans-MeSNO). Remarkably, the experimental difference in frequencies of N–O vibration for cis- and trans-MeSNO (21 cm^{-1}), is accurately

reproduced with our FPD scheme (19.9 cm^{-1}).

The analysis of the anharmonic corrections to vibrational frequencies reveals that the S–N mode in MeSNO is well described at harmonic level (-1.5 cm^{-1} correction to the harmonic value in cis-MeSNO, -7.6 cm^{-1} in trans-MeSNO). We compared two DFT methods, MPW2PLYPD and PBE0-GD3, with the same basis set def2-TZVPPD, and both methods gave similar results (388.4 cm^{-1} and 424.1 cm^{-1} for the harmonic S–N vibration, 1578 cm^{-1} and 1666.5 cm^{-1} for the harmonic N–O vibration in *cis*-MeSNO) (Tables 13 and 15).

In previous work,[71] we applied an automated vibrational self-consistent field (VSCF) and VCI procedures[120,121] to calculate the anharmonic vibrational frequencies of HSNO conformations in Molpro[76] code, using explicitly-correlated *ab initio* CCSD(T)-F12a method with aug-cc-pV(D+d)z basis set (which is similar to the VDZ-F12 basis set, used in the present work). In the case of HSNO, similarly to MeSNO, the S–N bond was found to have mostly harmonic character: the anharmonic correction in trans-HSNO is -6.1 cm^{-1}, in cis-HSNO -9.9 cm^{-1}.

On the other hand, the anharmonic correction to the N–O vibrational mode is significantly larger, -33.2 cm^{-1} for cis-MeSNO and -31.8 cm^{-1} in trans-MeSNO. In the case of HSNO,[21] *ab initio* anharmonic correction was calculated as -23.5 cm^{-1} in trans-conformer, and -19.9 cm^{-1} in cis-conformer.

The overall effect of anharmonic contribution lowers the ZPEs of MeSNO conformers by 0.9 kcal/mol for cis-MeSNO and for trans-MeSNO. This value is considerably larger comparing to the observed anharmonic effect in other small molecules, which rarely exceeds 0.5 kcal/mol.[46,47]

6. S–N bond energy profiles

In order to gain further insight into the properties of the S–N bond, we performed a series of *ab initio* energy scans along the S–N bond in cis-MeSNO, trans-MeSNO and the cis-trans isomerization TS. The vibrational frequency of S–N stretching in MeSNO is determined to be below 400 cm^{-1}, according to both experimental[115] and our computational results (Tables 12, 14), yet it demonstrates surprisingly harmonic behavior – the anharmonic correction is only -1.5 cm^{-1} in cis-MeSNO, -7.6 cm^{-1} in trans-MeSNO. To explore this surprising finding, we tested the performance of different *ab initio* methods, and applied the FPD protocol to obtain an accurate S–N bond energy profile in MeSNO. Those values can be used as the reference data to benchmark the performance of different DFT methods.

As previously mentioned, in traditional coupled cluster method, the contribution of perturbative triple excitations Δ(T) has almost no dependence on the basis set size when applied to the S–N bond length and BDE.[67] Previously,[71] we demonstrated that the contribution of perturbative quadruple excitations, Δ(Q), also weakly depends on the basis set size for the same set of the S–N bond properties. Here, we are adding to the set a newly developed distinguishable cluster approximation DCSD,[104,105] implemented in Molpro 2015.1 code, to compare its performance to traditional CCSD and CCSD(T) methods. The DCSD method has been shown to have a computational cost comparable to the CCSD method, but promises better accuracy.[104,105,122]

In Tables 16-18, the S–N bond PES energy values are listed with the corresponding bond distances for cis-MeSNO, trans-MeSNO and the isomerizaion TS, correspondingly. In all cases, the shortest S–N bond is predicted by the CCSD method (S–N bond distance 1.87 Å in cis-MeSNO, 1.86 Å in trans-MeSNO, 2.00 Å in the TS). Interestingly, the distinguishable cluster approximation, DCSD, performs almost as good as the more computationally expensive CCSD(T) method for cis-MeSNO and trans-MeSNO (minimum at the same 1.90 Å scan point), and significantly outperforms CCSD method in the case of transition state (2.05 and 2.00 Å, correspondingly). Further increase of the level of excitations in the coupled cluster method leads to continuing lengthening of the S–N bond. Non-perturbative treatment of triple excitations (CCSDT method) in the case of cis-MeSNO and trans-MeSNO increased the S–N bond length by 0.01 Å, but had no effect on already elongated S–N bond in the TS. The application of perturbative quadruple excitations CCSDT(Q) for the MeSNO system is limited, due to significantly longer CPU times and increased demand for high-capacity and high-throughput storage on the computational nodes. With the cc-pV(D+d) basis set, we observed further elongation of the S–N bond from the CCSDT(Q) level for all MeSNO cases.

Table 16. PES scan (kcal/mol) for the S–N bond in cis-MeSNO

r(S–N), Å	CCSD	DCSD	CCSD(T)	CCSDT	CCSDT(Q)
1.750	1.881	-	-	-	-
1.760	1.541	-	-	-	-
1.770	1.241	-	-	-	-
1.780	0.978	-	-	-	-
1.790	0.751	-	-	-	-
1.800	0.556	1.102	1.179	1.319	-
1.810	0.393	0.874	0.945	1.072	-
1.820	0.260	0.675	0.740	0.854	-
1.830	0.156	0.505	0.563	0.665	-
1.840	0.080	0.362	0.413	0.501	-
1.850	0.029	0.244	0.288	0.363	0.530
1.860	0.003	0.151	0.187	0.249	0.392
1.870	0.000	0.081	0.108	0.158	0.277
1.880	0.020	0.033	0.052	0.088	0.183
1.890	0.061	0.007	0.016	0.039	0.110
1.900	0.122	0.000	0.000 (1.903 Å)	0.010	0.055
1.910	0.203	0.013	0.003	0.000	0.020
1.920	0.302	0.044	0.024	0.008	0.001
1.930	0.419	0.092	0.061	0.033	0.000 (1.926 Å)
1.940	0.553	0.158	0.116	0.074	0.015
1.950	0.702	0.239	0.185	0.131	0.044
1.960	0.867	0.335	0.270	0.203	0.089
1.970	1.047	0.447	0.369	0.289	0.147
1.980	1.241	0.572	0.481	0.389	0.218
1.990	1.447	0.710	0.606	0.502	0.302
2.000	1.667	0.861	0.744	0.627	0.398

Table 17. PES scan (kcal/mol) for the S–N bond in trans-MeSNO

r(S–N), Å	CCSD	DCSD	CCSD(T)	CCSDT	CCSDT(Q)
1.750	1.608	-	-	-	-
1.760	1.306	-	-	-	-
1.770	1.039	-	-	-	-
1.780	0.807	-	-	-	-
1.790	0.608	-	-	-	-
1.800	0.440	0.981	1.104	1.258	-
1.810	0.301	0.774	0.886	1.026	-
1.820	0.190	0.593	0.695	0.821	-
1.830	0.106	0.440	0.530	0.642	-
1.840	0.047	0.311	0.390	0.487	-
1.850	0.012	0.206	0.273	0.356	0.540
1.860	0.000	0.123	0.178	0.247	0.406
1.870	0.010	0.062	0.104	0.159	0.293
1.880	0.041	0.022	0.050	0.091	0.200
1.890	0.091	0.002	0.016	0.043	0.126
1.900	0.160	0.000	0.000 (1.904 Å)	0.013	0.069
1.910	0.248	0.016	0.002	0.000	0.030
1.920	0.352	0.050	0.020	0.004	0.007
1.930	0.473	0.099	0.054	0.024	0.000 (1.930 Å)
1.940	0.610	0.165	0.104	0.060	0.008
1.950	0.761	0.245	0.168	0.110	0.029
1.960	0.927	0.340	0.246	0.174	0.065
1.970	1.107	0.448	0.337	0.252	0.113
1.980	1.300	0.570	0.441	0.342	0.174
1.990	1.504	0.704	0.557	0.445	0.246
2.000	1.721	0.851	0.684	0.559	0.330

Table 18. PES scan (kcal/mol) for the S–N bond in MeSNO cis-trans isomerization TS

r(S–N), Å	CCSD	DCSD	CCSD(T)	CCSDT	CCSDT(Q)
1.900	0.848	1.725	-	-	-
1.910	0.673	1.482	-	-	-
1.920	0.521	1.261	-	-	-
1.930	0.390	1.060	-	-	-
1.940	0.279	0.880	-	-	-
1.950	0.188	0.718	1.003	-	-
1.960	0.116	0.575	0.837	-	-
1.970	0.062	0.449	0.688	-	-
1.980	0.025	0.340	0.555	-	-
1.990	0.004	0.247	0.438	-	-
2.000	0.000	0.170	0.336	0.389	0.553
2.010	0.011	0.108	0.249	0.296	0.442
2.020	0.037	0.061	0.175	0.216	0.345
2.030	0.077	0.027	0.115	0.150	0.262
2.040	0.130	0.007	0.068	0.096	0.190
2.050	0.197	0.000	0.034	0.055	0.131
2.060	0.276	0.005	0.011	0.025	0.083
2.070	0.368	0.022	0.000	0.007	0.047
2.080	0.471	0.051	0.000 (2.075 Å)	0.000	0.021
2.090	0.586	0.091	0.011	0.003	0.006
2.100	0.711	0.142	0.031	0.016	0.000 (2.101 Å)
2.110	-	0.203	0.062	0.038	0.004
2.120	-	0.274	0.102	0.070	0.017
2.130	-	0.354	0.151	0.111	0.039
2.140	-	0.443	0.209	0.160	0.069
2.150	-	0.541	0.275	0.217	0.107
2.160	-	0.648	0.349	0.283	0.152
2.170	-	0.763	0.431	0.355	0.205
2.180	-	0.885	0.519	0.435	0.265
2.190	-	1.015	0.615	0.521	0.332
2.200	-	1.152	0.717	0.614	0.405

Graphical representation of the calculated one-dimensional S– N bond PES is shown on Figures 9-11. As mentioned above, the increase in number of excitations in coupled cluster theory, as well as the quality of treatment of those excitations, leads to elongation of the S–N bond. The most significant change in the bond length occurs after changing to DCSD from CCSD method, or switching from CCSD to CCSD(T). Further systematic increase in excitations level leads to slower changes in the bond lengths, which is similar to the convergence behavior with the increasing basis set size within those methods.

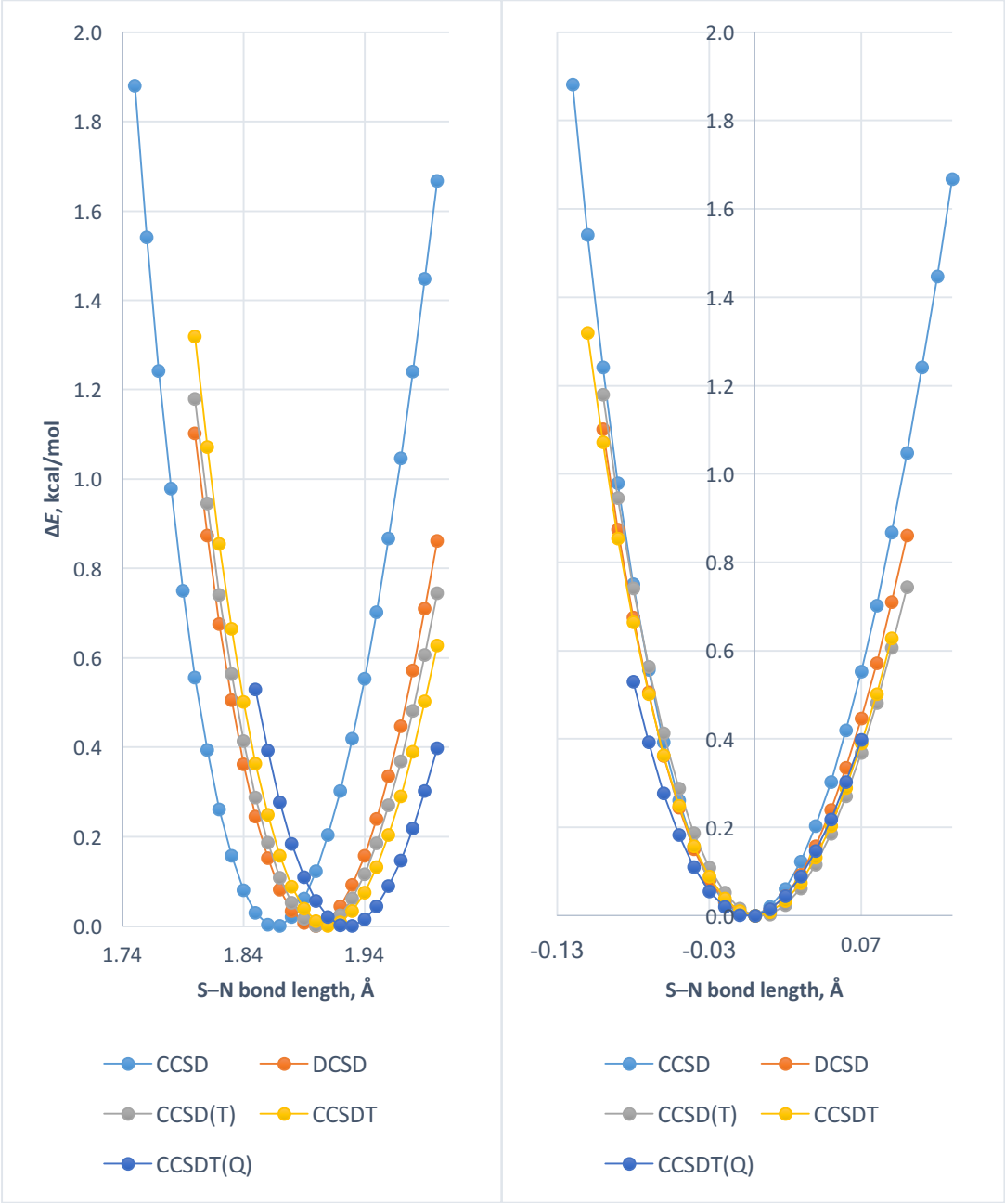

Figure 9. Cis-MeSNO ab initio S–N bond PES, non-normalized (A) and normalized (B), with cc-pV(D+d) basis set.

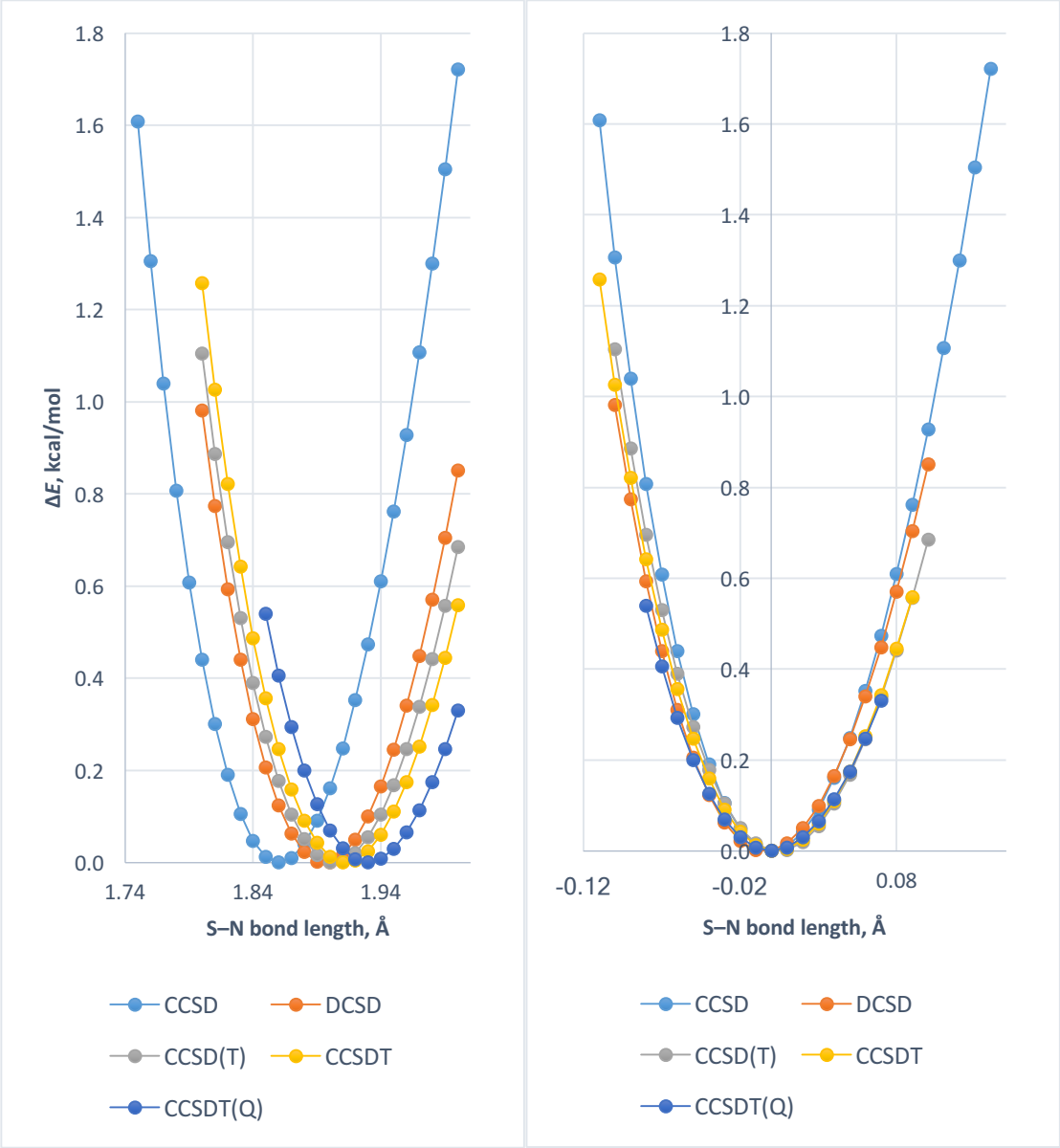

Figure 10. Trans-MeSNO ab initio S–N bond PES, non-normalized (A) and normalized (B), with cc-pV(D+d) basis set.

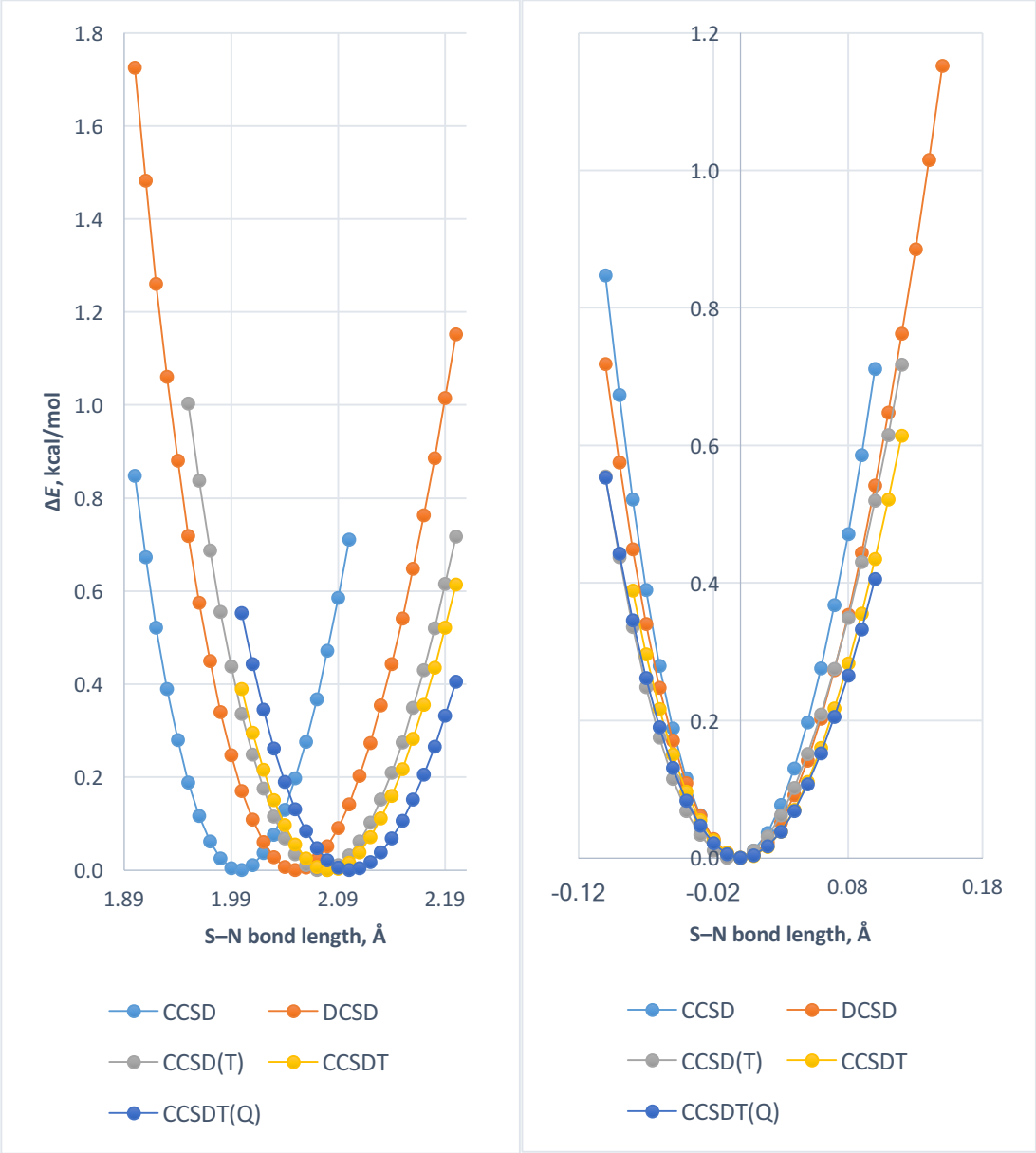

Figure 11. MeSNO cis-trans isomerizaiton TS ab initio S–N bond PES, non-normalized (A) and normalized (B), with cc-pV(D+d) basis set.

To evaluate the influence of the post-CCSD(T)-F12a/CBS corrections in the FPD scheme on the S–N bond PES, we separately investigated the (Q), ΔCV and ΔSR effects. We performed a series of single-point energy calculations along the S–N bond of cis-MeSNO, the results are presented in Table 19 and Figure 12.

Table 19. Ab Initio PES scan (kcal/mol) for the S–N bond in cis-MeSNO

r(S–N), Å	Δ*E*, CCSD(T)-F12a/CBS(T-Q)	Δ*E*, CCSD(T)-F12a/CBS(T-Q)+Δ(Q)	Δ*E*, CCSD(T)-F12a/CBS(T-Q)+ΔCV	Δ*E*, CCSD(T)-F12a/CBS(T-Q)+ΔSR
1.700	1.379	1.705	1.200	1.445
1.710	1.077	1.374	0.921	1.136
1.720	0.818	1.084	0.683	0.870
1.730	0.598	0.834	0.485	0.644
1.740	0.416	0.621	0.323	0.455
1.750	0.270	0.442	0.196	0.302
1.760	0.157	0.297	0.102	0.182
1.770	0.075	0.182	0.039	0.093
1.780	0.024	0.097	0.006	0.034
1.790	0.000	0.039	0.000	0.004
1.800	0.003	0.007	0.020	0.000
1.810	0.031	0.000	0.065	0.021
1.820	0.083	0.016	0.133	0.066
1.830	0.157	0.053	0.222	0.132
1.840	0.252	0.112	0.332	0.220
1.850	0.367	0.189	0.462	0.328
1.860	0.500	0.285	0.610	0.455
1.870	0.652	0.398	0.775	0.599
1.880	0.820	0.527	0.957	0.760
1.890	1.003	0.672	1.154	0.936
1.900	1.202	0.831	1.366	1.128

The position of the S–N bond length minima in cis-MeSNO is found to be relatively more sensitive to the Δ(Q) corrections, comparing to ΔCV and ΔSR. Therefore, an ideal FPD scheme, tailored to predict the most accurate structures of RSNOs, should account for excitations beyond triple in the coupled cluster theory.

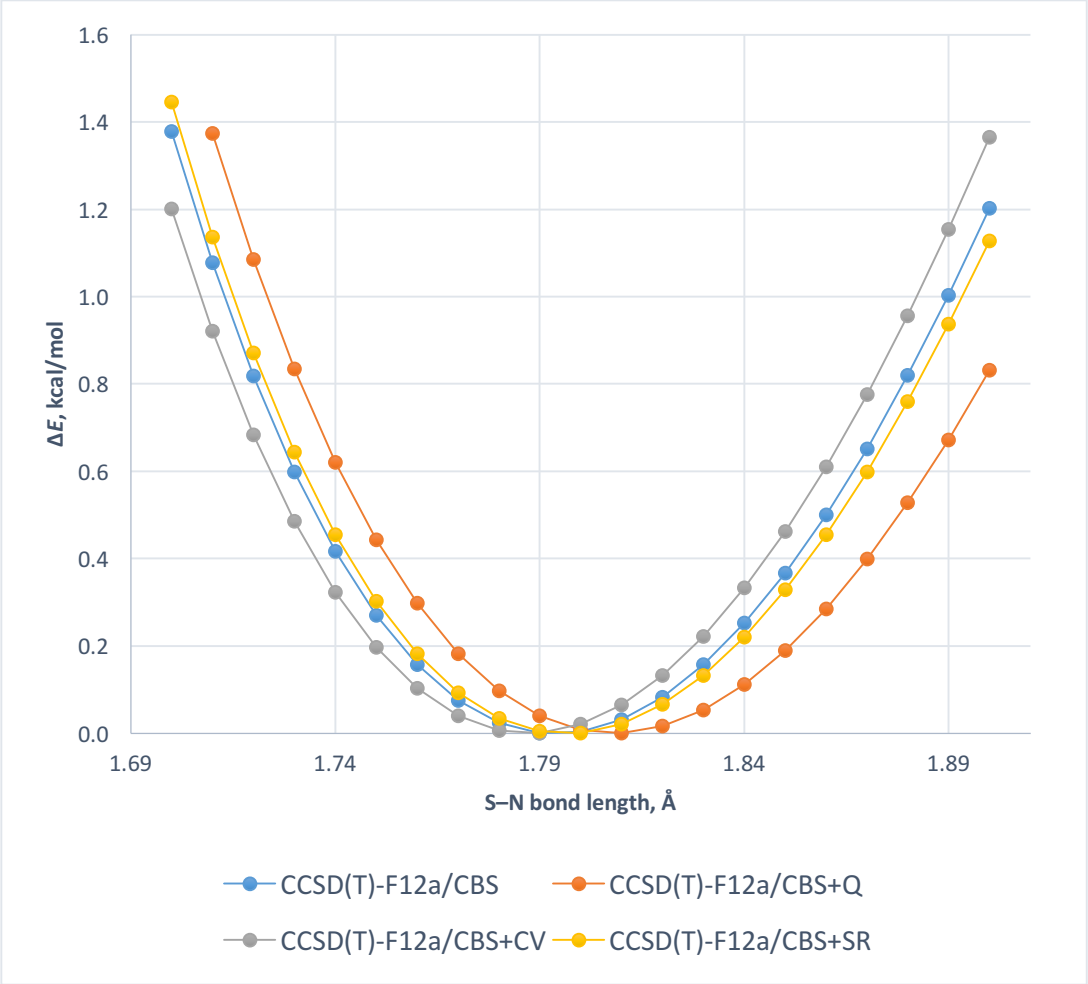

Figure 12. Ab Initio PES scan (kcal/mol) for the S–N bond in cis-MeSNO

Overlapping the positions of the minima in Figures 9-11 allowed us to evaluate the shape of S–N bond PES, and reproducibility of the results, obtained with the coupled cluster methods of increasing level of complexity. As the result, we observe no significant change in the shape of the PES at different levels of theory. This leads us to the conclusion, that harmonic S–N bond character prevails, and the anharmonic corrections can be omitted at the first approximation for the corresponding ZPE calculations.

This is an important conclusion, because the remarkably low S–N bond vibrational frequency in RSNOs leads to unusually high contribution of ΔZPE in computed reaction barriers and reaction energies when this bond is converted into other, more typical covalent bonds (~2.5 kcal/mol).[49] Therefore, a higher anharmonicity of the S–N bond could create a significant problem for accurate RSNO reaction energies. Our results suggest that the harmonic approximation is sufficient in this case.

7. Benchmarking of DFT methods

To assist further evaluations of the accuracy of more approximate methods (DFT, in the present work) we applied a variation of the FPD approach to generate a set of reference data on MeSNO structure and properties. The main difference from the described above FPD schemes is the omission of ΔSR and ΔSO effects, which are not implemented in DFT methods, available in Gaussian 09. Inclusion of the ΔSR and ΔSO corrections to the reference data can lead to false results in evaluation of the performance of DFT methods. Tables 20-22 contain the FPD reference data, and corresponding results of DFT calculations with larger and more accurate def2-TZVPPD basis set, and smaller and more computationally efficient def2-SV(P)+d.

In cis-MeSNO and trans-MeSNO, the most accurate S–N bond lengths (def2-TZVPPD basis set) were obtained with double-hybrid B2PLYP and B2PLYPD methods. For example, the S–N bond length in cis-MeSNO, calculated with the FPD approach, and B2PLYP/def2-TZVPPD method, differs only by 0.001 Å (1.810 Å with the FPD, 1.811 Å with B2PLYP). In the isomerization TS, MPW2PLYP and MPW2PLYPD double hybrids perform among the best: 1.949 Å S–N bond length with the FPD, 1.960 Å with MPW2PLYP and 1.960 Å with MPW2PLYPD.

In reproducing S–N BDE, PBE0 and PBE0-GD3 methods demonstrate an excellent performance (32.7 kcal/mol reference value, 31.8 kcal/mol obtained with PBE0/def2-TZVPPD), while double-hybrid DFT methods tend to underestimate the BDE value (by 2.8 kcal/mol in the best case of B2PLYPD/def2-TZVPPD combination).

Table 20. Cis-MeSNO, ab initio and DFT properties

Method	r(S–N), Å	r(N–O), Å	r(C–S), Å	∠SNO, °	D_0(S–N), kcal/mol
CBS(T-Q)+ΔQ+ΔCV+ΔZPE	1.810	1.189	1.787	117.51	32.67
DFT methods with def2-TZVPPD basis set					
B3LYP	1.816	1.182	1.800	117.83	28.92
PBE0	1.779	1.179	1.782	117.91	31.83
PBE0-GD3	1.779	1.179	1.783	117.98	32.54
PBE0-1/3	1.760	1.176	1.778	118.14	28.86
ωB97XD	1.767	1.181	1.789	118.12	28.94
B2PLYP	1.811	1.190	1.794	117.61	29.21
B2PLYPD	1.812	1.190	1.796	117.72	29.92
MPW2PLYP	1.794	1.188	1.792	117.79	28.32
MPW2PLYPD	1.795	1.188	1.794	117.87	28.83
DFT methods with def2-SV(P)+d basis set					
B3LYP	1.830	1.181	1.797	117.68	29.64
PBE0	1.795	1.177	1.780	117.85	31.58
PBE0-GD3	1.794	1.177	1.782	117.92	32.27
PBE0-1/3	1.769	1.174	1.778	118.17	28.28
ωB97XD	1.774	1.181	1.788	118.06	28.92
B2PLYP	1.825	1.187	1.792	117.62	26.86
B2PLYPD	1.826	1.187	1.794	117.72	27.57
MPW2PLYP	1.807	1.185	1.790	117.82	26.16
MPW2PLYPD	1.807	1.185	1.792	117.89	26.67

In the case of the relative energy of cis-MeSNO and trans-MeSNO, PBE0 and double-hybrids B2PLYP and MPW2PLYP perform among the best with a larger def2-TZVPPD basis set, but all DFT methods tend to overestimate the relative stability of cis-MeSNO with a smaller def2-SV(P)+d basis set. Isomerization barrier height in the MeSNO molecule is better reproduced with the double-hybrids MPW2PLYP and MPW2PLYPD.

Table 21. Trans-MeSNO, ab initio and DFT properties

Method	r(S–N), Å	r(N–O), Å	r(C–S), Å	∠SNO, °	$\Delta E_{(\text{cis-trans})}$, kcal/mol
CBS(T-Q)+ΔQ+ΔCV+ΔZPE	1.820	1.186	1.793	115.62	1.13
DFT methods with def2-TZVPPD basis set					
B3LYP	1.827	1.177	1.805	116.50	0.82
PBE0	1.790	1.175	1.788	116.45	1.10
PBE0-GD3	1.791	1.175	1.789	116.45	1.34
PBE0-1/3	1.772	1.172	1.784	116.23	1.06
ωB97XD	1.779	1.177	1.793	115.84	1.05
B2PLYP	1.819	1.186	1.800	116.50	1.10
B2PLYPD	1.821	1.186	1.802	116.46	1.35
MPW2PLYP	1.803	1.183	1.798	116.31	1.11
MPW2PLYPD	1.804	1.183	1.799	116.29	1.29
DFT methods with def2-SV(P)+d basis set					
B3LYP	1.847	1.175	1.802	116.83	1.35
PBE0	1.813	1.171	1.786	116.85	1.59
PBE0-GD3	1.814	1.171	1.787	116.84	1.82
PBE0-1/3	1.790	1.169	1.783	116.59	1.55
ωB97XD	1.791	1.176	1.792	116.11	1.54
B2PLYP	1.842	1.181	1.798	116.94	1.50
B2PLYPD	1.843	1.181	1.800	116.91	1.74
MPW2PLYP	1.823	1.179	1.795	116.72	1.55
MPW2PLYPD	1.824	1.179	1.797	116.70	1.73

Table 22. MeSNO cis-trans isomerization TS, ab initio and DFT properties

Method	*r*(S–N), Å	*r*(N–O), Å	*r*(C–S), Å	∠SNO, °	∠CSNO, °	Δ*E*≠, kcal/mol
CCSD(T)-F112a/CBS(T-Q)+ΔQ+ΔCV+ΔZPE	1.949	1.166	1.805	113.09	85.42	12.71
DFT methods with def2-TZVPPD basis set						
B3LYP	1.987	1.155	1.818	113.84	85.39	13.70
PBE0	1.939	1.154	1.800	113.71	85.08	14.62
PBE0-GD3	1.939	1.153	1.801	113.72	85.28	14.66
PBE0-1/3	1.912	1.152	1.795	113.67	85.00	14.22
ωB97XD	1.924	1.157	1.805	113.51	85.70	13.35
B2PLYP	1.984	1.163	1.814	113.63	85.04	13.65
B2PLYPD	1.985	1.162	1.816	113.65	85.34	13.71
MPW2PLYP	1.960	1.161	1.811	113.62	85.06	13.56
MPW2PLYPD	1.961	1.161	1.812	113.62	85.30	13.60
DFT methods with def2-SV(P)+d basis set						
B3LYP	2.009	1.157	1.815	113.57	86.14	14.42
PBE0	1.966	1.153	1.799	113.49	85.77	15.16
PBE0-GD3	1.966	1.153	1.799	113.51	86.01	15.19
PBE0-1/3	1.936	1.151	1.794	113.48	85.74	14.72
ωB97XD	1.942	1.158	1.803	113.30	86.55	14.02
B2PLYP	2.009	1.162	1.810	113.46	85.92	13.99
B2PLYPD	2.010	1.162	1.812	113.49	86.22	14.04
MPW2PLYP	1.984	1.161	1.807	113.43	86.00	13.96
MPW2PLYPD	1.985	1.161	1.808	113.44	86.24	13.99

An accurate one-dimensional S–N bond PES was generated with the use of FPD approach, to test the performance of selected DFT methods (Figures 13-16). The FPD scheme included CCSD(T)-F12a/CBS energies, augmented with the Δ(Q) an ΔCV corrections. In all cases, the best performing methods are MPW2PLYP and MPW2PLYPD, with a larger def2-TZVPPD basis set and a smaller def2-SV(P)+d basis

set. The worst performing DFT method is PBE0-1/3, which systematically underestimates the S–N bond lengths.

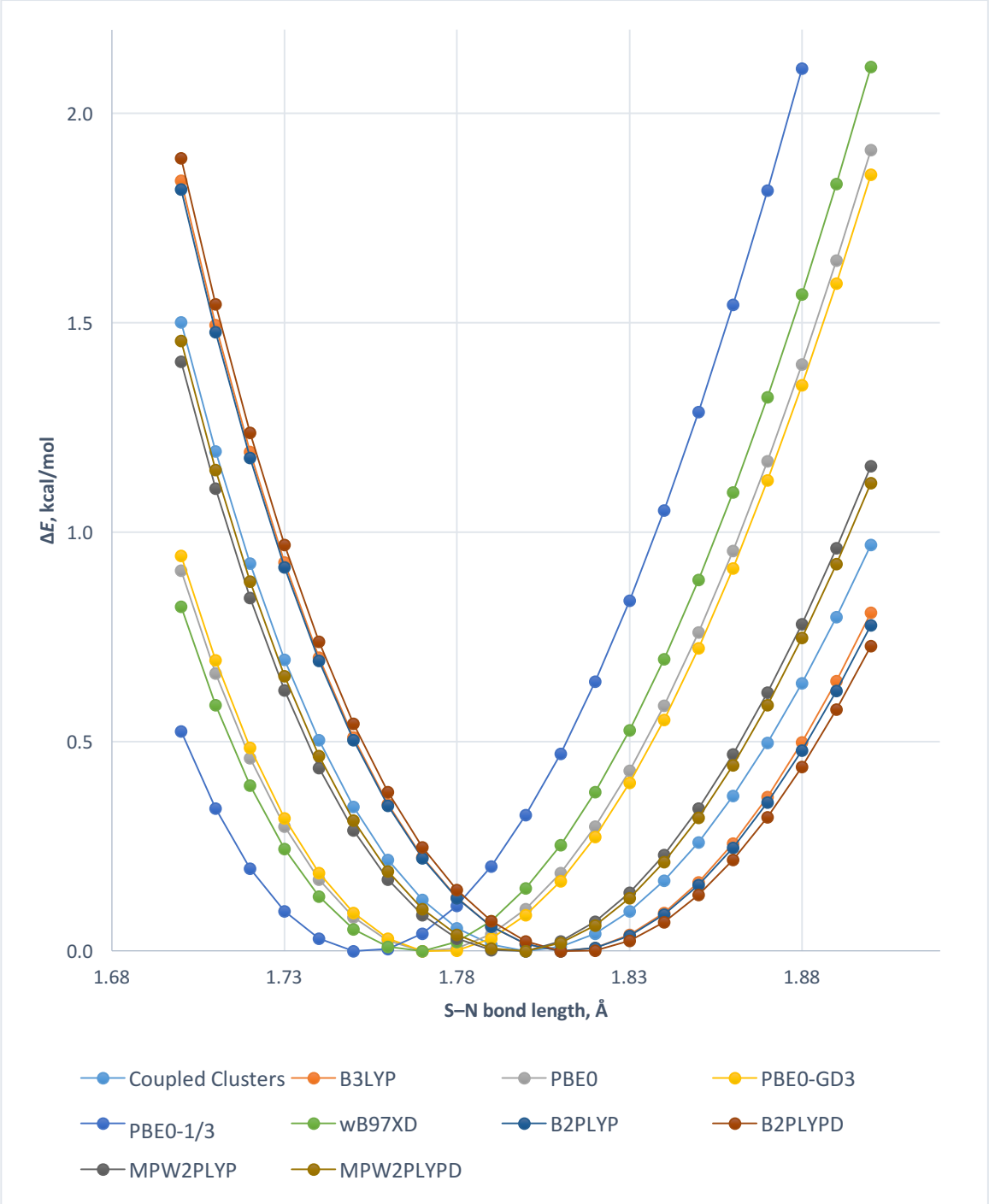

Figure 13. S–N bond energy profile (non-normalized) in cis-MeSNO, calculated with FPD protocol (Coupled Clusters) and DFT methods (using def2-TZVPPD basis set)

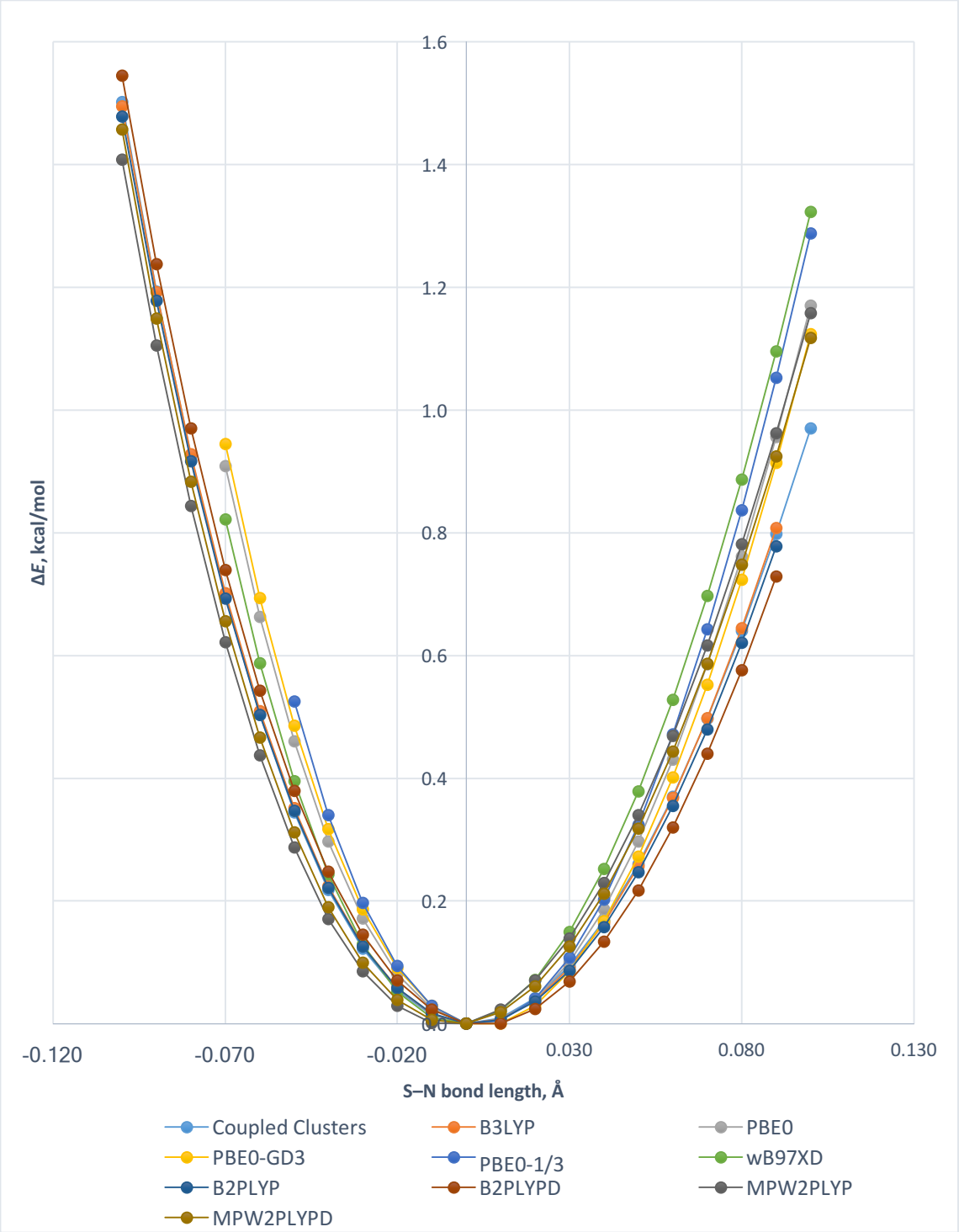

Figure 14. S–N bond energy profile (normalized) in cis-MeSNO, calculated withFPD protocol (Coupled Clusters) protocol and DFT methods (using def2-TZVPPD basis set)

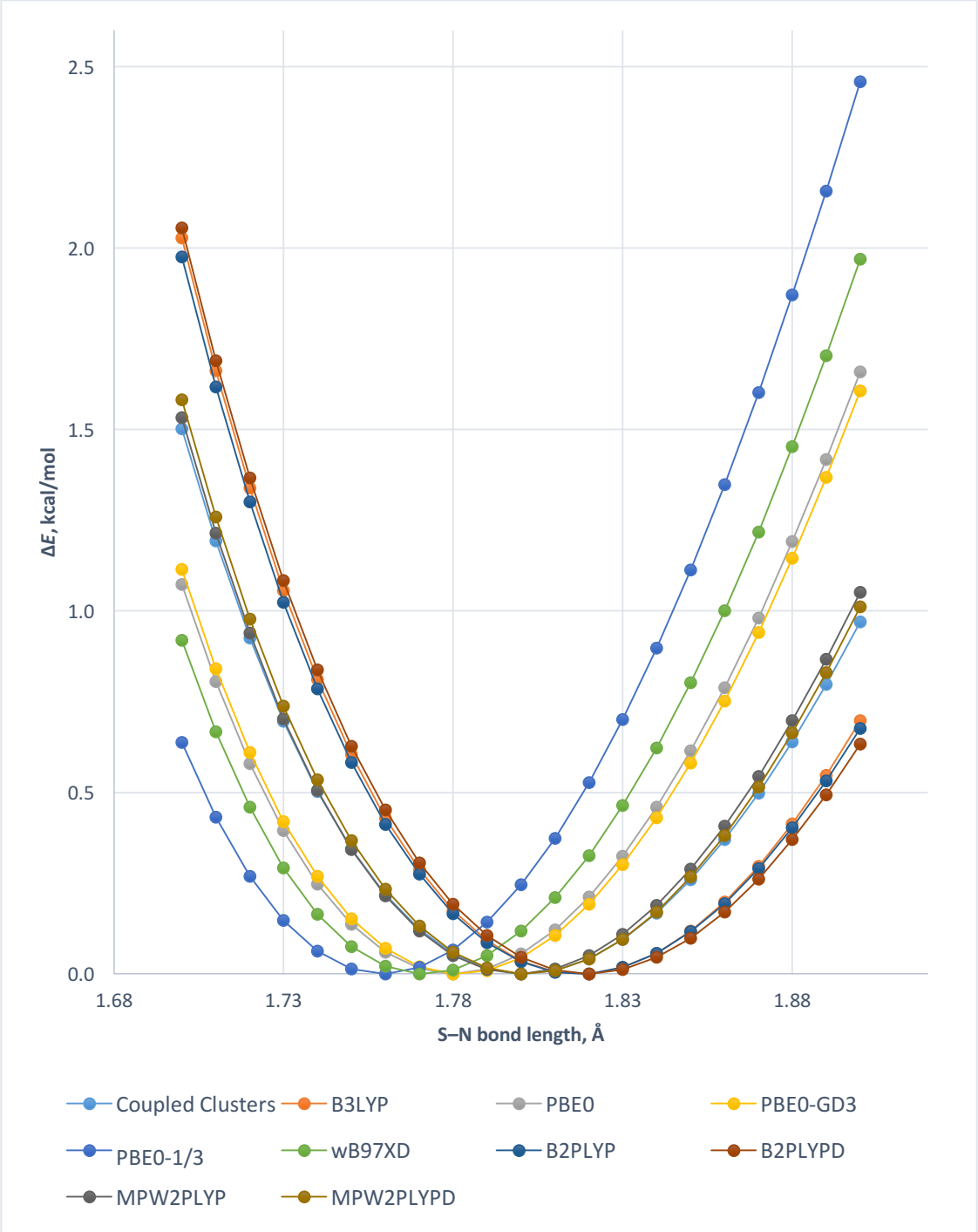

Figure 15. S–N bond energy profile (non-normalized) in cis-MeSNO, calculated with FPD protocol (Coupled Clusters) and DFT methods (using def2-SV(P)+d basis set)

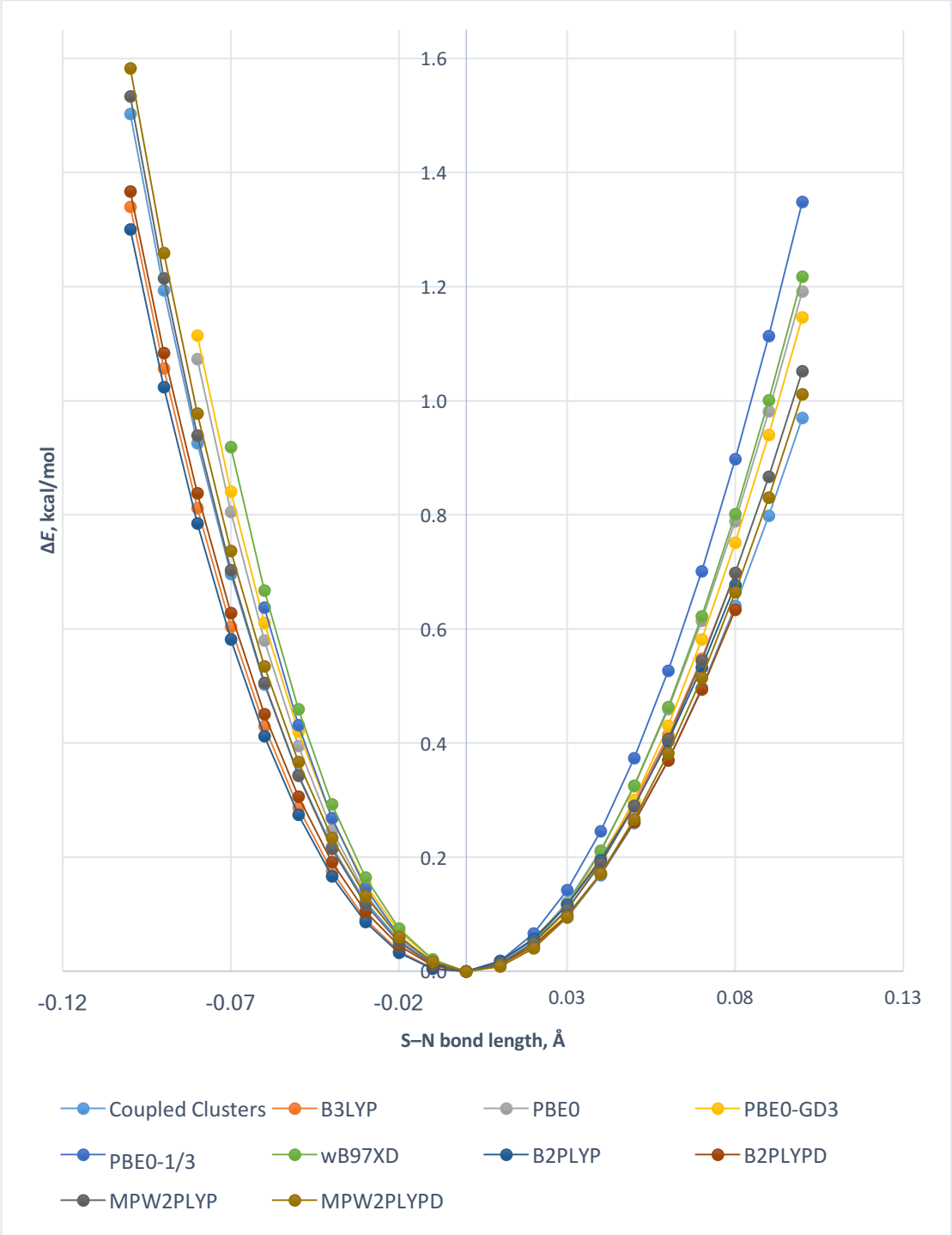

Figure 16. S–N bond energy profile (non-normalized) in cis-MeSNO, calculated with FPD protocol (Coupled Clusters) and DFT methods (using def2-SV(P)+d basis set)

The important harmonic vibrational modes of cis-MeSNO and trans-MeSNO (Tables 23-26) are, on average, better reproduced with the double-hybrid DFT

methods (B2PLYPD and MPW2PLYPD). For example, the closest to the FPD reference harmonic S–N vibration frequency in cis-MeSNO (399.7 cm^{-1}) is calculated with the MPW2PLYPD/def2-TZVPPD approach (388.4 cm^{-1}). The corresponding N–O vibration is also in excellent agreement with the reference: 1571.1 cm^{-1} with the FPD, 1578.3 cm^{-1} with the MPW2PLYPD/def2-TZVPPD. We do not recommend using a smaller basis set, def2-SV(P)+d, for the accurate calculations: with all DFT methods, the N–O vibrational frequency is significantly overestimated: in the worst case, a frequency of 1756.3 cm^{-1} was calculateed with the PBE0-GD3/def2-SV(P)+d combination vs. 1575.1 cm^{-1} calculated with FPD.

Table 23. Cis-MeSNO harmonic vibrational frequencies (with def2-TZVPPD basis set)

Mode	B3LYP	PBE0-GD3	ωB97XD	B2PLYPD	MPW2PLYPD	CCSD(T)-F12a/CBS (T-Q)
1 A"	105.4	105.7	77.7	103.7	101.6	84.6
2 A'	252.5	264.6	256.4	261.3	266.3	280.1
3 A"	298.4	311.1	303.4	301.3	303.1	291.0
4 A' (S–N)	376.6	424.1	444.4	370.1	388.4	399.7
5 A'	658.0	677.1	673.8	662.8	666.8	662.4
6 A'	728.9	759.9	757.3	738.6	744.8	754.3
7 A'	959.3	953.2	960.2	963.0	969.9	962.5
8 A"	962.5	958.2	971.6	967.4	974.9	970.8
9 A'	1333.5	1321.9	1337.6	1338.0	1346.5	1334.3
10 A"	1467.8	1456.5	1472.4	1475.2	1484.0	1477.2
11 A'	1472.2	1461.6	1476.7	1479.1	1488.2	1480.8
12 A' (N–O)	1627.0	1666.5	1662.8	1553.7	1578.3	1575.1
13 A'	3023.3	3031.7	3046.1	3023.2	3043.8	3028.4
14 A'	3109.7	3129.6	3142.0	3123.9	3141.4	3127.3
15 A"	3140.3	3164.7	3175.4	3161.2	3176.4	3157.2
ZPE, kcal/mol	27.9	28.1	28.2	27.9	28.1	28.0

Table 24. Cis-MeSNO harmonic vibrational frequencies (with def2-SV(P)+d basis set)

Mode	B3LYP	PBE0-GD3	ωB97XD	B2PLYPD	MPW2PLYPD	CCSD(T)-F12a/CBS (T-Q)
1 A"	147.2	145.7	117.8	142.5	136.4	84.6
2 A'	268.7	279.9	284.5	276.9	282.6	280.1
3 A"	303.5	316.0	310.2	304.7	307.2	291.0
4 A' (S–N)	369.3	408.9	440.1	359.2	380.9	399.7
5 A'	671.8	689.9	688.0	677.9	682.2	662.4
6 A'	740.9	768.6	769.1	751.4	757.8	754.3
7 A'	966.2	967.5	977.7	978.3	984.5	962.5
8 A"	969.5	970.1	977.8	982.4	988.3	970.8
9 A'	1332.3	1331.9	1346.3	1353.2	1360.0	1334.3
10 A"	1456.7	1456.3	1467.3	1473.8	1482.1	1477.2
11 A'	1457.7	1456.4	1468.5	1475.0	1483.2	1480.8
12 A' (N–O)	1714.5	1756.3	1745.0	1653.8	1674.9	1575.1
13 A'	2996.6	3011.3	3024.0	3005.2	3028.5	3028.4
14 A'	3097.6	3125.5	3136.4	3118.2	3138.9	3127.3
15 A"	3132.7	3166.4	3172.5	3158.6	3176.9	3157.2
ZPE, kcal/mol	28.1	28.4	28.5	28.2	28.4	28.0

Table 25. Trans-MeSNO harmonic vibrational frequencies (with def2-TZVPPD basis set)

Mode	B3LYP	PBE0-GD3	ωB97XD	B2PLYPD	MPW2PLYPD	CCSD(T)-F12a/CBS (T-Q)
1 A"	130.0	131.4	117.3	131.3	129.5	119.5
2 A'	229.6	237.8	235.9	229.6	235.0	227.5
3 A"	236.1	242.4	241.3	239.3	239.0	235.6
4 A' (S–N)	372.5	409.5	424.0	368.0	384.5	394.2
5 A'	662.2	683.6	687.2	664.9	671.5	669.6
6 A'	726.8	758.8	757.0	735.3	742.2	751.8
7 A'	965.5	959.5	970.6	974.3	980.3	1011.0
8 A"	986.7	984.3	996.2	992.9	1000.2	953.5
9 A'	1349.3	1339.0	1358.7	1358.5	1366.3	1352.6
10 A"	1460.4	1449.4	1465.3	1468.0	1476.5	1468.3
11 A'	1485.0	1475.3	1490.5	1493.5	1502.2	1494.5
12 A' (N–O)	1657.0	1698.3	1688.5	1582.3	1604.3	1593.5
13 A'	3039.2	3051.0	3061.4	3044.2	3063.0	3046.2
14 A'	3123.3	3145.2	3154.8	3139.5	3157.1	3142.3
15 A"	3140.4	3164.5	3172.4	3160.8	3176.9	3150.6
ZPE, kcal/mol	28.0	28.2	28.3	28.0	28.2	28.0

Table 26. Trans-MeSNO harmonic vibrational frequencies (with def2-SV(P)+d basis set)

Mode	B3LYP	PBE0-GD3	ωB97XD	B2PLYPD	MPW2PLYPD	CCSD(T)-F12a/CBS (T-Q)
1 A"	146.9	148.6	135.1	146.5	143.7	119.5
2 A'	235.9	244.0	245.4	235.0	240.6	227.5
3 A"	247.8	254.5	248.6	251.3	250.3	235.6
4 A' (S–N)	369.8	400.7	422.8	362.4	379.9	394.2
5 A'	669.8	688.0	692.8	673.3	680.0	669.6
6 A'	739.4	768.3	769.3	750.0	757.8	751.8
7 A'	971.0	970.5	979.9	986.8	992.5	1011.0
8 A"	988.0	991.4	1001.1	1001.2	1007.6	953.5
9 A'	1344.1	1343.7	1359.8	1367.2	1374.0	1352.6
10 A"	1446.8	1445.8	1457.6	1463.7	1471.7	1468.3
11 A'	1468.7	1469.8	1481.4	1487.2	1495.5	1494.5
12 A' (N–O)	1755.8	1797.6	1779.3	1695.8	1714.4	1593.5
13 A'	3015.9	3034.3	3041.1	3027.0	3047.9	3046.2
14 A'	3114.1	3143.6	3152.4	3135.7	3155.7	3142.3
15 A"	3131.6	3165.0	3170.2	3157.0	3175.4	3150.6
ZPE, kcal/mol	28.1	28.4	28.5	28.2	28.4	28.0

D. Conclusions

In this work, we for the first time applied highly accurate *ab initio* FPD protocol to investigate structure and properties of the MeSNO molecule. As the result, we gathered a set of the accurate properties of cis-MeSNO, trans-MeSNO and the cis-trans isomerization TS. This set includes geometric parameters (Figure 6), vibrational frequencies (Tables 12-14), relative energies of the cis- and trans-conformers (cis-MeSNO is more stable than trans-MeSNO by 1.15 kcal/mol in the gas phase, and by 1.13 kcal/mol in solution), S–N bond dissociation energy (32.4 kcal/mol in gas phase, 32.2 kcal/mol in solution), as well as the activation barrier of cis-trans isomerization (12.65 kcal/mol in the gas phase, 13.22 kcal/mol in water, 12.53 kcal/mol in diethylether). We also for the first time assessed the anharmonicity of the S–N bond stretching vibration in MeSNO molecule: our results suggest that despite having unusually low stretching frequency (FPD value 398.2 cm^{-1} in cis-MeSNO, and 386.1 cm^{-1} in trans-MeSNO) this bond has a small anharmonic character.

This dataset was used to benchmark the performance of DFT methods, and identify the most reliable ones to study the larger RSNOs, i.e. MPW2PLYP and MPW2PLYPD double hybrids for calculation of the geometric properties, vibrational frequencies and isomerization barriers, and PBE0 / PBE0-GD3 for the S–N BDEs.

Chapter III: Proximal Charged Residues Regulate the Conformational Dynamics of S-Nitrosated Cysteine Residues in Proteins

A. Introduction

The biological importance of S-nitrosothiols (RSNOs), relatively unstable derivatives of thiols (RSH), have attracted significant attention in recent years.[19,64,65,123] Although the ubiquity of regulated biological RSNO reactions is now well established, the atomic-level mechanisms governing those processes are yet to be fully understood. Experimental study of S-nitrosothiols is limited due to their thermal instability[36] and only a handful of experimentally derived structural data points is available.[67]

S-Nitrosated cysteine residues in peptides and proteins act as storage pool of nitric oxide NO, a major gasotrasmitter (gaseous signaling molecule *in vivo*), and the regulated S-nitrosation/denitrosation of specific cysteine residues in proteins is involved in a multitude of key biological processes across all branches of the tree of life[1,124], from immune response in plants to neurotransmission in humans. Moreover, the smallest RSNO—thionitrous acid HSNO—has been recently proposed to be a short-lived endogenous biological species involved in signaling processes.[125-127]

In the X-Ray structures, small-molecule RSNOs tend to adopt a planar conformation, with either cis- or trans-orientation along the S–N bond.[109-111,116,128-132] This phenomenon was previously rationalized,[67] involving a resonance description of the -SNO group. Thus, one of the key resonance structures (***D***) in

RSNOs possesses a double bond between S and N atoms, therefore, suppressing free rotation around the S–N bond (Figure 17):

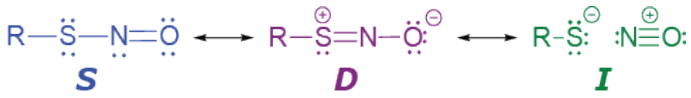

Figure 17. Resonance description of the SNO group.

On the contrary, analysis of few in number crystallographic structures of S-nitrosated proteins (Table 27) reveals multiple entries with non-planar CSNO dihedral angles in corresponding CysNO residues.

Table 27. Structural parameters of S-nitrosated Cys residues in proteins, according to X-Ray crystallographic studies.

PDB code, protein name	X-ray resolution, Å	CysNO residue	S–N bond length, Å	CSNO dihedral angle, °	Reference
1BUW, human hemoglobin	1.90	Chain B, 93	1.717	87.5	[133]
		Chain D, 93	1.762	75.6	
2CI1, dimethylarginine dimethylamino-hydrolase	1.08	83	1.646	69.5	[134]
2IIY, human thioredoxin	1.70	62	1.759	1.3	[135]
		69	1.803	0.7	
2IFQ, human thioredoxin	1.20	Chain A, 67	1.783	1.2	
		Chain C, 67	1.797	151.9	
2HXK, human thioredoxin	1.65	Chain A, 62 (1)	1.806	0.4	
		Chain A, 62 (2)	1.803	1.8	
		Chain A, 69	1.805	0.5	
		Chain B, 62	1.806	0.6	
		Chain B, 69	1.840	2.5	
		Chain C, 62	1.802	4.7	
		Chain C, 69 (1)	1.806	179.1	

		Chain C, 69 (2)	1.809	3.3	
2NRM, blackfin tuna myoglobin	1.09	10	1.799	3.1	[136]
3EU0, protein-tyrosine phosphatase 1B	2.70	215	1.665	41.1	[137]
2Y34, prolyl hydroxylase domain-containing enzyme (PHD) isoform 2 (EGLN1)	2.01	302	1.630	93.5	[138]
2Y33	2.00	302	1.788	76.1	[138]
3V4N, Entero-coccus faecalis hydroxymethyl-glutaryl-CoA synthase	1.60	Chain A, 111	1.632	145.4	[139]
		Chain B, 111	1.636	151.1	
		Chain C, 111	1.631	4.9	
		Chain D, 111	1.628	42.9	
4F0M, RuBisCO	2.25	181	1.662	111.2	[140]
		460	1.655	75.7	
4F0K, RuBisCO	2.05	181	1.661	150.0	
		460	1.656	91.0	
4F0H, RuBisCO	1.96	181	1.583	177.8	
		460	1.652	73.5	
4IAH, RuBisCO	2.80	122	1.620	54.8	[141]
4OO5, human thioredoxin	1.54	62	1.746	1.4	Montfort et al.
4L21, Cimex nitrophorin F64V	1.65	60	1.824	0.2	Montfort et al.
4L20, Cimex nitrophorin A21V	1.68	60	1.834	178.0	Montfort et al.
4RKY, protein deglycase DJ-1	1.50	106	1.618	159.8	[33]

In recent theoretical work,[6] it was shown that complex and unique electronic structure of the SNO group, as well as reactivity and properties of RSNOs in general, can be dramatically altered by interaction with Lewis acids, suggesting a wide range

of possibilities for specific/general acid and metal-ion catalytic control of RSNO reactions.[6,7,48,106,112,142] A coordinated Lewis acid changes the balance between the two antagonistic components (***D*** and ***I***) and thus changes RSNO reactivity: S-coordination promotes the ionic component and thus is expected catalyze N-atom directed nucleophilic attack/NO^+ transfer, whereas O- and N-coordination should promote S-atom directed nucleophilic attack.[101,103]

An alternative mechanism of protein influence on the properties of SNO group is via an electric field effect,[143] which can also shift the balance between ***D*** and ***I*** resonance structures and lead to a downstream effect of tunable reactivity.

In current work, we perform a computational study of some of the factors of protein environment on the conformational dynamics of the CysNO residue. Commonly used molecular dynamics (MD) simulations of S-nitrosated proteins rely on the predefined set of parameters (Force Field). Inaccurate description of the S–N bond torsion in CysNO can lead to diminished predictive quality of such calculations.

Due to the large size of a typical protein, computational cost of traditional electronic structure calculations is prohibitively high. Fortunately, the ONIOM family of hybrid quantum mechanics/molecular mechanics methods[144,145] have been proven to be useful tools for the theoretical treatment of large molecular systems where different levels of theory applied to different parts of a molecule. In this model, a large molecule is divided into multiple fragments, allowing a combination of expensive QM and inexpensive classical molecular mechanics (MM) force field methods. For example, Figure 18[146] depicts an example of a 2-layer separation in the

ONIOM model: *Real* system incorporates the whole molecule, and *Model* system only includes a small portion, where the highest precision is needed.

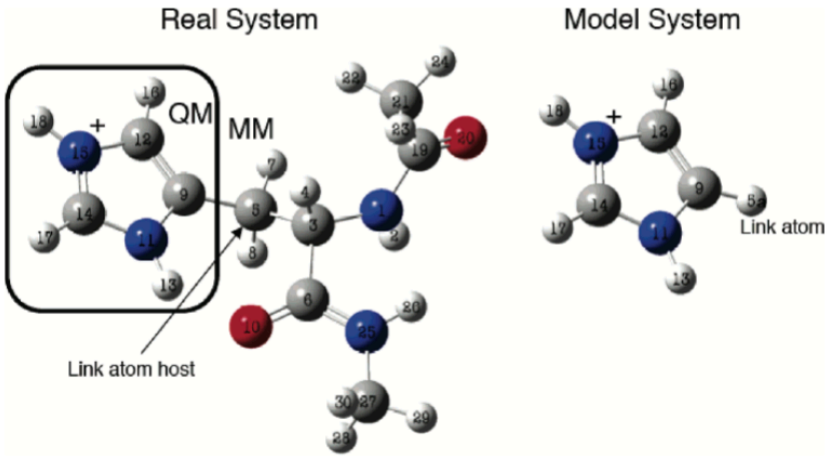

Figure 18. 2-layer ONIOM model[1]

The energy of such system is calculated according to the formula[146]:

$$E^{\mathrm{ONIOM(QM:MM)}} = E^{\mathrm{QM}}_{\mathrm{model}} + E^{\mathrm{MM}}_{\mathrm{real}} - E^{\mathrm{MM}}_{\mathrm{model}}.$$

B. Computational Details

All calculations in this study were performed with the Gaussian 09 package[56]. Hybrid quantum mechanics/molecular mechanics (QM/MM) calculations of α-helix models were performed with the two-layer mechanical embedding ONIOM[144] technique with inclusion of solvation effects (ONIOM-PCM)[147] using diethyl ether (ε = 4.24) solvent parameters to mimic the protein environment.

An artificial 18-residue α-helix model, composed of alanine residues with CysNO at the 11th position, was generated using an in-house code based on the molecular modeling toolkit (MMTK) library[148]. A single charged residue (Lys, Arg,

His, Asp, Glu), or a pair of positively and negatively charged residues were placed at 1, 3, and 4 positions relative to CysNO.

High-level layer of the ONIOM model included charged residue and CysNO atoms (including corresponding side chain atoms) and was treated at Density Functional Theory (DFT) level, with either Perdew–Burke–Ernzerhof hybrid functional[94] (PBE0) or MPW2PLYPD double hybrid functional.[93] Double-and triple-ζ basis sets def2-SV(P) and def2-TZVPPD by Weigend and Ahlrichs[95] with diffuse functions by Rappoport and Furche[149] were obtained from the EMSL Basis Set Exchange Database.[82,150] The def2-SV(P) basis set was further augmented by a tight d function at the sulfur atom with ζ = 2.994,69 and the resulting basis set is denoted as def2-SV(P)+d. Low-level layer of the ONIOM model utilized molecular mechanics method with Amber94 force field.[151] Custom force field parameters for the SNO group were adopted from the literature.[6]

All structures (both stationary points and the transition states) in the α-helix model were subjected to fully relaxed optimization with no geometrical constraints, followed by harmonic frequency calculations, using PBE0/def2-SV(P)+d method for the high-level layer of the ONIOM model, followed buy the single-point electronic energy calculations with MPW2PLYPD/def2-TZVPPD formalism for the high-level layer of the ONIOM model. Nature of all stationary points was confirmed by the absence of imaginary frequencies (for the minima), or the presence of one characteristic imaginary frequency (for the transition states).

Simulations of the DJ-1 protein were performed with three-layer ONIOM[144,145] technique. Gaussian 09 input files were generated from the X-ray

strcuture, PDB:4RKY[33] using an in-house code based on the Molecular Modeling Toolkit (MMTK) library[148]. High-level layer of ONIOM included S-nitrosated Cys106 residue atoms and Glu18 atoms (including their side chains) and was treated at PBE0/def2-SV(P)+d level of theory for geometry optimization and harmonic frequency calculations, followed by MPW2PLYPD/def2-TZVPPD single-point calculations of the electronic energy. Medium layer, consisting of atoms in the direct proximity of Cys106 residues, was optimized with Hartree-Fock method[152-154] with STO-3G basis set[155,156] to accommodate for conformational changes of the SNO group. Low-level layer of the ONIOM model included the rest of the protein molecule, and used molecular mechanics method with Amber94 force field[151]. Low-level atoms was kept frozen during geometry optimization.

C. Results and Discussion

1. Charged Residue Control of CysNO cis-trans Isomerization: An Artificial α-Helix Model

It has been demonstrated previously[6] that charged residues can significantly alter the electronic structure of the -SNO group. For instance, Talipov et al. [6] with Natural Resonance Theory (NRT)[157] determined that in free cis-MeSNO, resonance structures ***D*** and ***I*** have 22% and 10% weights at the PBE0/def2-SV(P)+d level of theory, correspondingly (Figure 19). In the same study, they demonstrated that coordination of truncated model of Lysine (Lys) residue at the O atom of the MeSNO molecule causes increase of the resonance weight of structure ***D*** to 39%, and decrease in structure ***I*** to 2%. Similarly, Lys coordination at the N atom of MeSNO leads to 30% resonance weight of structure ***D***, and 4% weight of structure ***I***. Coordination of Lys at S atom decreases the weight of structure ***D*** to 14% and increased contribution of structure ***I*** to 17%.

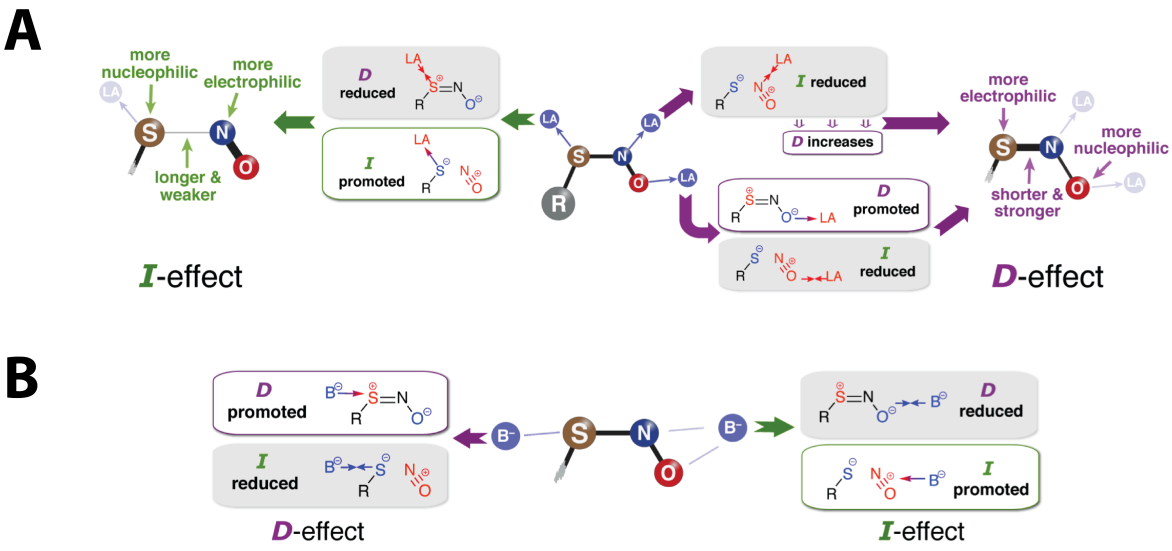

Figure 19. Influence of positively (A) and negatilevy (B) charged aminoacids on the electronnic structure of the -SNO group. Adapted from Ref.[6]

Given that resonance weights of structures ***D*** and ***I*** are expected to correlate the double-bond character of the S–N bond in CysNO, they can also correlate with the cis-trans isomerization barrier height. Therefore, coordination of charged amino acid residues, resulting in change of the resonance weights of structures **D** and ***I*** in the -SNO group, should affect the conformational dynamics of the CysNO in proteins.

Indeed, in the case of truncated residue model, the barrier height for cis-trans isomerization is significantly changed by coordination of a charged residue. Figure 20 shows such example. We used one of the best performing DFT functionals, MPW2PLYPD and PBE0, to calculate the cis-trans isomerization barriers in truncated residues model. Without Lys residue, coordinated at the S atom, isomerization barrier was calculated as 13.2 kcal/mol, but Lys coordination lowered it to 9.6 kcal/mol.

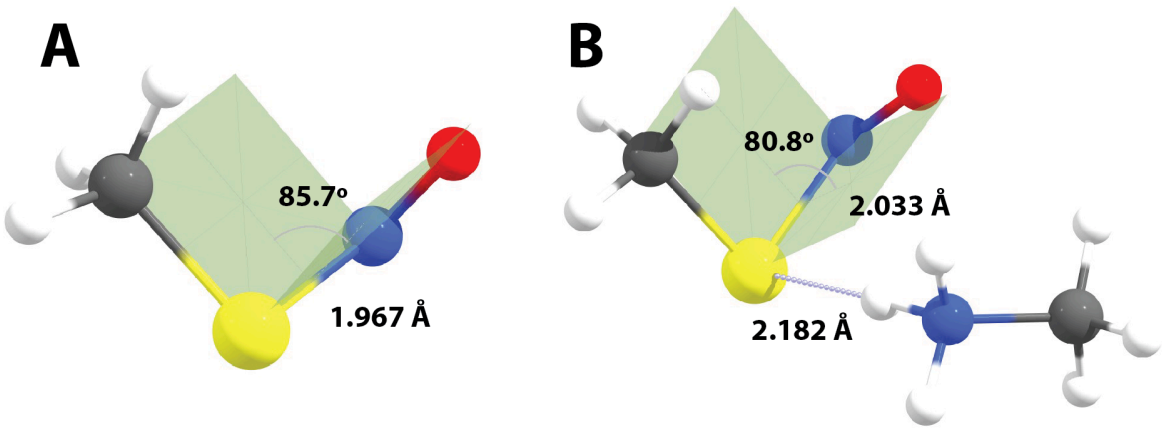

Figure 20. The transition state of cis-trans isomerization in truncated residues model (A - CysNO with no charged residues present, B - truncated Lys is coordinated at the S atom of CysNO), calculated at the MPW2PLYPD/def2-TZVPPD//PBE0/def2-SV(P)+d level

Although truncated models can be useful to understand the influence of charged residues on the barriers of cis-trans isomerizaion in a protein-like environment, in the real proteins the situation is more complex because of the variety of possible coordination modes, imposed by the secondary and tertiary structure of the protein. Therefore, to better assess the influence of spatial constraints on the CysNO conformational dynamics, we used an 18-residue α-helix ONIOM model (Figure 21) of with CysNO at the 11th position (Table 28). The α-helix model allows us to search for the most prominent arrangement of charged residues, which can be searched for in the real or engineered proteins and studied experimentally.

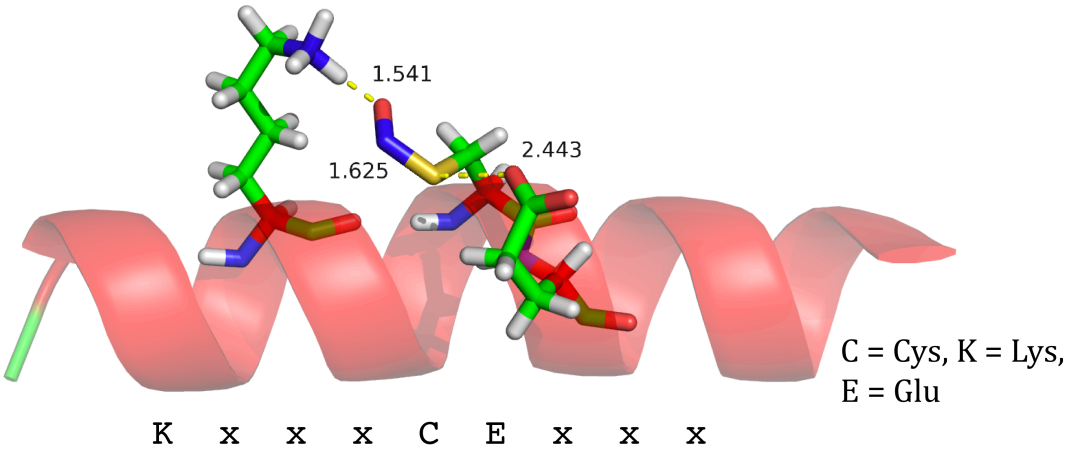

- '**HIGH**' layer (QM): PBE0/def2-SV(P)+d optimization and vibrational frequencies, MPW2PLYPD/def2-TZVPPD single-point energies
- '**LOW**' layer (MM): Amber94 FF
- PCM (Diethyl Ether, ε = 4.24)

Figure 21. 18-residue α-helix ONIOM model with two charged residues, coordinated to the CysNO.

Without charged residues, CysNO embedded in α-helix shows similar properties to the truncated CysNO model[6]: trans-conformation is more stable comparing to cis by 0.87 kcal/mol (compared to 1.2 kcal/mol in the truncated model), and the trans-conformation has a marginally longer S-N bond: 1.823 Å comparing to 1.808 Å in cis-form (1.757 Å and 1.768 Å in truncated model, correspondingly).

Table 28. Sequence code (Ala and CysNO are denoted as 'x' and 'C', respectively), cis and trans-CysNO relative energies, S-N bond lengths in optimized structures, CSNO dihedral angles, activation barriers of cis-trans isomerization reaction.

Structure	r(S-N), Å	ΔH ($\Delta H^{\neq}$), kcal/mol	ΔG ($\Delta G^{\neq}$), kcal/mol	CSNO dihedral angle, °
α-helix cis	1.808	-	-	0.94
α-helix trans	1.823	0.9	0.6	177.59
α-helix TS1	1.990	10.6	11.9	83.59
α-helix TS2	2.008	11.2	12.5	-88.55
KxxxCxxxx cis	1.845	-	-	2.82
KxxxCxxxx trans	1.850	2.0	2.2	179.89
KxxxCxxxx TS1	2.062	9.6	10.2	85.28
KxxxCxxxx TS2	2.054	10.6	10.7	-85.71
xxxKCxxxx cis	1.666	-	-	1.71
xxxKCxxxx trans	1.705	0.8	0.3	179.22
xxxKCxxxx TS1	1.927	15.5	14.7	87.33
xxxKCxxxx TS2	1.901	15.7	16.0	-87.58
xxxRCxxxx cis	1.844	-	-	1.02
xxxRCxxxx trans	1.856	2.2	1.8	175.75
xxxRCxxxx TS1	2.031	9.6	9.8	81.73
xxxRCxxxx TS2	2.052	10.5	10.7	-90.68
xxxxCxxxK cis	1.674	-	-	0.66

xxxxCxxxK trans	1.716	2.4	1.1	178.26
xxxxCxxxK TS1	1.914	19.9	18.4	96.63
xxxxCxxxK TS2	1.896	18.6	17.9	-88.47
ExxxCxxHx cis	1.630	-	-	7.29
ExxxCxxHx trans	1.698	0.5	-0.4	175.93
ExxxCxxHx TS1	1.877	19.5	19.4	86.83
ExxxCxxHx TS2	1.896	18.5	18.6	-87.90
ExxxCxxxK cis	1.627	-	-	2.09
ExxxCxxxK trans	1.702	5.5	6.8	175.92
ExxxCxxxK TS1	1.853	22.0	21.1	85.78
ExxxCxxxK TS2	1.873	18.3	17.5	-90.80
KxxxCExxx cis	1.624	-	-	7.06
KxxxCExxx trans	1.654	3.0	1.6	179.94
KxxxCExxx TS1	1.855	29.9	28.8	87.43
KxxxCExxx TS2	1.876	24.2	23.7	-89.08
KxxxCxxEx cis	1.627	-	-	7.79
KxxxCxxEx trans	1.665	2.3	2.4	177.44
KxxxCxxEx TS1	1.854	23.6	23.1	88.04
KxxxCxxEx TS2	1.867	18.7	18.8	-88.36
xExxCxxKx cis	1.629	-	-	7.15
xExxCxxKx trans	1.689	5.8	6.6	173.16
xExxCxxKx TS1	1.856	23.7	25.2	85.96
xExxCxxKx TS2	1.851	22.1	23.1	-88.89
xKxxCxxDx cis	1.616	-	-	14.67
xKxxCxxDx trans	1.693	5.7	7.4	167.32
xKxxCxxDx TS1	1.884	21.6	22.2	90.67
xKxxCxxDx TS2	1.928	18.5	19.1	-84.03

To estimate the barrier of CysNO isomerization, we located both transition states connecting cis- and trans-conformations (Figure 22). Each structure was characterized by calculation of the harmonic frequencies (no imaginary frequencies for cis and trans conformations, one imaginary frequency for each transition state). Electronic energies of all structures were recalculated with MPW2PLYPD/def2-TZVPPD formalism to achieve better accuracy as discussed previously.[71]

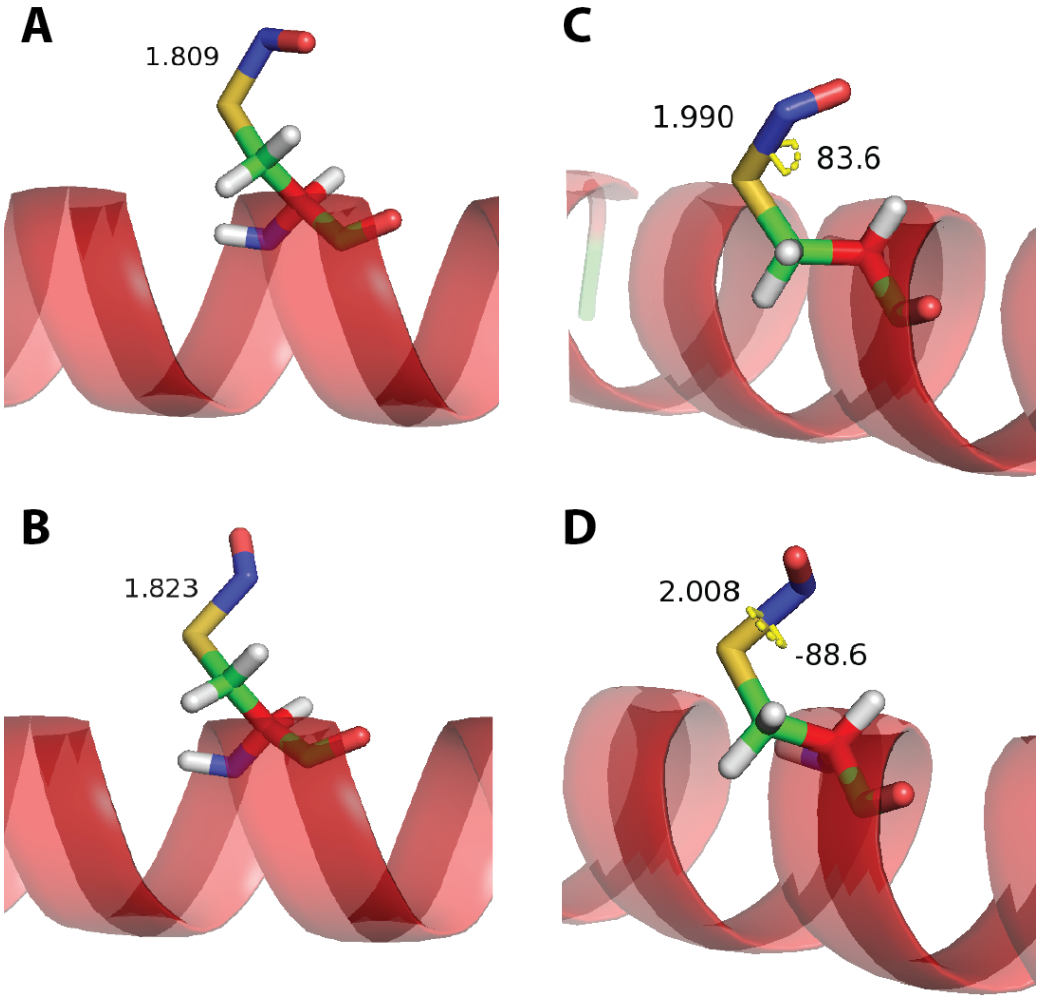

Figure 22. CysNO residue embedded in α-helix ONIOM model (A - cis, B- trans conformations, C, D - transition states). Highlighted: S–N bond lengths, CSNO dihedral angles.

Figure 22 illustrates one of the key features of α-helix ONIOM model comparing to truncated residues: the aminoacid backbone creates a noticeable anisotropy around the CysNO residue, previously not observed in the truncated model. Two transition state structures differ from each other in S–N bond lengths (1.990 Å and 2.008 Å), CSNO dihedral angles (83.6° and -88.6°), as well as activation barriers (10.6 and 11.2 kcal/mol, respectively).

Isomerization reaction barriers of CysNO embedded in the α-helix are in good agreement with both the experimental and theoretical results for model systems published in the literature. Arulsamy et al.[111] reported $\Delta G^{\neq}$ for cis-trans interconversion of tertiary $(CH_3)_3CSNO$ as 10.7 ± 0.7 kcal/mol determined via variable-temperature ^{15}N NMR experiment over the range of temperatures from +65 to -81°C, and in the same work 12.9 kcal/mol barrier was predicted for CH_3SNO isomerizarion using B3LYP/6-311+G(d) level of theory. Bartberger et al. reported[116] $\Delta G^{\neq}$ of isomerization for CH_3CH_2SNO as 11.1 kcal/mol using similar ^{15}N NMR technique.

To investigate the effect of the proximal charged residues on the CysNO isomerization within α-helix, we chose the structures from[6] with maximum ΔR(S–N) value, directly proportional to the strength of the residue influence on the -SNO group (Table 28).

Relative stability of cis and trans-CysNO was noticeably affected by the coordination of one charged residue to the -SNO group: trans-conformation was destabilized by more than 1 kcal/mol in cases of KxxxCxxxx, xxxRCxxxx and xxxxCxxxK (in all models, Ala and CysNO are denoted as ‘x’ and ‘C’, respectively), and

virtually remained intact in case of xxxKCxxxx. No inversion of stability between cis-CysNO and trans-CysNO was observed.

In contrast, the S–N bond lengths, as well as activation barriers of isomerization reaction were altered in a more dramatic way. The one-residue model demonstrated the possibility of both weak enhancement and strong diminishing of rotation around the S-N bond, with noticeable anisotropy of the α-helix environment still in place.

In case of KxxxCxxxx, cis-CysNO has elongated compared to non-coordinated CysNO S-N bond: 1.845 Å vs. 1.808 Å. This effect is caused by the S-N bond destabilizing coordination of positively charged Lys residue near S atom of the SNO group (Figure 23). Both transition states also have elongated S-N bond compared to uncoordinated CysNO in the α-helix: 2.054 Å and 2.062 Å vs. 1.990 Å and 2.008 Å, and have lower isomerization barriers: and 9.6 and 10.6 kcal/mol vs. 10.6 and 11.2 kcal/mol. Similar weak activation is observed in xxxRCxxxx model, with elongation of the S–N bonds in cis-CysNO and both transition states.

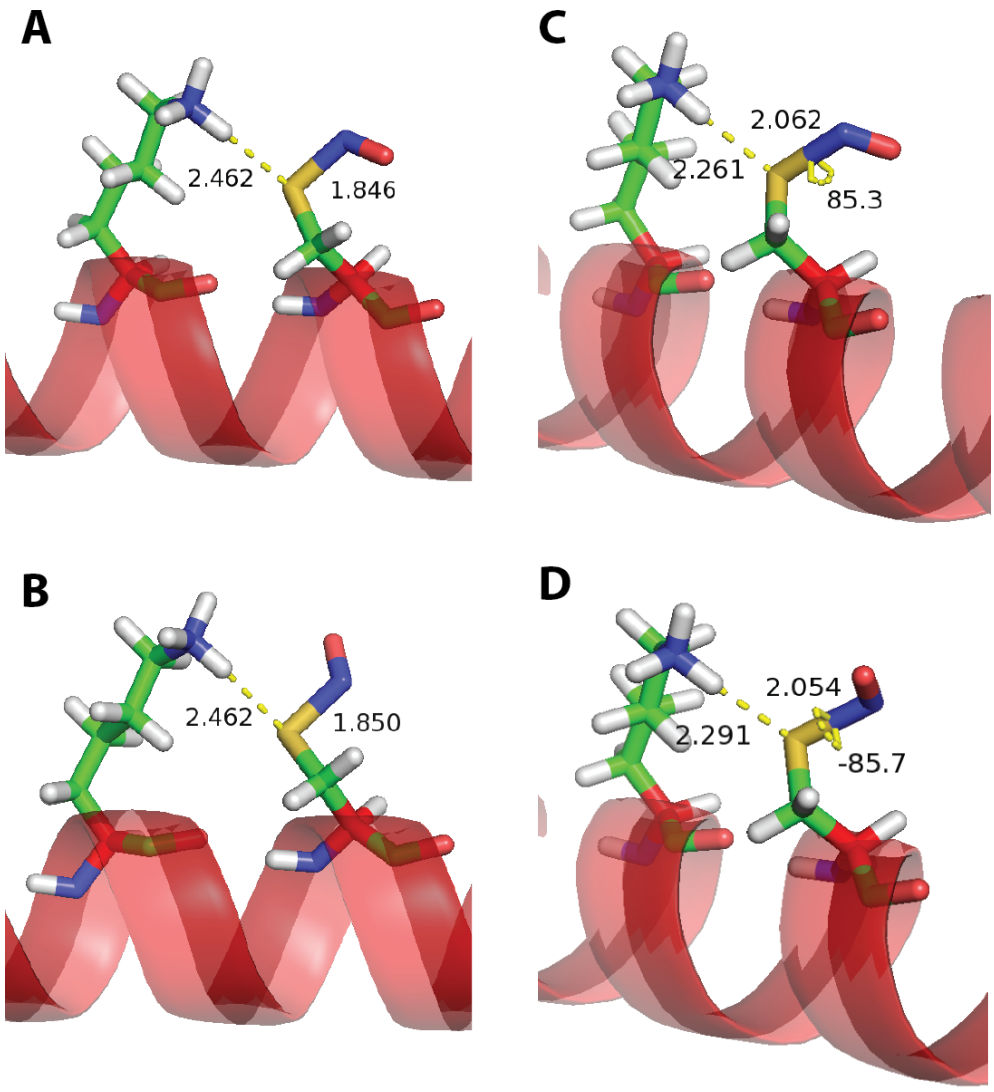

Figure 23. KxxxCxxxx in cis (A), trans (B) conformations, and both transition states(C, D). Highlighted: S-N bond lengths, distance from charged residue to S atom, CSNO dihedral angles.

This effect of positively charged residue coordination near S atom of the CysNO isomerization transition state is similar to its coordination with cis-CysNO[6]: increase in resonance weight of ionic structure I and corresponding decrease of the weight of structure D was linked to weaker S–N bond and more flexible CSNO dihedral angle in the SNO group.

In the case of xxxKCxxxx and xxxxCxxxK models, an opposite effect is observed: charged Lys residue caused contraction of the S–N bond in CysNO and corresponding restriction of its isomerization. In the xxxxCxxxK model, cis-conformation has much shorter (1.674 Å), and, therefore, more rigid CSNO torsion: $\Delta H^{\neq}$ of cis-trans isomerization is 18.6 kcal/mol (19.0 kcal/mol for the second TS).

With two residues of an opposite charge embedded in the α-helix model (see Table 28), more combinatorial possibilities lead to a greater structural flexibility and potential cooperativity effect on the CysNO. Thus, relative stability of cis-CysNO and trans-CysNO varies more strongly compared to one charged residue: in ExxxCxxHx, both conformations are closer in energy, with trans-CysNO becomes marginally more stable, judging by the ΔG value. ExxxCxxxK, xExxCxxKx and xKxxCxxDx models strongly favor cis-CysNO over the trans comformation (by 5.5, 5.8 and 5.7 kcal/mol), and KxxxCExxx, KxxxCxxEx models demonstrate moderate increase in the relative stability of the cis-CysNO (by 3.0 and 2.3 kcal/mol, respectively).

Shorter S–N bond lengths in transition states for CysNO isomerization with 2 charged residues are correlated with higher barrier heights: the strongest inhibition of S–N bond rotation is observed in KxxxCExxx (24.2 and 30.0 kcal/mol for two possible transition states, Figure 24) and xExxCxxKx (22.1 and 23.7 kcal/mol) cases. Such increase in activation energy from more favorable non-coordinated CysNO transition state ($\Delta G^{\neq}$ 11.9 kcal/mol) to more favorable KxxxCExxx transition state ($\Delta G^{\neq}$ 23.7 kcal/mol) would result in more than an 8 orders of magnitude decrease of the corresponding reaction rate constant at 293 K.

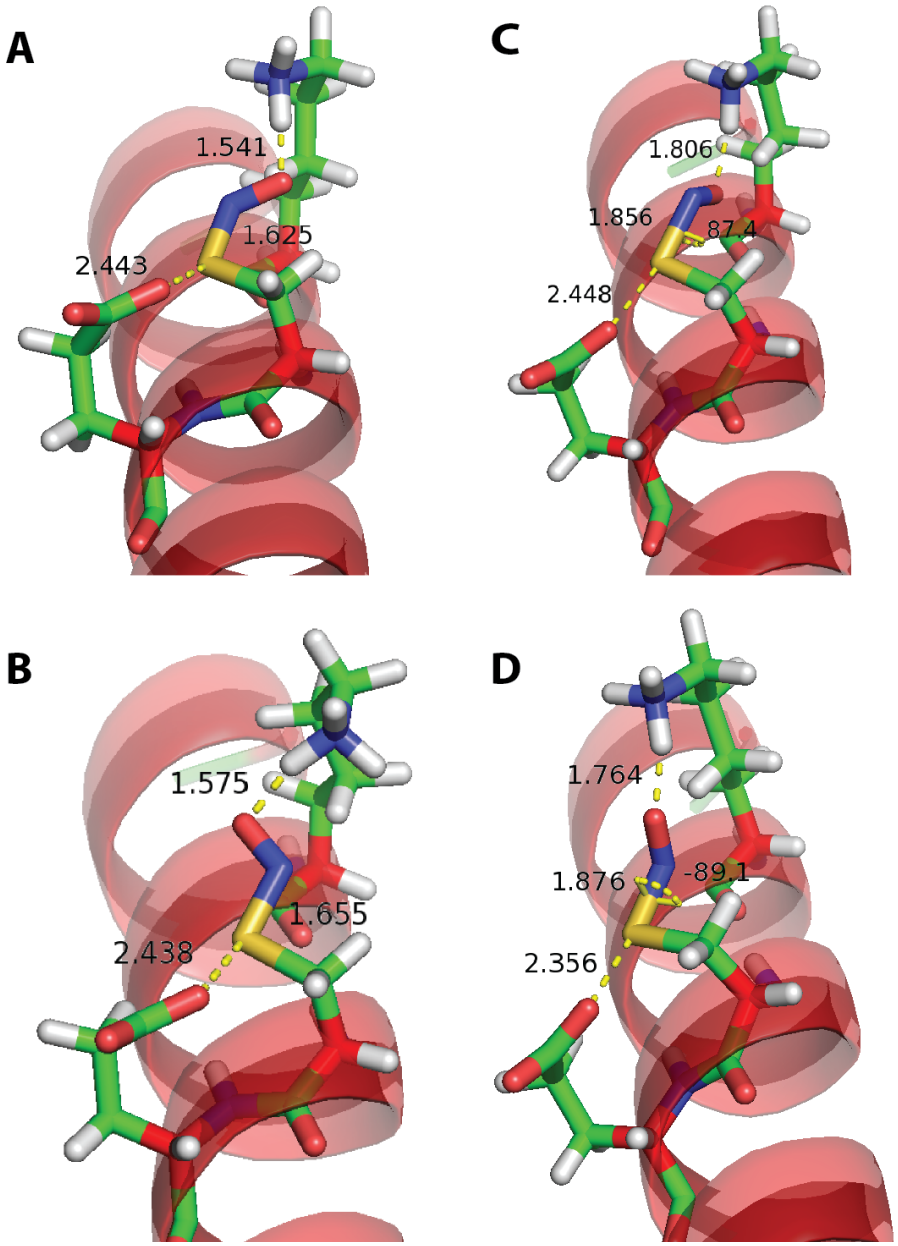

Figure 24. KxxxCExxx in cis (A), trans (B) conformations, and both transition states (C, D). Highlighted: S-N bond lengths, distance from charged residue to S atom, CSNO dihedral angles.

Another remarkable feature of coordination of the two charged residues α-helix model is an increase in anisotropy of the CysNO environment: in case of KxxxCExxx model, rotation in one direction instead of another leads to a change in activation barrier over 5 kcal/mol. Similar preference of one isomerization pathway

over another is observed in ExxxCxxxK, KxxxCxxEx and xKxxCxxDx cases. Hence, even a small 18-reside length α-helix resembles one of the most characteristic features of the tightly regulated protein environment: steric control.

After collecting a pool of data for 1- and 2-residue models, dependence of the activation barriers on the S–N bond lengths in transition states emerged. Figures 25 and 26 illustrate this trend for $\Delta H^{\neq}$ and $\Delta G^{\neq}$. Overall, a clear trend is observed, with a single outlier: one of the two KxxxCExxx transitions states. It was found that the steric clash of SNO group and α-helix backbone resulted in disproportional increase of activation barrier in this case.

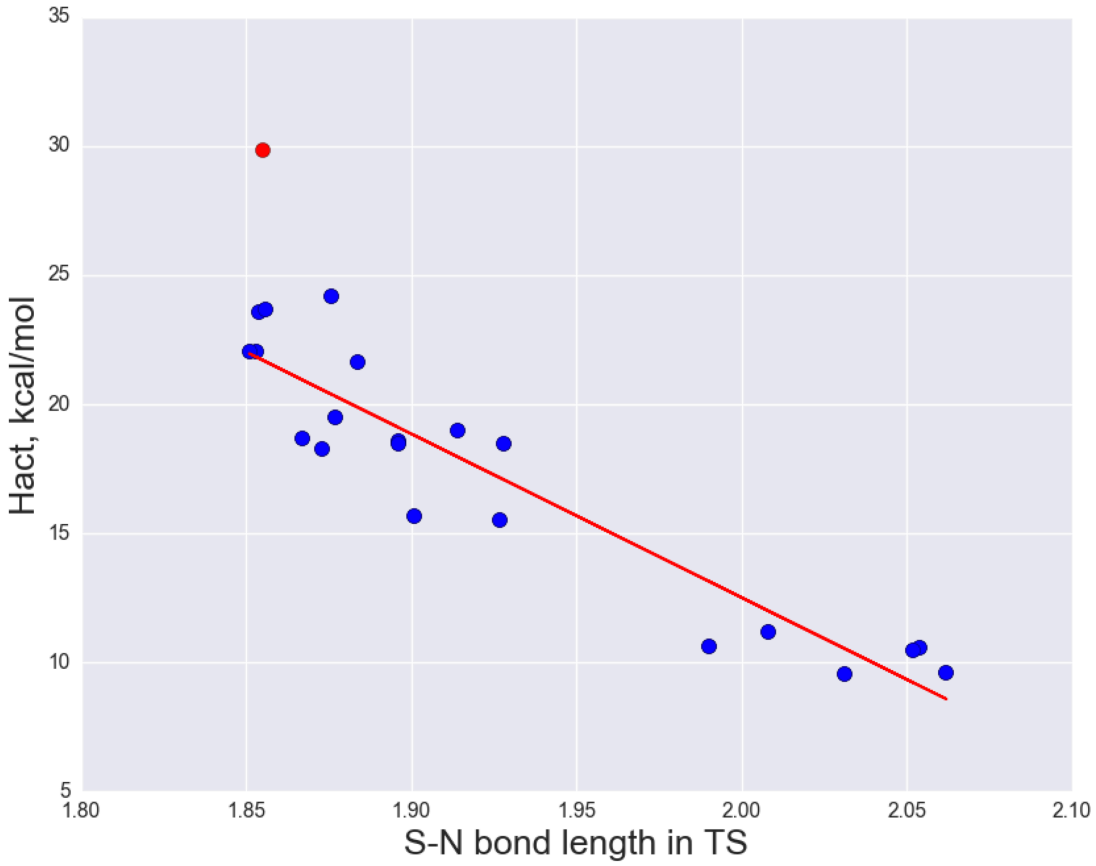

Figure 25. Linear regression results for $\Delta H^{\neq}$ vs. r(S–N) in TS (slope -63.4, intercept 139.3, r^2 0.8705). An outlier (KxxxCExxx) structure is shown in red.

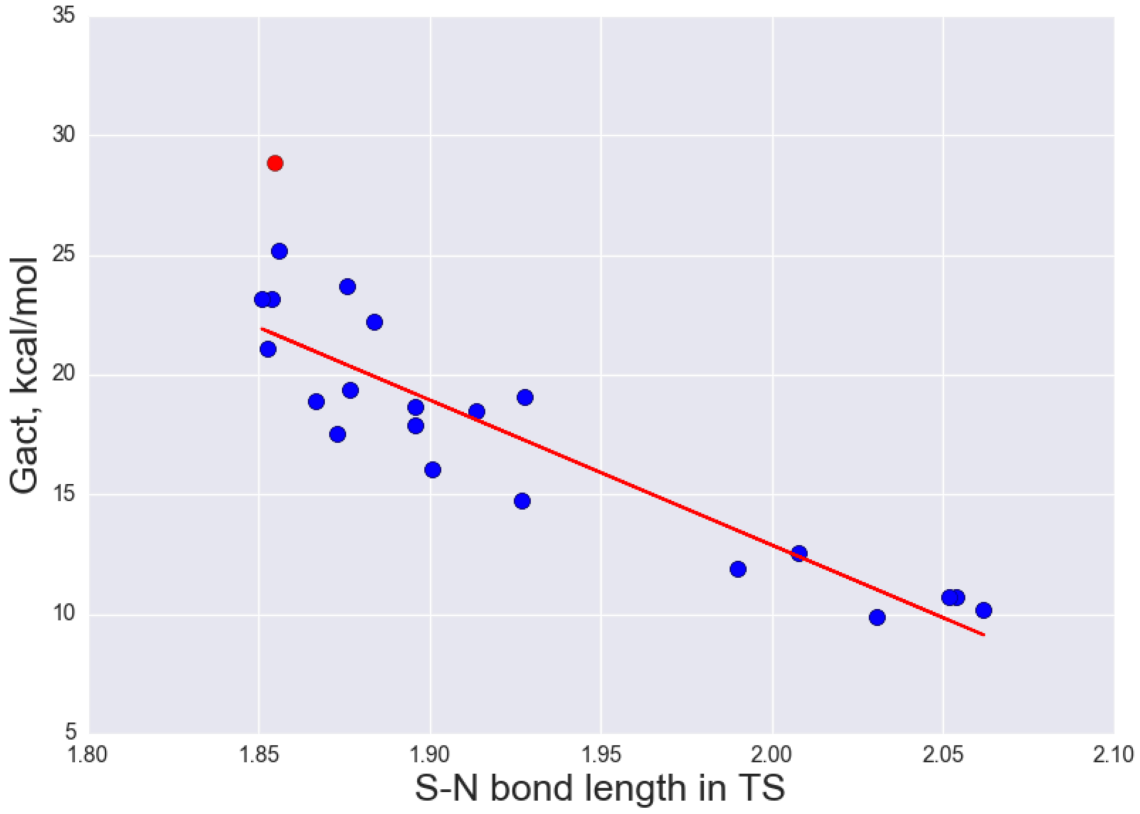

Figure 26. Linear regression results for $\Delta G^{\neq}$ vs. r(S–N) in TS (slope -60.7, intercept 134.2, r^2 0.8437). An outlier (KxxxCExxx) structure is shown in red.

According to this model, significant decrease in activation barrier can be achieved at the S–N bond length of 2.1 Å or higher in the transition state (0.04 Å bond length increase comparing to the non-coordinated CysNO transition state).

Despite the relative simplicity of the α-helix ONIOM model, it revealed that charged residues significantly affect relative stability of cis- and trans-conformations of CysNO, as well as the barriers of their interconversion.

2. Protein Control of CysNO Conformation: The DJ-1 Protein Model

To further investigate the factors affecting isomerization of CysNO in the protein environment, a DJ-1 protein (PDB code 4RKY) was selected for current study. Recent X-Ray structure of DJ-1 by Choi et al.[33] (resolution 1.5 Å) revealed an unusual trans-conformation of S-nitrosated Cys106 residue (CSNO dihedral angle 159.8°), contrary to most of the known reliable identified S-nitrosated cysteine residues in proteins detected by X-Ray crystallography (Table 27), which adopt a cis-form.

DJ-1, a small protein of 188 residues, is proposed by Choi et al.[33] to be a trans-S-nitrosylase, an enzyme, capable of transferring the NO moiety to another proteins[37]. S-nitrosation of Cys106 in DJ-1 was shown in[33,158] to be crucial in protection of neuronal cells from oxidative stress and, therefore, prevention of neurodegenerative diseases, such as Alzheimer's disease, from development. In particular, Cys106 DJ-1 was S-nitrosated *in vitro* by exposing it to 25 μM CysNO.[33] Mutation of Cys106 abolished the effect of CysNO on SNO-DJ-1 formation.

It was previously found that DJ-1 contains ionizable acidic residue Glu18 in close proximity to the S-atom of S-nitrosated Cys106 (O…S distance 3.426 Å).[158] Corresponding X-Ray crystallography reveal that Glu18 alters Cys106 acidity and creates more susceptible target for S-nitrosation by forming a hydrogen bond between deprotonated S atom of the Cys106 residue and protonated O atom of the carboxylic group of Glu18 (Figure 27). This hydrogen bond formation was accounted for significant depression of the pKa value of Cys106 (determined in this

study as 5.4 ± 0.1), by effectively stabilizing Cys106 thiolate anion in DJ-1. Based on our α-helix ONIOM studies, S-nitrosated DJ-1 protein represents a promising model to study CysNO isomerization reaction in protein environment.

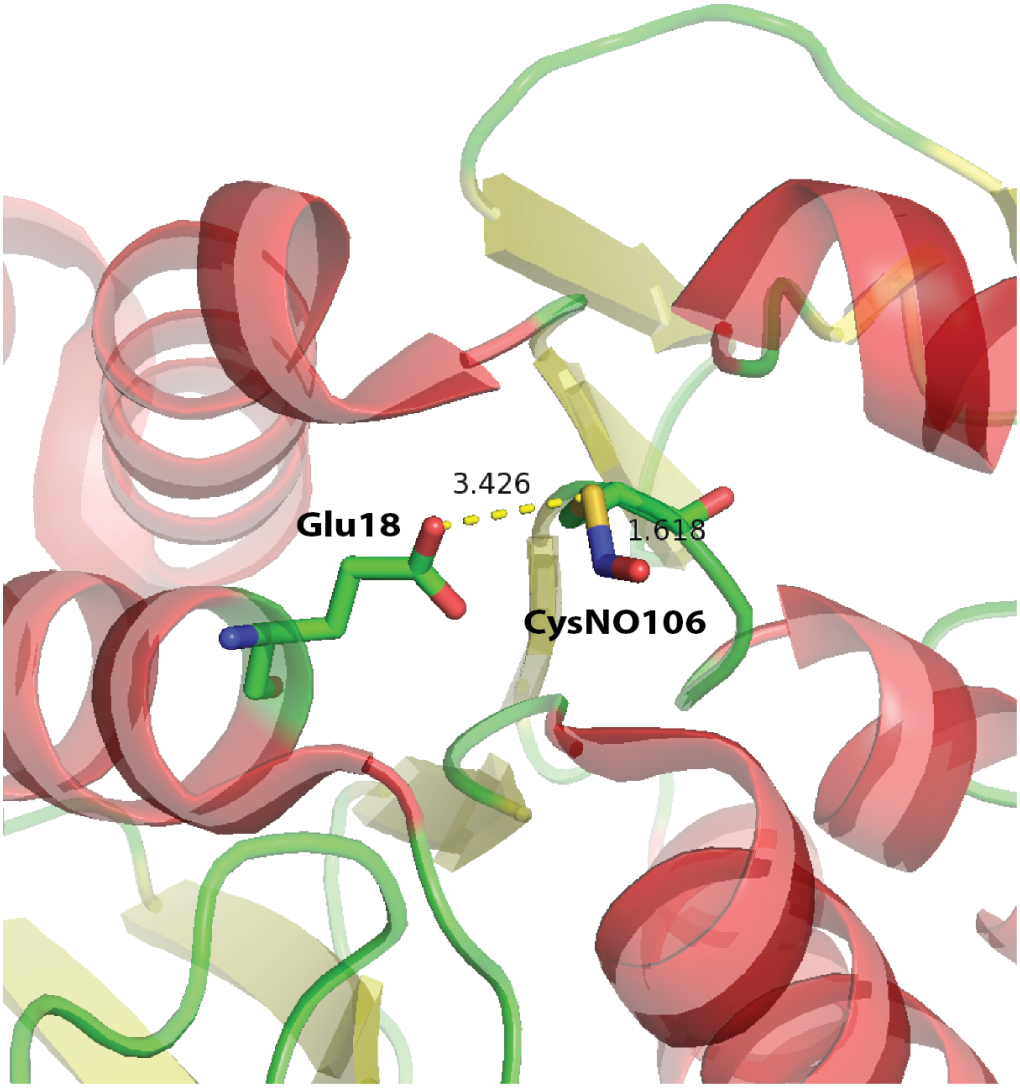

Figure 27. Crystal structure of the S-nitrosated Cys106 and proximal Glu18 residue in DJ-1 protein (Choi et al., 2014). Highlighted: S–N bond length in CysNO106, distance from Glu18 to the S atom of SNO group.

In this study, we created a three-layer ONIOM model from the PDB entry 4RKY using in-house Python code based on MMTK toolkit[148]. The model utilizes quantum-mechanical approach for the high-layer and middle-layer atoms, and

molecular mechanical approach for the low-layer atoms. S-nitrosated Cys106 and deprotonated Glu18 residues with corresponding side chains (high-layer atoms) are described with PBE0/def2-SV(P)+d methodology. Surrounding Cys106 residues (Cys106 pocket with the total of 26 residues, middle-layer atoms) with corresponding side chains were treated with HF/STO-3G approach, and the rest of the protein molecule was included into the computational scheme by Amber94[151] force field. Due to the nature of the three-layer ONIOM model, high-level QM atoms are excluded from the MM layer, and, therefore, no external force field parameters were required to describe the properties of SNO group, contrary to the two-layer α-helix ONIOM model.

Starting atomic coordinates for the ONIOM model of DJ-1 (Figure 27) were based on crystallographic data from 4RKY PDB file. After optimizing the positions of high- and medium-level atoms, we observe conservation of the trans-conformation of S-nitrosated Cys106: CSNO dihedral angle is 179.1°, and deviates insignificantly from trans-CysNO in α-helix ONIOM model (177.6°) (Figure 28).

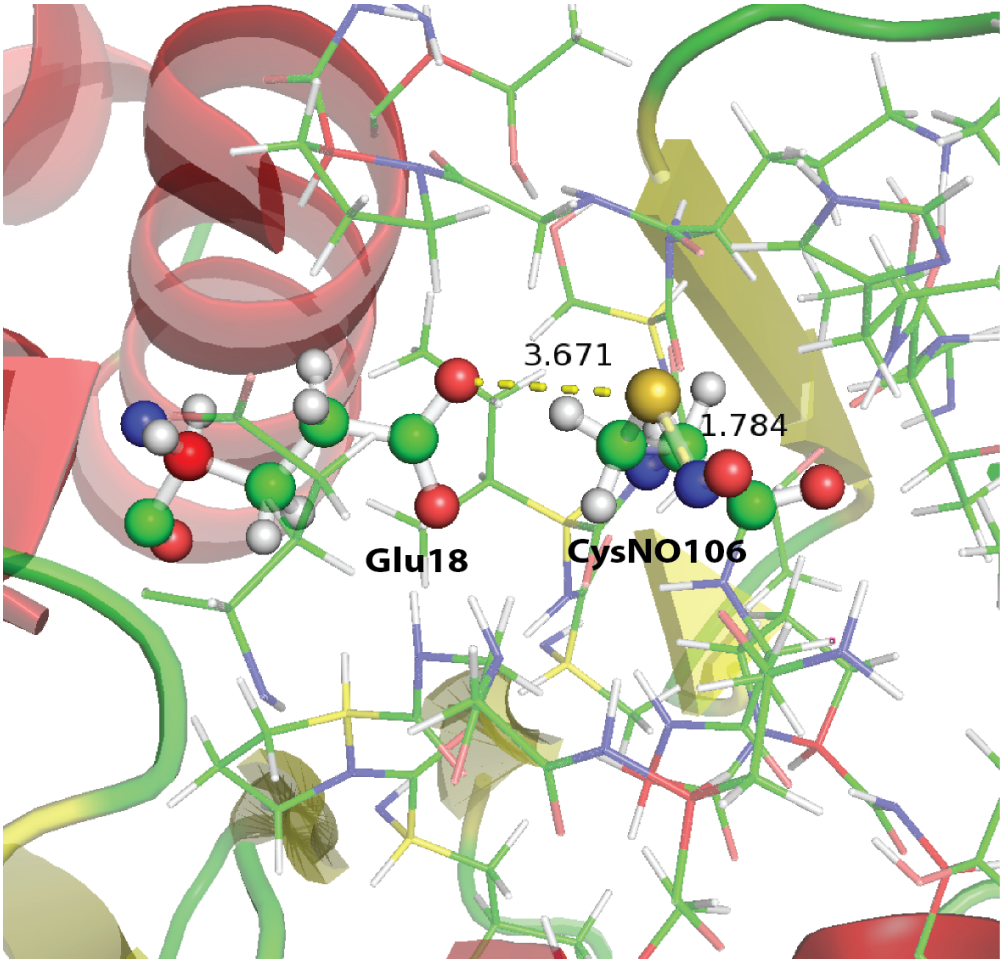

Figure 28. Optimized ONIOM model of trans-CysNO106 and proximal Glu18 residues in DJ-1 protein. Ball-and-stick view is used for the high-level layer of atoms (CysNO106 and Glu18), stick representation is used for the medium-layer atoms (CysNO pocket), and cartoon representation is used for the rest of the protein molecule. Highlighted: S–N bond length in CysNO106, distance from Glu18 to the S atom of SNO group.

Optimized S–N bond length in CysNO is 1.783 Å, 0.040 Å shorter than the S–N bond of trans-CysNO in α-helix ONIOM model. Glu18 residue remained in close proximity of the SNO group: the O…S distance increased from 3.426 Å in X-Ray structure to 3.670 Å in the optimized model. These results are in qualitative agreement with previously published data[6], where a Lewis base, coordinated near S-atom of the SNO group, stabilizes it and shortens the S-N bond.

Optimized structure of cis-conformation of the S-nitrosated Cys106 is shown

in Figure 29. The CSNO dihedral angle remains close to the cis-CysNO in the α-helix model (3.6° vs. 0.9°), whereas the S–N bond length decreases by 0.022 Å (1.786 Å vs. 1.808 Å). Glu18 residue remains 3.638 Å away from the S atom of the SNO group.

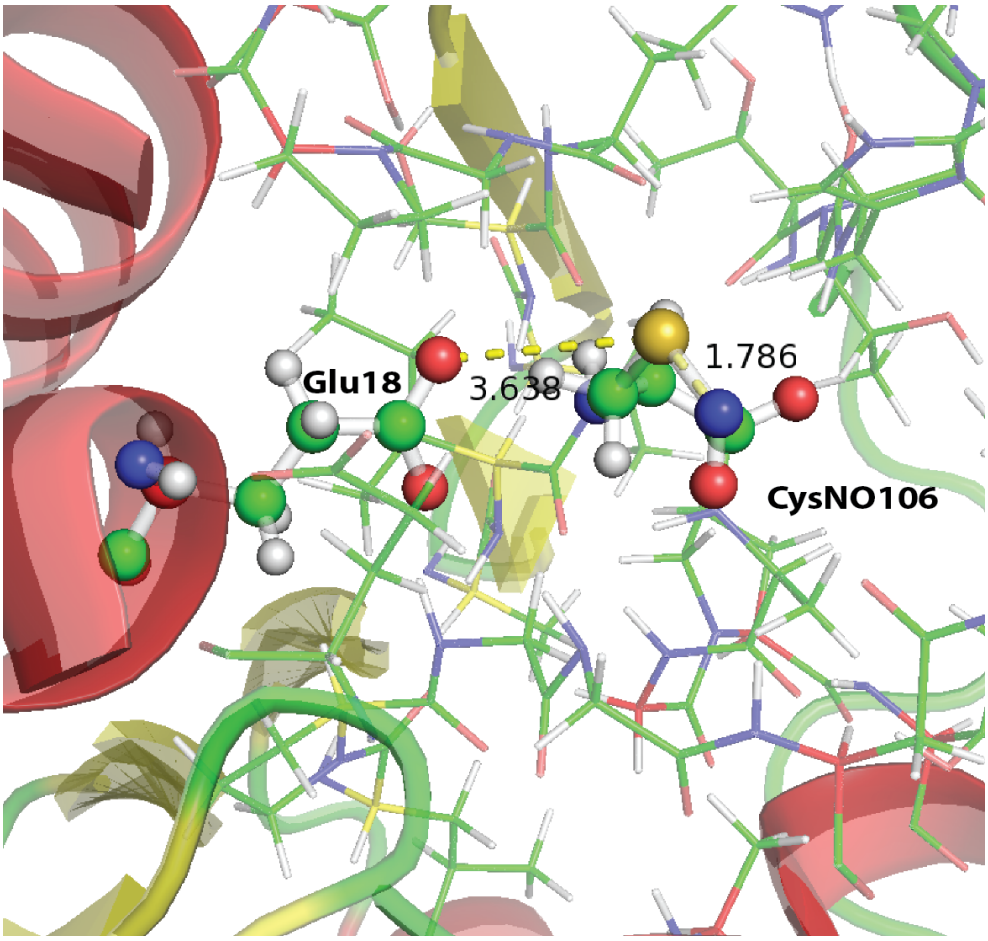

Figure 29. Optimized ONIOM model of cis-CysNO106 and proximal Glu18 residues in DJ-1 protein. Ball-and-stick view is used for the high-level layer of atoms (CysNO106 and Glu18), stick representation is used for the medium-layer atoms (CysNO pochet), and cartoon representation is used for the rest of the protein molecule. Highlighted: S–N bond length in CysNO106, distance from Glu18 to the S atom of SNO group.

Calculations of the relative stability of cis- and trans-CysNO conformations in DJ-1 confirmed experimental findings: protein environment favors trans-CysNO over cis-CysNO (1.3 kcal/mol ΔH, 1.6 kcal/mol ΔG).

To estimate the influence of steric effects on the conformations of the SNO group, we used another X-ray structure of non-S-nitrosated DJ-1 1P5F from Wilson et al. (resolution 1.10 Å) (Wilson, Collins, Hod, Ringe, & Petsko, 2003), and applied in-house Python code (S-nitrosator algorithm, Dr. Marat Talipov and Dr. Maxim Ivanov) to *in silico* S-nitrosate Cys106. This algorithm only uses Amber 94 force field to minimize repulsion of the newly placed NO moiety from the intact surrounding residues, and only takes into account steric interactions. It was found that *in silico* cis-CysNO106 is more stable than the trans-conformation, leading to the conclusion that Cys106 pocket can easily accommodate both conformations.

To estimate energetic barriers of cis-trans isomerization of S-nitrosated Cys106, we optimized two corresponding transition states, connecting both conformations (Figure 30). Similarly to the α-helix ONIOM model, anisotropy of the protein environment causes differences in the structure and energetic barriers in DJ-1 in clockwise and counterclockwise rotation around the S–N bond.

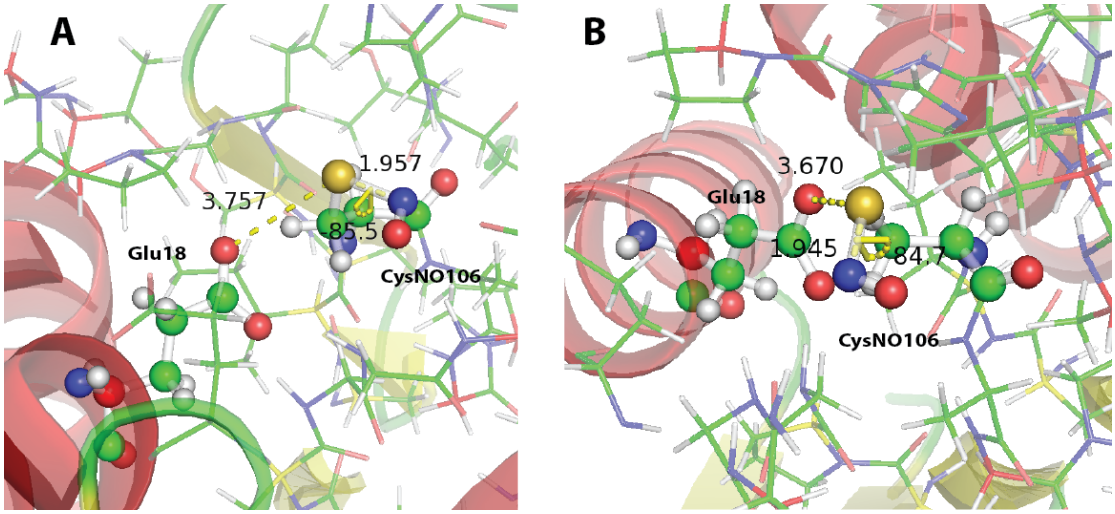

Figure 30. Optimized ONIOM model of two transition states of cis-CysNO106 isomerization. Ball-and-stick view is used for the high-level layer of atoms (CysNO106 and Glu18), stick representation is used for the medium-layer atoms (CysNO pocket), and cartoon representation is used for the rest of the protein molecule. Highlighted: S–N bond length in CysNO106, distance from Glu18 to the S atom of SNO group, CSNO dihedral angle.

Both transition states have one imaginary frequency, responsible for rotation around the S–N bond. The S–N bond lengths in optimized transition states and corresponding barriers (1.957 Å, 13.6 kcal/mol $\Delta H^{\neq}$ and 1.945 Å, 15.6 kcal/mol $\Delta H^{\neq}$) are in good agreement with our findings derived from the α-helix ONIOM model. Thus, activation barriers predicted by the S–N bond length (15.2 kcal/mol for 1.957 Å, 16.0 kcal/mol for 1.945 Å,) differs by 1.6 and 0.4 kcal/mol from the calculated ones. Increase of the rotation barrier from 11.9 kcal/mol in alpha-helix to 14.6 kcal/mol in DJ-1 leads to more than a 100-fold decrease in corresponding cis-trans monomolecular rate constant at 293 K.

The Glu18 position in optimized transition states remained coordinated near the S atom of SNO group: O…S distances are 3.757 Å and 3.670 Å. Therefore, a proposed role of the Glu18 residue is not only to convert Cys106 into an easier target for S-nitrosation by depressing its pKa value, but also to stabilize the

resulting trans-CysNO and limit the rotation around S–N bond. In future work, we propose to study S-nitrosation reaction between Cys106 of DJ-1 and HSNO, as well as the transfer of NO moiety from DJ-1 to target proteins.

With calculated transition states CSNO dihedral angles of -85.5° and 84.7°, all PDB structures (Table 27) with CSNO dihedral angle deviating strongly from 0° or 180° call for additional attention. For example, bent SNO group (CSNO dihedral angle 87.5° for Chain B, 75.6° for Chain D) of S-nitrosohemoglobin by Chan et al.[133] was later re-identified as a thionitroxide radical, RS-NH-O•, in Ref.[159].

One can draw a conclusion that the protein environment influences S-nitrosated Cys106 via both steric and electrostatic interactions (in the DJ-1 case, the interaction between Glu18 and the SNO group is found to be the major governing force in regulating the barrier of cis-trans interconversion). At the same time, strong influence of charged residues on the activation barriers of CysNO isomerization reaction makes MD simulations of S-nitrosated proteins challenging. Namely, proposed force field parameters for CysNO,[160] especially the energy profile of CSNO torsion, do not take into account specific electrostatic interactions of the proximal charged residues with the SNO group. Therefore, diligent consideration of all possible sources of errors is required in MD simulations of S-nitrosoproteins.

D. Conclusions

In this work, we demonstrated that protein environment significantly affects the structure, relative stability of cis-trans conformers, as well as the barriers of cis-trans isomerization of CysNO, in α-helix model or in a DJ-1 protein, by steric and electrostatic influence on the SNO group. Thus, the S–N bond length in cis-conformation of the KxxxCExxx double-coordinated model is significantly shorter (1.624 Å,) comparing to non-coordinated cis-CysNO an α-helix (1.808 Å). The activation barrier of cis-trans isomerization reaction has increased, correspondingly, by almost 14 kcal/mol (from 10.6 to 24.2 kcal/mol). This phenomenon stress the fact that S-nitrosothiols are unique biochemical entities in a sense of malleability of their electronic structure, and can impose significant challenges for the experimental and computational studies.

The ability of ONIOM approach to combine both the accuracy of the DFT methods and scalability of molecular mechanics (MM) grants one the toolkit to access the reactivity of CysNO in proteins. The observed deviations from planarity (e.g. cis- or trans-conformations) of the SNO group in the experimental structures of S-nitrosated proteins are not supported by the performed in this work calculations. Our results robustly demonstrate that neither α-helix nor DJ-1 protein models can stabilize the 'bent' conformations of CysNO, moreover, it was repeatedly shown to be the transition state structures of corresponding CysNO cis-trans isomerization reactions.

In ongoing work, we are expanding the ONIOM α-helix and DJ-1 models to investigate the influence of proximal charged residues on the mechanism of trans-S-nitrosation reaction.

Chapter IV: Making S-Nitrosothiols 'Click'

A. Introduction

S-nitrosation of the cysteine residues in proteins with formation of corresponding S-nitrosoproteins is a highly important biological process, attracting significant interest in life sciences and medicine.[2,21] Unfortunately, S-nitrosoproteins are challenging to study experimentally, due to their lability: to reliably determine protein S-nitrosation sites, unstable SNO groups must be converted into more stable species. Despite a significant effort,[3,161] an efficient and selective single-step chemical labeling reaction that yields a robust RSNO derivative is yet to be found.[161]

Most of the currently used methods to identify S-nitrosated cysteine residues in proteins are complex and error prone, as they require prior labeling of far more numerous unmodified cysteine residues (Figure 31).[162-165]

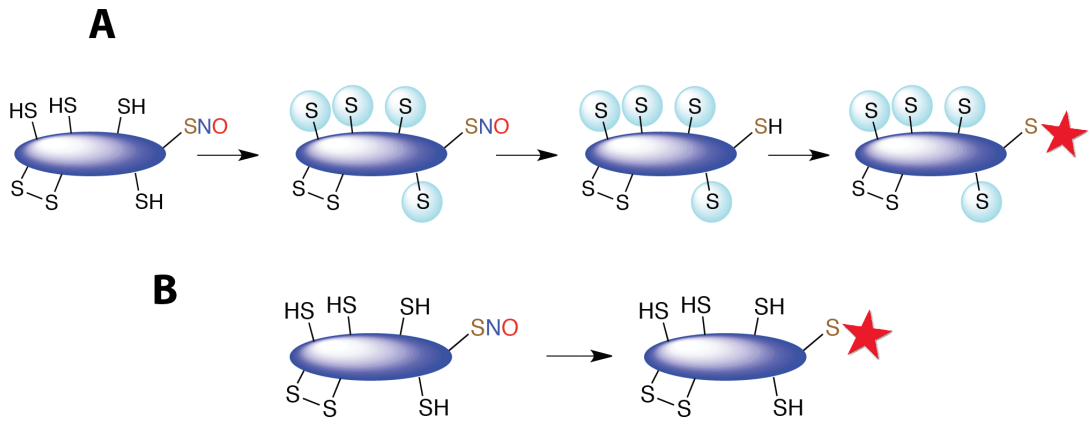

Figure 31. Currently implemented (A) and optimized (B) protocols of CysNO labeling.

An inspiring example of efficient chemical labeling is the famous click[166] reaction, or 1,3-dipolar azide-alkyne cycloaddition, that is widely used in chemical

biology.[167,168] In this work, we computationally demonstrate that RSNOs can be activated by the addition of Lewis acids (LAs) to readily undergo (3+2) cycloadditions, and propose that development of LA-linked reagents may provide a powerful single-step chemical labeling method with great potential for studies of S-nitrosated proteins.

We base our design of efficient RSNO cycloaddition reactions on the insights into the electronic structure of the SNO group[67] that, however, can be rationalized using the concept of resonance structures. In the resonance description of RSNOs,[112] the conventional structure ***S*** (with single S–N bond) (Figure 17) is augmented by zwitter-ionic resonance structure ***D*** (with double S–N bond) and ion-pair structure ***I*** (no covalent bond between the S and N atoms).

Importantly, structures ***D*** and ***I*** can be referred to as antagonistic structures, as they imply significantly different bonding patterns and formal charges in the SNO group. ***D*** *vs* ***I*** antagonism rationalizes the unusual properties of the S–N bond that exhibits partial double bond character[116], despite being unusually long and weak.[106] It also accounts for the dramatic effect of Lewis acid coordination on the stability of the S–N bond.[6,169]. Moreover, the two antagonistic structures correlate with the dual reactivity of RSNOs towards nucleophiles that can attack the –SNO group either at S or at N atoms. The first mode of reactivity is promoted by structure ***D***, and the second—by structure ***I*** (Figure 32).[7]

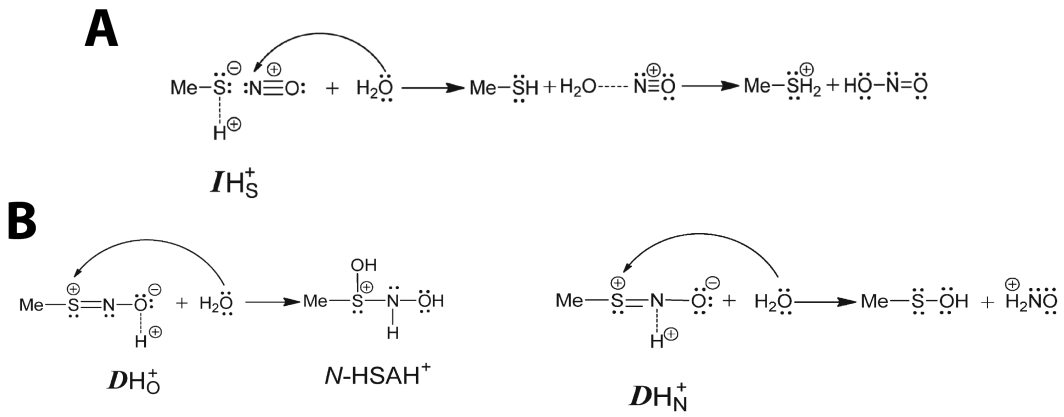

Figure 32. N-atom (A) vs S-atom (B) nucleophilic attack, promoted by the CH_3SNO protonation on S (A) and O, N atoms (B), respectively. Adapted from Ref.[7]

B. Computational Details

The electronic structure calculations were performed with CBS-QB3[119,170] composite methodology and density functional theory (DFT) using hybrid Perdew-Burke-Ernzerhof functional PBE0,[56,94,171] as implemented in Gaussian 09 package.[56] DFT calculations were performed with def2-SV(P) double-zeta quality basis set by Ahlrichs and co-workers,[95] with a tight d-function added for sulfur atoms; the resulting basis set is referred to as def2-SV(P)+d. Because CBS-QB3 calculations are feasible only for small molecules (up to 16 heavy atoms), only PBE0 calculations were used for the reactions involving cyclooctyne derivatives or a tris(pentafluorophenyl)borane (BCF) group. For other reactions studied (Tables 29, 30), CBS-QB3 and PBE0 provide a generally consistent description (Appendix A, Tables A1-A5).

All calculations, including geometry optimizations and vibrational frequencies calculations,[172] included solvation effects using the polarized continuum solvent model (PCM)[96] with acetonitrile solvent parameters, as implemented in

Gaussian 09. Natural bond orbital[157]l (NBO) and natural resonance theory (NRT)[173] analyses were performed using the NBO 5.0 program[174] for the PBE0/def2-SV(P)+d calculation results.

The electronic structure calculations of AdSNO and LA complexes were performed with dispersion-corrected PBE0-GD3[99] DFT functional in combination with the def2-SV(P)+d basis set, with PCM solvent parameters for diethylether. Time-dependent DFT calculations (TD-DFT) were used to estimate the main features of UV/visible spectra of free and LA-binded AdSNO molecule in solution, using time-dependent variation of the PBE0-GD3 functional with def2-TZVPPD basis sets[95] (PCM solvent parameters were set for toluene).

C. Results and Discussion

1. Proof of the concept

Based on the resonance description of the electronic structure of S-nitrosothiols (Figure 33 A), we hypothesized that RSNOs can demonstrate dual reactivity towards alkenes and alkynes. The three characteristic resonance structures ***S***, ***D*** and ***I*** imply single, double and ionic S–N bond, correspondingly. The resonance components ***D*** and ***I*** are antagonistic, as they imply opposite bonding patterns, charge distributions, and hence opposite reactivities. Natural bond orbital (NBO) interactions behind structures ***D*** and ***I*** are shown on Figure 33 B. The structure ***D*** (promoted by the π-conjugation n_S–>π^*_{N-O}) is expected to give rise to a (3+2) cycloaddition reaction, similarly to the classical 1,3-dipole cycloadditions. Resonance structure ***I*** (promoted by the negative hyperconjugation n_O–>σ^*_{S-N}) should lead to the carbon-carbon bond insertion into the S–N bond.

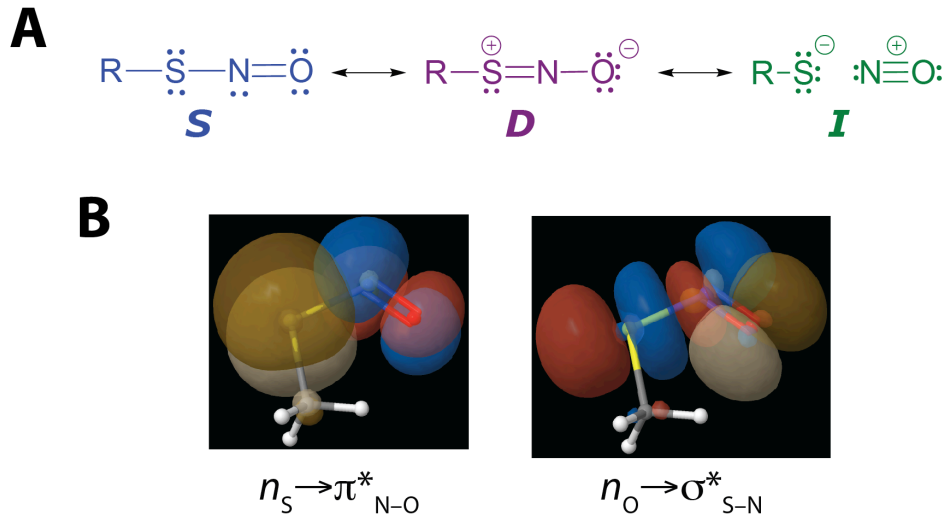

Figure 33. Resonance description of RSNO electronic structure (A); natural bond orbital (NBO) interactions behind structures D and I (B).

Indeed, we found transition states (TSs) for both reaction modes for the methyl-substituted CysNO model (CH_3SNO) and a model alkyne (dimethylacetylene) (Figure 34 A) using CBS-QB3 methodology with PCM solvation. Similarly to the two modes of RSNO hydrolysis reaction, promoted either by structures ***D*** or ***I***,[7] the S–N bond contracts in the cycloaddition TS_{Cycl} (from 1.84 Å in CH_3SNO/alkyne pre-reactional complex to 1.66 Å in the TS), which is consistent with the elevated ***D*** character. On the other hand, the S–N bond significantly elongates in the S–N insertion TS_{Ins} (from 1.84 Å to 2.30 Å, correspondingly), which is consistent with the elevated ***I***-character.

The (3+2) cycloaddition pathway is characterized by synchronous formation of the S–C and O–C bonds, as suggested by intrinsic reaction coordinate (IRC) analysis (Figure 34 B). In fact, the IRC profiles for RSNO cycloaddition are remarkably similar to the IRC profiles of azide (3+2) cycloaddition with the same dipolarophile molecule, known as an archetype 1,3-dipolar cycloaddition reaction.

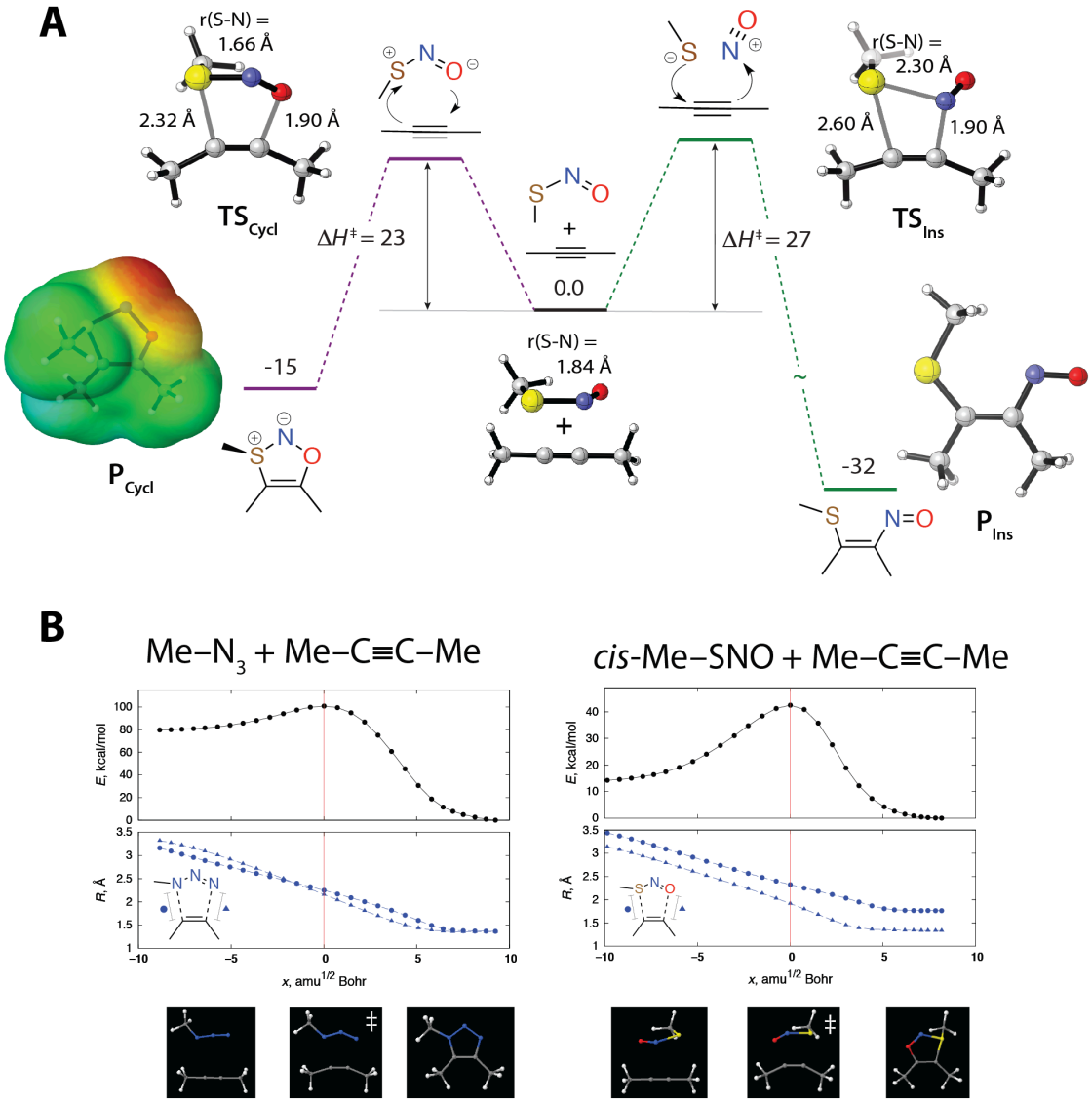

Figure 34. CBS-QB3 calculated enthalpic profiles (in kcal/mol) for the (3+2) cycloaddition and the S–N bond insertion reaction between model RSNO and alkyne, with the corresponding TS and product structures; the cycloaddition product P_{Cycl} structure is shown with corresponding electrostatic potential map (A). Intrinsic reaction coordinate (IRC) profiles and evolution of lengths of the newly formed bonds for (3+2) cycloadditions of model azide and RSNO with an alkyne (B).

Both reactions have significantly high activation enthalpies (23–27 kcal/mol), close in energy to that of homolytic S–N bond dissociation in RSNOs (~30 kcal/mol),[36,72] a monomolecular process that is likely to prevail over the

bimolecular reactions with alkenes or alkynes. Although the (3+2) cycloaddition pathway has a lower activation barrier, its product P_{Cycl} is less thermodynamically stable than the S–N bond insertion product P_{Ins}. The latter is similar to the products of radical reactions of RSNOs with alkenes and alkynes initiated by the S–N photolysis or thermolysis,[175] so it is possible that the direct S–N bond insertion pathway may contribute to the thermally-activated reactions.

To independently evaluate the relative energetics of the (3+2) cycloaddition and S–N bond insertion pathways, we located corresponding transition states and reaction products of CH_3SNO and C_2H_2 in the gas phase, using an accurate, but computationally expensive *ab initio* method CCSD(T)-F12a/VDZ-F12 (Figure A1, Tables A1-A4). The transition state structures for both (3+2) cycloaddition and S–N bond insertion mechanisms, as well as their activation barriers and reaction energies, are in qualitative agreement with the abovementioned CBS-QB3 reaction profiles of CH_3SNO and C_4H_6 in acetonitrile. Thus, the activation barrier of (3+2) cycloaddition is lower compared to the S–N bond insertion (26.8 kcal/mol vs. 31.0 kcal/mol, respectively), while the S–N bond insertion reaction is significantly more exothermic (-36.3 vs. -13.6 kcal/mol for the (3+2) cycloaddition).

2. Modulation of RSNO reactivity

In principle, both reactions (Figure 34 A) can be used for chemical labeling of –SNO groups, if the activation barriers are sufficiently lowered. As we have recently demonstrated,[7,112] coordinating a Lewis Acid (LA) to the –SNO group atoms can

dramatically alter the reactivity of RSNOs by promoting one of the antagonistic resonance structures ***D*** or ***I***, at the expense of the other. S-coordination of a LA should promote structure ***I*** due to favorable interaction with the S– atom that bears a formal negative charge in that structure, and reduce ***D*** that implies positively charged S^+ atom. Therefore, coordination of the LA moiety at the S atom should facilitate the S–N bond insertion reaction.

On the other hand, O-coordination of the LA molecule to RSNO should favor structure ***D*** with negatively charged O^-, and disfavor ***I*** with its cationic NO^+ moiety. N-coordination should also disfavor ***I*** due to the similar LA—NO^+ interaction and, therefore, indirectly promote ***D***.[112] Therefore, but O- and N-coordination should in theory facilitate the (3+2) cycloaddition pathway. Indeed, the O- and N-coordination of a model LA (BF_3) lead to significant reduction of the calculated reaction cycloaddition barriers, $\Delta H^{\ddagger}$ = 16 and 12 kcal/mol, respectively (Figure 35).

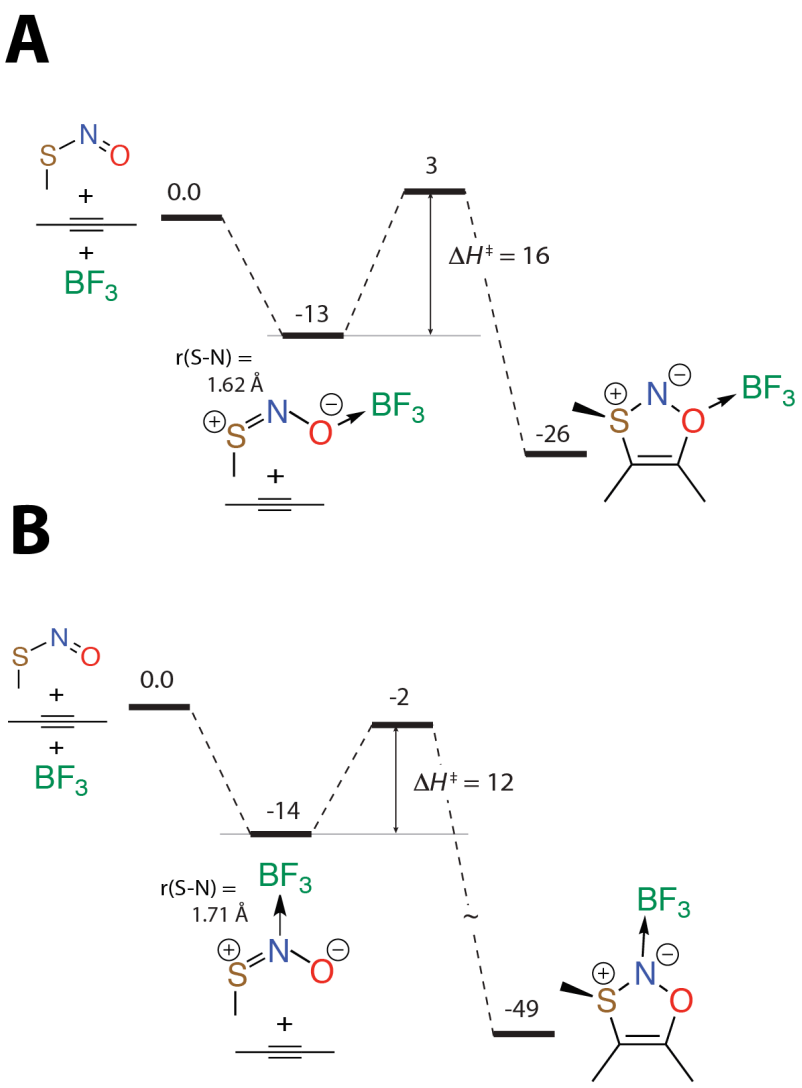

Figure 35. Enthalpic profiles (in kcal/mol) for the (3+2) cycloaddition between a model RSNO and alkyne catalyzed by O- and N- coordination of a LA (BF_3) (A and B, respectively). In the LA complexes, RSNO is drawn with D resonance structure, which is promoted by the LA coordination.

Natural resonance theory[173] (NRT) calculations show that the resonance contribution of structure ***D*** increases from 25% in free CH_3SNO to 52% and 34% for O- and N-coordinated BF_3–CH_3SNO complexes, respectively. The resonance weight of structure ***I*** drops from 8% to ~4% in both cases. These changes correlate with

significant shortening of the S–N bond in O- and N-coordinated BF_3–CH_3SNO complexes (by ~0.2 and ~0.1 Å, respectively). Although O-coordination of the LA is better at promoting resonance weight of structure ***D***, N-coordination results in 4 kcal/mol lower activation barrier of (3+2) cycloaddition reaction (Figure 35). This surprising effect is related to the increased basicity of the N atom in the heterocyclic cycloaddition product P_{Cycl} with S^+–N^- dipolar bond and significant negative charge on N, as clearly seen on the electrostatic potential map (Figure 35 A). Delocalization of the emerging negative charge on N atom by a N–>LA dative bond leads to stabilization of the TS and overall increased driving force of the reaction, which has much higher exothermicity ΔH_{rxn} = -35 kcal/mol, compared to uncatalyzed and O-coordinated LA-catalyzed reactions (-15 and -13 kcal/mol, respectively).

As expected, S-coordination of BF_3 promotes the S–N bond insertion pathway (Figure 36). However, the S-coordinated CH_3SNO-BF_3 complex is much weaker (ΔH_{LA} = -2 kcal/mol) than O- and N-coordinated forms (ΔH_{LA} ≈ -14 kcal/mol), which are stabilized by stronger N–>B and O–>B dative bonds. Although it may be possible to use a soft LA that would preferentially bind to the S atom, promotion of structure ***I*** would also further destabilize the S–N bond. Thus, promoting (3+2) cycloaddition pathway by LA N-coordination is a more practical strategy for designing an efficient RSNO labeling reaction.

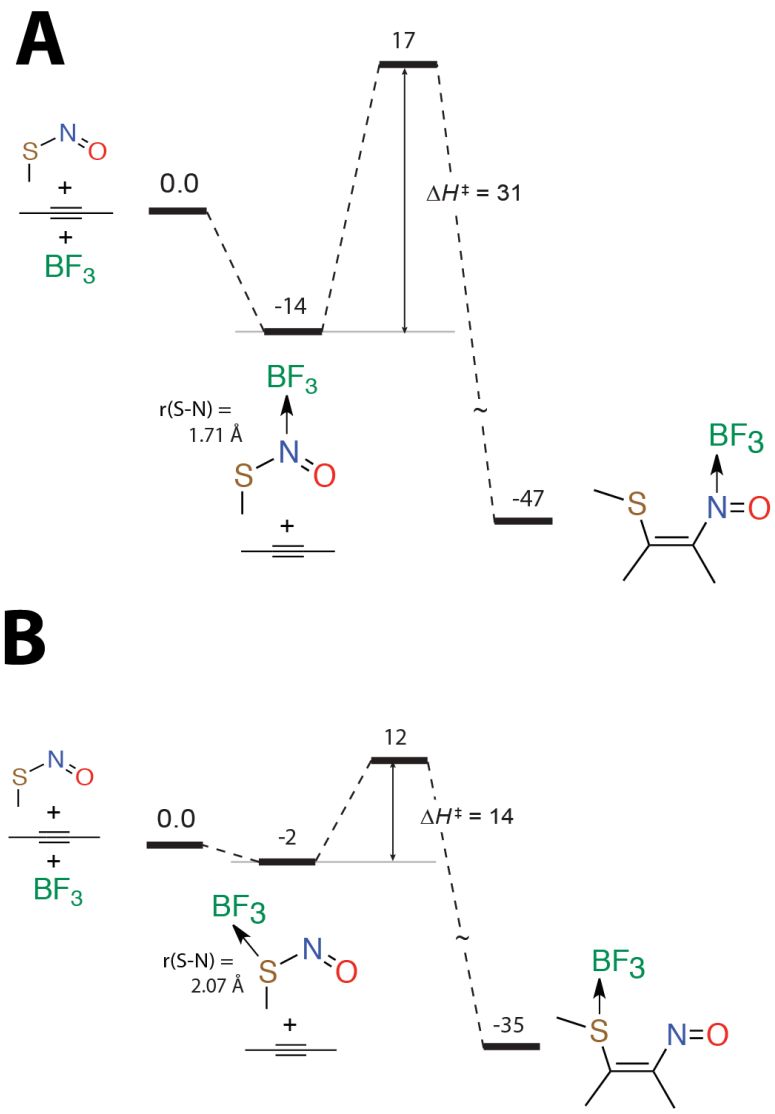

Figure 36. Enthalpic profiles for the S–N bond insertion reaction between model RSNO and alkyne: A) reaction inhibited by the LA N-coordination, and B) reaction catalyzed by the LA S-coordination.

Even with the assistance of LA catalysis, (3+2) cycloaddition barrier is still too high to make a good RSNO labeling reaction candidate. Moreover, LA-catalyzed reaction is a two-step process, involving the LA coordination at first followed by actual cycloaddition step, and requires high LA concentrations that may lead to

undesirable side reactions. The first problem can be addressed by using strain-activated alkynes and alkenes, developed for copper-free click chemistry (Figure 37, Table 29).[167,168]

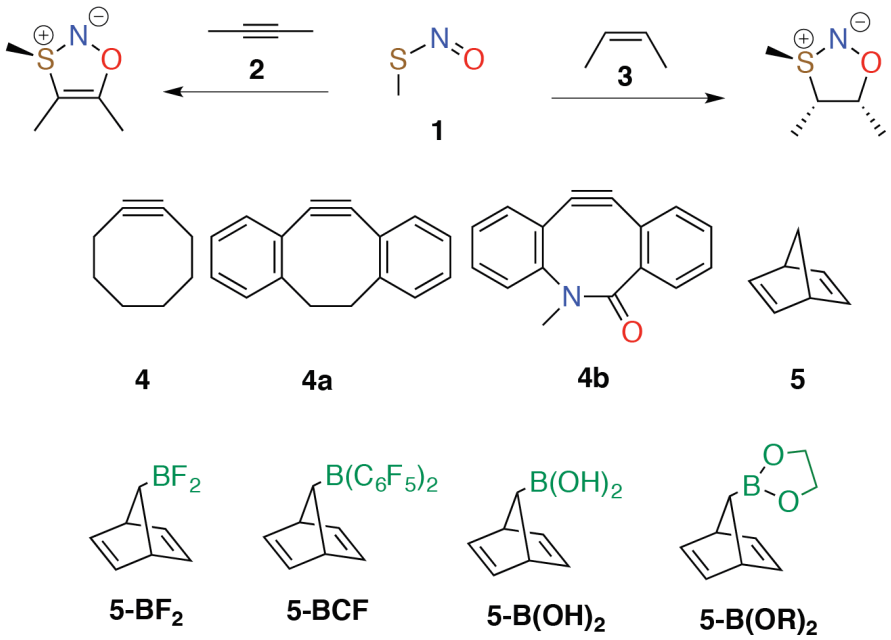

Figure 37. Prototypical (3+2) cycloaddition reaction between CH_3SNO (1), alkyne (2), alkene (3), click-chemistry reagents (4-5) and customized LA-linked reagents (5-x).

Table 29. Enthalpies of coordination of cis-CH_3SNO and Lewis Acids, 3+2 cycloaddition activation and reaction enthalpies, CH_3-S BDEs and LA binding enthalpies in 3+2 cycloaddition products (kcal/mol). Values in [Brackets] are the result of CBS-QB3 calculations in acetonitrile, the remaining results are obtained with PBE0/def2-SV(P)+d approximation also in acetonitrile.*

Reagent	LA	ΔH_{LA}	$\Delta H^{\neq}_{rxn}$	ΔH_{rxn}	$\Delta H^{\neq}_{reverse}$	BDE (S–C)	$\Delta H_{LA\text{-}P}$
2	-	-	28.1 [23.4]	-12.7 [-14.1]	40.8 [37.5]	29.2 [32.1]	-
2	BF_3 at N	-15.5 [-13.4]	17.0 [12.3]	-33.6 [-34.1]	50.7 [46.4]	40.6 [43.4]	-36.4 [-33.5]
	BF_3 at O	-12.2 [-12.5]	20.2 [17.4]	-10.8 [-11.4]	31.0 [28.8]	35.0 [37.6]	-10.3 [-10.5]
3	-	-	26.0 [20.9]	5.7 [-0.3]	20.3 [21.1]	30.4 [37.4]	-
3	BF_3 at N	-15.5 [-13.5]	12.4 [7.7]	-16.7 [-20.5]	29.0 [28.2]	44.2 [49.6]	-37.9 [-33.7]
	BF_3 at O	-12.2 [-12.5]	15.3 [10.8]	-2.7 [-7.5]	18.0 [18.3]	40.4 [46.7]	-20.7 [-19.8]
4	-	-	15.4	-23.4	38.8	28.8	-
4	BF_3 at N	-15.5	5.5	-44.6	50.1	40.4	-36.6
	BF_3 at O	-12.2	7.3	-20.9	28.1	33.7	-9.7
4a	-	-	14.7	-14.8	29.5	25.6	-
4a	BF_3 at N	-15.5	6.9	-38.8	44.3	41.7	-39.5
	BF_3 at O	-12.2	14.8	-6.4	21.7	31.7	-3.9
4b	-	-	8.3	-35.7	44.0	30.4	-
4b	BF_3 at N	-15.5	2.5	-54.4	56.9	42.7	-34.2
	BF_3 at O	-12.2	5.3	-32.1	37.4	35.4	-8.7
5	-	-	19.9 [14.8]	-7.5 [-11.5]	27.4 [26.3]	31.2 [37.6]	-
5	BF_3 at N	-15.5	9.1	-28.3	37.4	44.0	-36.2
	BF_3 at O	-12.2	8.6	-15.3	23.9	41.6	-20.0
5-BF_2	-BF_2 at N	-8.6 [-8.7]	7.8 [5.4]	-30.3 [-31.1]	38.0 [36.5]	60.6 [65.8]	-
5-$B(OH)_2$	-$B(OH)_2$ at N	-1.4	16.9	-18.7	35.6	45.0	-
5-$B(OR)_2$	-$B(OR)_2$ at N	3.9	9.2	-26.4	35.7	47.6	-
5-BCF	-BCF at N	-15.6	4.6	-32.9	37.5	60.3	-

* Reaction parameters are calculated relative to the separate dienophile and LA/cis-CH_3SNO complex for non-LA-linked reagents, and relative to the prereactive complexes for LA-linked dienophile reagents.

Table 30. Gibbs free energies of coordination of cis-CH_3SNO and Lewis Acids, 3+2 cycloaddition activation and reaction enthalpies. Values in [Brackets] are the result of CBS-QB3 calculations in acetonitrile, the remaining results are obtained with PBE0/def2-SV(P)+d approximation also in acetonitrile.*

Reagent	LA	ΔG_{LA}	$\Delta G^{\neq}_{rxn}$	ΔG_{rxn}	$\Delta G^{\neq}_{reverse}$	$\Delta G^{\neq}_{LA\text{-}P}$
2	-	-	40.0 [33.6]	-0.2 [-3.2]	40.2 [36.8]	-
2	BF_3 at N	-5.9 [-3.9]	28.4 [22.0]	-20.9 [-23.1]	49.3 [45.1]	-26.6 [-21.9]
	BF_3 at O	-2.9 [-3.1]	32.6 [26.7]	1.8 [-2.2]	30.7 [28.9]	-0.9 [0.5]
3	-	-	26.0 [20.9]	20.9 [15.4]	19.4 [20.2]	-
3	BF_3 at N	-5.9 [-3.9]	26.4 [22.6]	-1.2 [-5.0]	27.6 [27.7]	-26.1 [-21.4]
	BF_3 at O	-2.9 [-3.1]	30.6 [25.9]	13.2 [8.0]	17.4 [17.9]	-9.3 [-7.5]
4	-	-	26.7	-10.7	37.5	-
4	BF_3 at N	-5.9	16.0	-31.3	47.3	-26.5
	BF_3 at O	-2.9	19.1	-8.4	27.5	-0.5
4a	-	-	26.3	-3.2	29.6	-
4a	BF_3 at N	-5.9	17.8	-26.5	44.3	-29.2
	BF_3 at O	-2.9	26.8	5.0	21.7	5.4
4b	-	-	20.5	-22.5	43.0	-
4b	BF_3 at N	-5.9	13.8	-40.9	54.7	-24,3
	BF_3 at O	-2.9	18.0	-18.5	36.6	1.0
5	-	-	34.2 [28.9]	7.5 [3.3]	26.6 [25.6]	-
5	BF_3 at N	-5.9	23.3	-13.3	36.6	-24.8
	BF_3 at O	-2.9	23.8	0.7	23.1	-8.4
5-BF_2	-BF_2 at N	4.4 [4.4]	13.3 [9.0]	-20.3 [-26.4]	33.6 [35.5]	-
5-$B(OH)_2$	-$B(OH)_2$ at N	7.4	24.3	-10.2	34.5	-
5-$B(OR)_2$	-$B(OR)_2$ at N	17.5	12.2	-22.2	34.4	-
5-BCF	-BCF at N	0.1	6.5	-29.9	36.4	-

* Reaction parameters are calculated relative to the separate dienophile and LA/cis-CH_3SNO complex for non-LA-linked reagents, and relative to the prereactive complexes for LA-linked dienophile reagents.

CH_3SNO (3+2) cycloaddition barriers are 6–13 kcal/mol lower for the strain-activated cyclooctyne 4 or norbornadiene 5, compared to the model reagents 2 (alkyne) and 3 (alkene), see Table 28. Nonetheless, these reaction barriers are still high compared to the click reactions of the same dipolarophile molecules with azides.[176,177]

LA-assisted cycloadditions with strain-activated alkynes demonstrate a promising improvement over the non-catalyzed reactions. For example, the reaction of the N-coordinated BF_3-CH_3SNO complex with 4b, biarylazacyclooctynone (BARAC),[178] a powerful click chemistry reagent, has a predicted activation enthalpy of 2.5 kcal/mol (at PBE0/def2SV(P)+d level). However, the requirement of preliminary RSNO/LA complexation, as well as possible LA dissociation from the cycloaddition product, may complicate further practical implementation in proteomic analysis for an efficient CysNO detection.

To overcome these problems, we propose to use customized reagents that combine both strain-activated carbon-carbon double/triple bond and a LA moiety in one molecule. Ideally, both components of the reagent molecule should be linked together by a rigid scaffold and located in a specific spatial arrangement, resembling the structure of LA-catalyzed cycloaddition TS_{Cycl} (Figure 34).

We tested a variety of scaffolds based on existing copper-free click chemistry reagents[167,168] (Table 29) and found that norbornadiene[168] scaffold can combine a strain-activated C=C double bond and a LA moiety in a near-attack[179]arrangement perfect for the cycloaddition reaction (Figures 38, 39).

Norbornadiene (reagent 5) is predicted to undergo (3+2) cycloaddition with RSNO relatively easily ($\Delta H^{\ddagger}$ = 15 kcal/mol, Figure 38), and the reaction is greatly enhanced by N-coordination of BF_3 ($\Delta H^{\ddagger}$ = 4 kcal/mol).

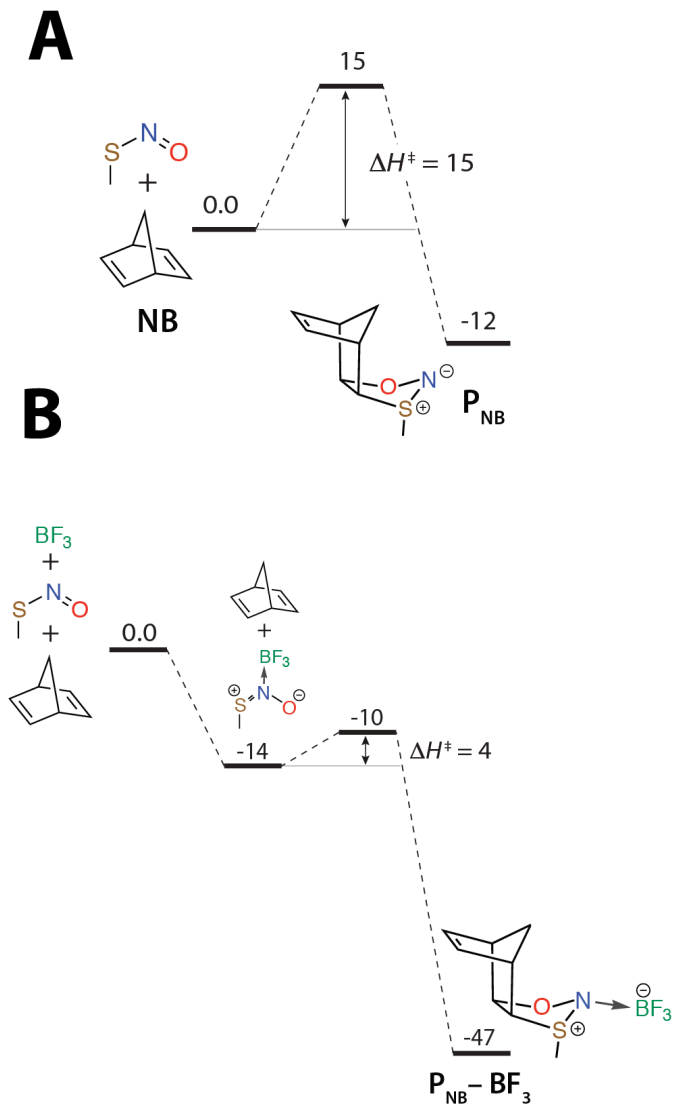

Figure 38. Enthalpic profiles (in kcal/mol) for (3+2) cycloaddition reactions between norbornadiene NB (reagent 5) and a model RSNO (A), NB and RSNO activated by N-coordiantion of BF_3 (B).

A prototype linked reagent 5-BF_2 with a LA group –BF_2 attached to the bridging carbon N-coordinates to MeSNO less exothermally than BF_3 (ΔH_{LA} = -9 vs -

14 kcal/mol respectively), although the subsequent cycloaddition is as easy ($\Delta H^{\ddagger}$ = 5 kcal/mol, Figure 39). Importantly, the cycloaddition step is a monomolecular, not bimolecular, reaction of the donor-acceptor complex between CH_3SNO and 5-BF_2. The reaction product is 40 kcal/mol lower in enthalpy than the separated reactants, and has an adamantane-like cage (Figure 39) that incorporates the –SNO group ligated by two covalent and one strong (~30 kcal/mol) N–B dative bond.

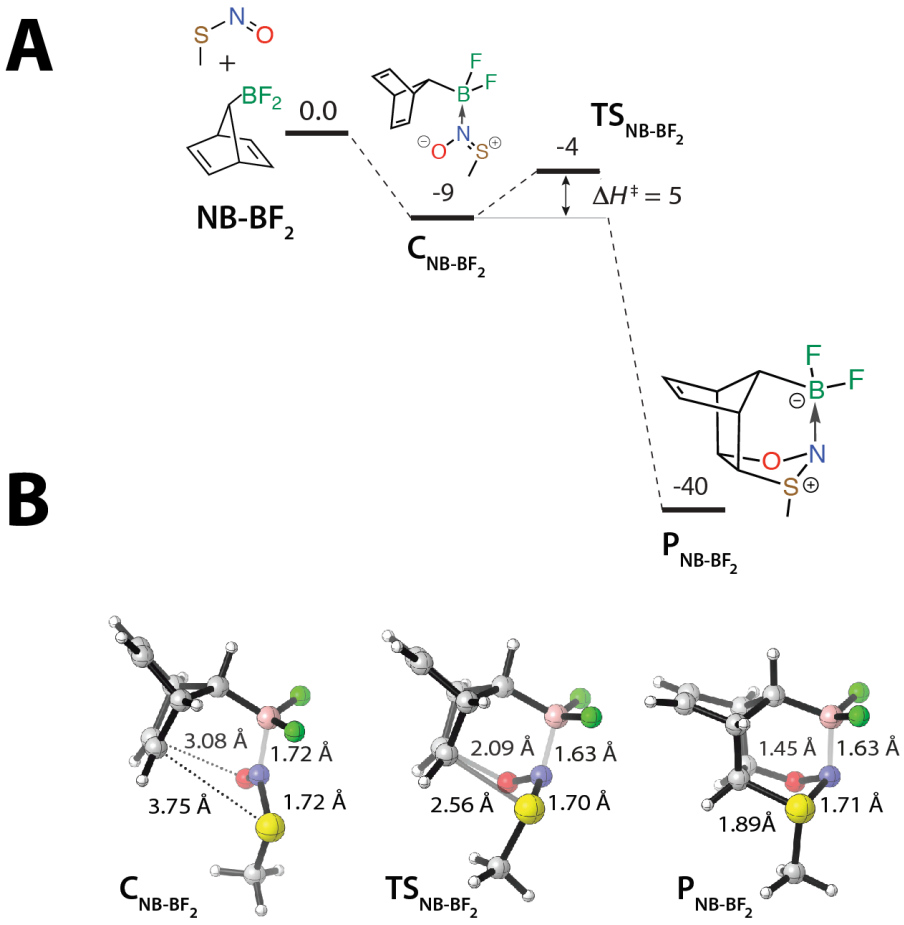

Figure 39. Enthalpic profiles (in kcal/mol) for (3+2) cycloaddition reactions between LA-linked norbornadiene NB-BF_2 (reagent 5-BF_2) and RSNO (A); calculated structures for the pre-reactive complex C_{NB}-BF_2, transition state TS_{NB}-BF_2, and product P_{NB}-BF_2 of the RSNO—NB-BF_2 cycloaddition reaction (B).

In terms of free energies, the overall reaction of CH_3SNO with 5-BF_2 is more thermodynamically favorable than BF_3-activated reaction with 5 (ΔG_{rxn}= -26 vs -20 kcal/mol, respectively, Figure 40) with a significantly lower activation barrier ($\Delta G^{\ddagger}$= 9 vs 18 kcal/mol, respectively). Thus, although the concentrations of the donor-acceptor 5-BF_2–RSNO complexes may be lower than BF_3–RSNO complexes, the overall cycloaddition process should be much more efficient with 5-BF_2.

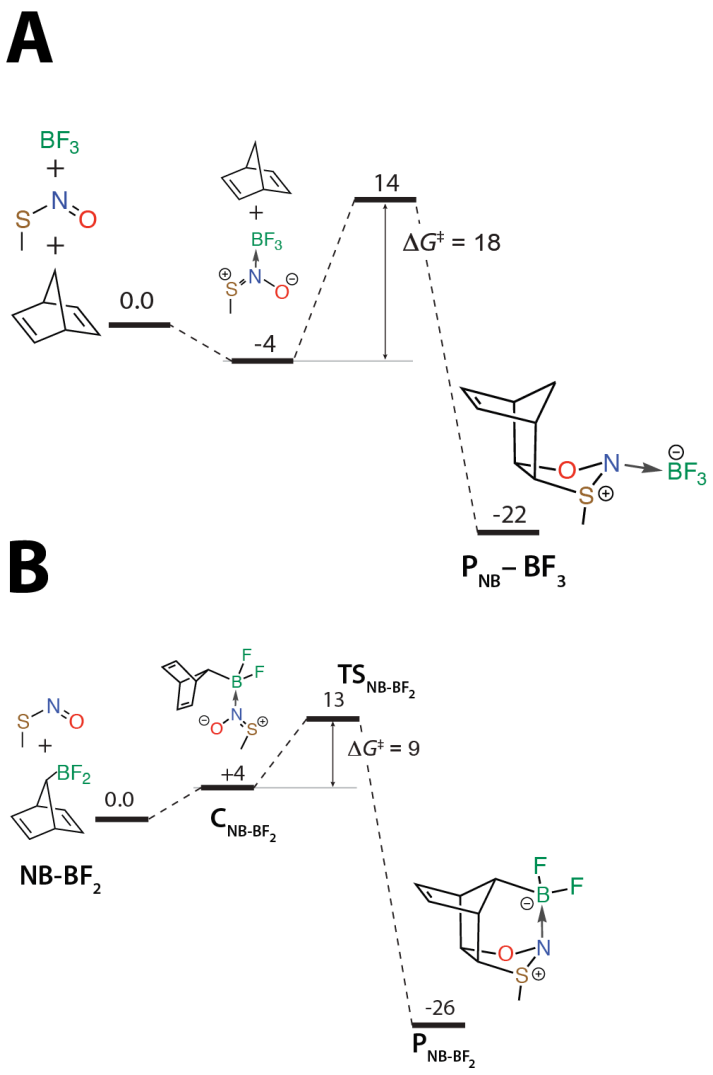

Figure 40. Gibbs free energy profiles (in kcal/mol) for (3+2) cycloaddition reactions between reagent 5 and RSNO, activated by N-coordiantion of BF_3 (A); LA-linked norbornadiene NB-BF_2 (reagent 5-BF_2) and RSNO (B).

In the case of the LA-linked reagent, a combination of several factors gives rise to reaction that could be comparable in efficiency with click chemistry[167,168] reactions. The initial N-coordination partially compensates the entropic penalty for bringing the C=C and SNO groups together, helps them to attain a proper near-attack orientation (Figure 39 B), and catalyzes the ensuing monomolecular cycloaddition. As the reaction proceeds, the developing negative charge on the N atom strengthens the N→LA dative bond, driving the reaction downhill. Norbornadiene scaffold provides nearly ideal spatial arrangement of the alkene and LA moieties, although future design of RSNO labeling reagents could be also based on other activated alkenes and alkynes,[167,168] as well as other Lewis acids. Our preliminary results demonstrate that modulation of the strength of the LA component leads to corresponding changes in reactivity: a reagent with stronger LA (5-BCF) has more exothermic binding enthalpies and lower (3+2) activation barriers, than the weaker LA reagents (5-$B(OH)_2$ and 5-$B(OR)_2$) (Figure 41).

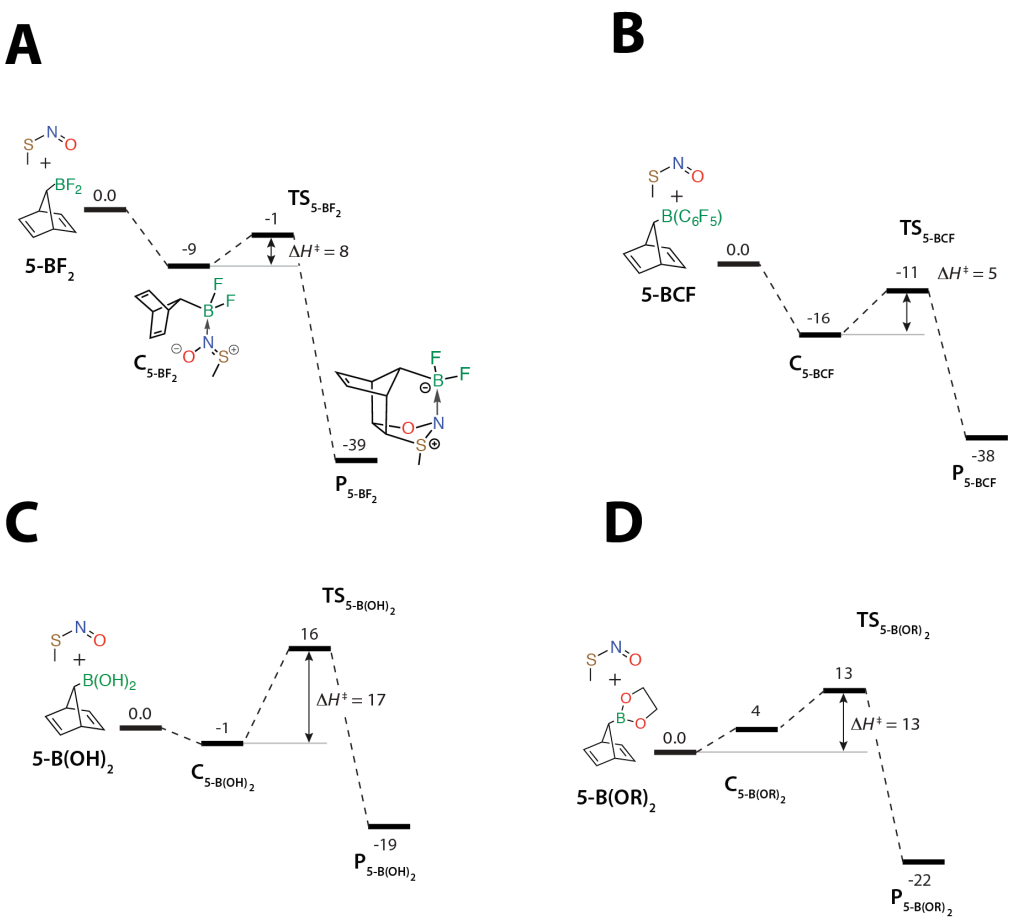

Figure 41. Enthalpic profiles (in kcal/mol) of LA-linked reagents, calculated with PBE0/def2-SV(P)+d approximation in acetonitrile: 5-BF_2 (A), 5-BCF (B), 5-$B(OH)_2$, 5-$B(OR)_2$.

3. Boron-based Lewis acids: N vs. O coordination

(3+2) Cycloaddition reactions of RSNOs can be correlated with the contribution of the zwitterionic structure ***D***, which is promoted by N or O-coordination of a Lewis acid to the SNO group. However, efficient catalysis of (3+2) cycloaddition specifically requires LA coordination on N atom, because strengthening of the N–B dative bond in the cycloaddition product with negatively charged N atom is essential for the increase of the driving force of the reaction.

Considering that O and N atoms in RSNOs have comparable basicity, it is important to ensure N-coordination of the Lewis acid for efficient catalysis of RSNO cycloaddition reactions. Therefore, we investigated coordination of boron-based Lewis acids on the example of the model tertiary RSNO, the adamantil-SNO (AdSNO), with BCF in collaboration with T. Warren group (Georgetown University).

Computationally (Table 31), at the PBE0-GD3BJ/def2-SV(P)+d (PCM, diethylether) level BCF coordination to the SNO group atoms is the most preferable in the case of O-coordination. In fact, given that the O atom has two lone pairs, we observed two possible coordination structures (Figure 42). The second structure is about 3 kcal/mol higher in energy.

Table 31. Calculated parameters of the AdSNO-LA complexes.

Complex	ΔH, kcal/mol	S–N, Å	ΔS–N, Å	S–N BDE, kcal/mol	ΔS–N BDE, kcal/mol
Trans-AdSNO/BF_3 complexes					
Trans-O #1	0.0	1.630	-0.135	43.0	10.9
Trans-O #2	0.5	1.632	-0.134	42.5	10.4
Trans-N	2.7	1.709	-0.057	38.8	6.7
Trans-S	8.6	1.828	+0.062	24.1	-8.0
Trans-AdSNO/BCF complexes					
Trans-O #1	0.0	1.615	-0.151	49.0	16.9
Trans-O #2	3.1	1.623	-0.143	45.9	13.8
Trans-N	5.8	1.728	-0.037	42.3	10.3
Trans-S	13.3	1.916	+0.150	15.0	-17.1

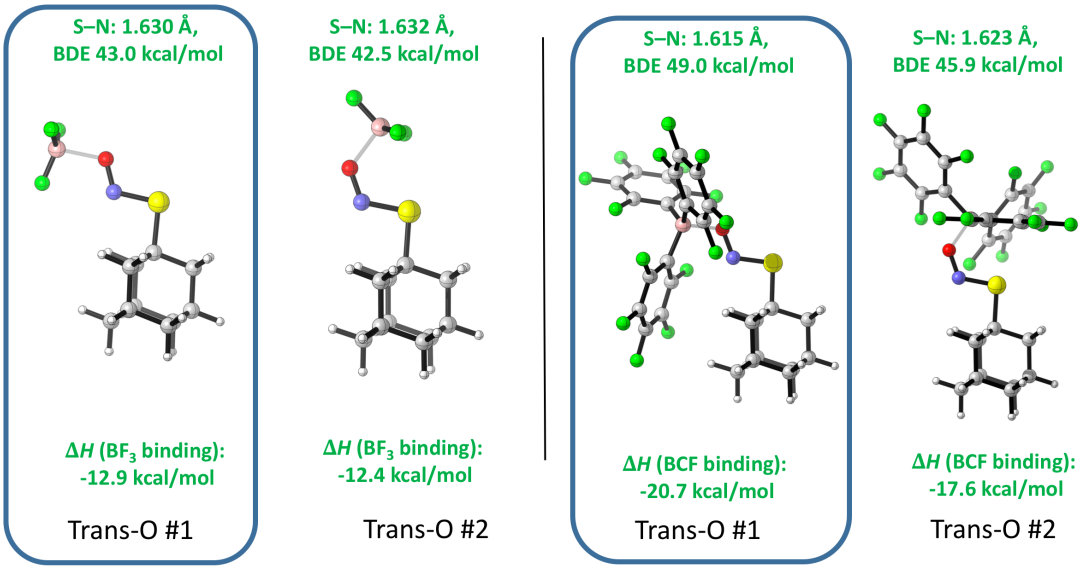

Figure 42. Trans-AdSNO O-coordinated complexes with BF_3 and BCF in diethylether (S–N bond length for the free trans-AdSNO is 1.766 Å, S–N BDE 32.1 kcal/mol). More stable structures are circled.

N-coordination is less favorable, about 6 kcal/mol higher in energy than the lowest O-coordination structure, while S-coordination is least probable as the S-coordinated complex is more than 13 kcal/mol higher in energy (Figure 43).

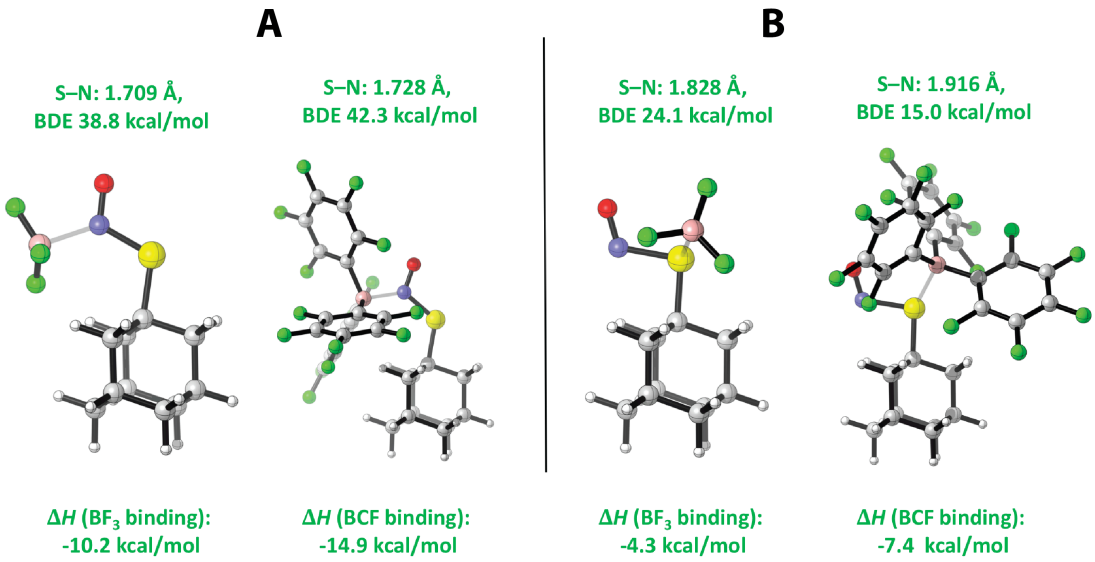

Figure 43. Trans-AdSNO N-coordinated complexes (A) and S-coordinated complexes (B) with BF_3 and BCF in diethylether.

Similar relative energies are observed in the case of coordination if a weaker LA, BF_3, although the O vs. N-coordination structure energy difference is smaller, about 3 kcal/mol, likely due to the less prominent steric repulsion with the adamantyl moiety.

The calculated modulation of the S–N bond properties follows the expected trends, commensurate with the strength of the Lewis acid. In particular, O-coordination shortens the S–N bond by 0.15 Å for the BCF and by 0.14 Å for BF_3, and significantly increases the S–N bond dissociation energy (by 17 and 11 kcal/mol, respectively). N-coordination has a weaker effect on the S–N bond shortening (0.06 and 0.04 Å) and strengthening (10 and 7 kcal/mol). S-coordination expectedly lengthens and weakens the S–N bond (by 0.15 and 0.06 Å, 17 and 8 kcal/mol for BCF and BF_3).

In addition to the calculated properties of the S–N bond, we were able to quantify the observed modulation of the SNO group electronic structure using Natural Resonance Theory (NRT) for the lowest-energy O-coordinated AdSNO/BF_3 complex (Figure 44), which demonstrates significant (13%) increase in the contribution of the structure ***D*** at the expense the structure ***I*** (6%) and structure ***S*** (7%).

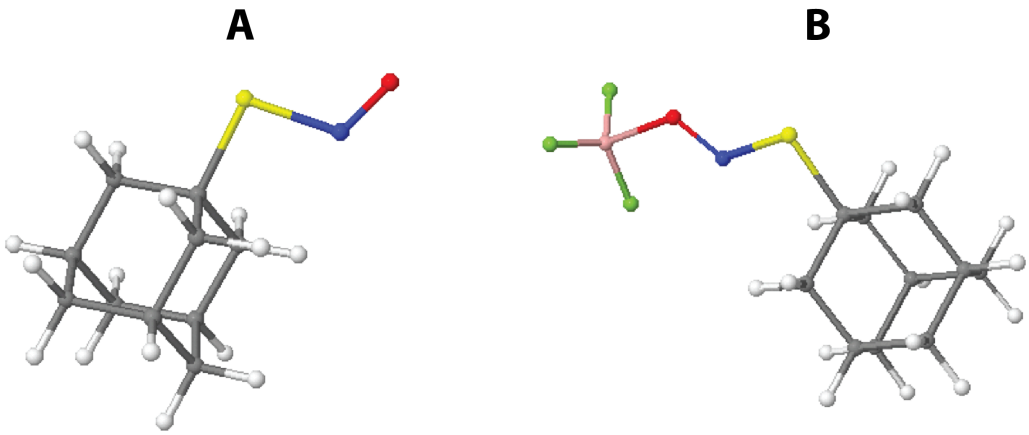

Figure 44. S, D and I balance in free trans-AdSNO (A) and in O-coordinated BF3 complex (B).

In agreement with our computational results, suggesting that the O-coordinated AdSNO/BCF complex is the lowest energy structure, our collaborators at Prof. Warren lab (A. McQuilken, T. Warren, unpublished) were able to prepare and isolate the O-coordinated complex, and to experimentally determine its structure using X-ray spectroscopy (Figure 45). These experimental results for the first time provided a direct evidence of dramatic shortening of the S–N bond upon O-coordination of Lewis acids. The calculated and experimental values of the S–N bond length in this complex are in excellent agreement with each other (1.62 Å calculated, 1.63 Å experimental).

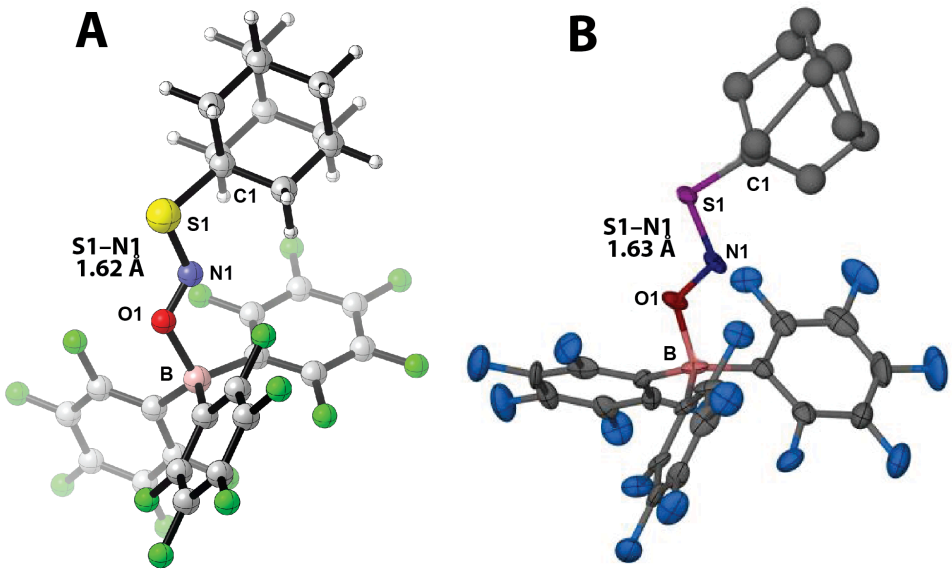

Figure 45. Experimental (on the right) and theoretically predicted (on the left) structures of the oxygen-bound AdSNO/BCF adduct.

The time-dependent DFT calculations (TD-DFT) of the excited states of free AdSNO and O-coordinated AdSNO/LA complex support complex formation not only in the form of a crystal, but also in solution, since the calculations predict the disappearance of a weak symmetry-forbidden n–>π* transition ≈600 nm in the O-coordinated complex, which is consistent with experimentally observed bleaching of the corresponding absorption band (Figure 46, A. McQuilken, T. Warren, unpublished). This bleaching occurs due to the lowering of the energy of corresponding n orbital in AdSNO/BCF complex after the formation of dative O–B bond.

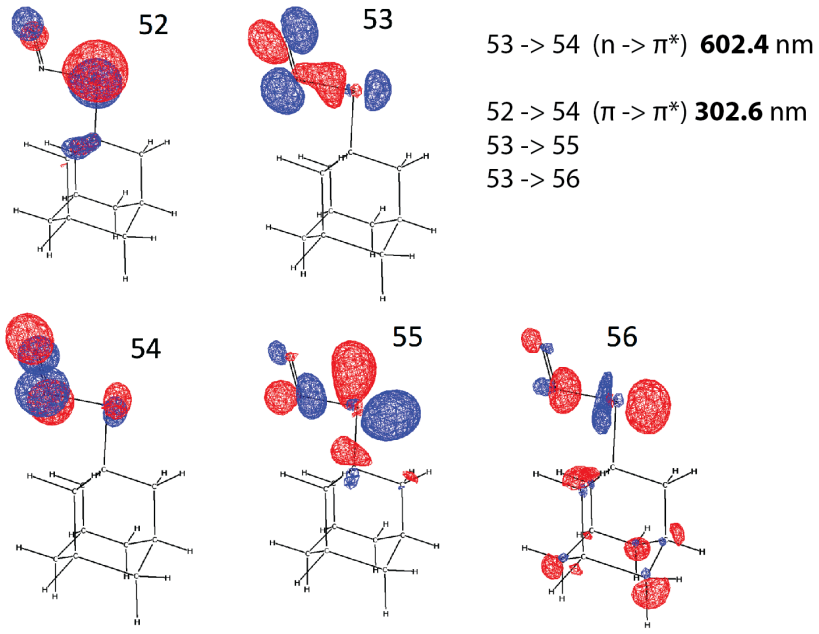

Figure 46. Electronic transitions in free AdSNO, calculated with TD-PBE0-GD3/def2-TZVPPD, PCM (toluene).

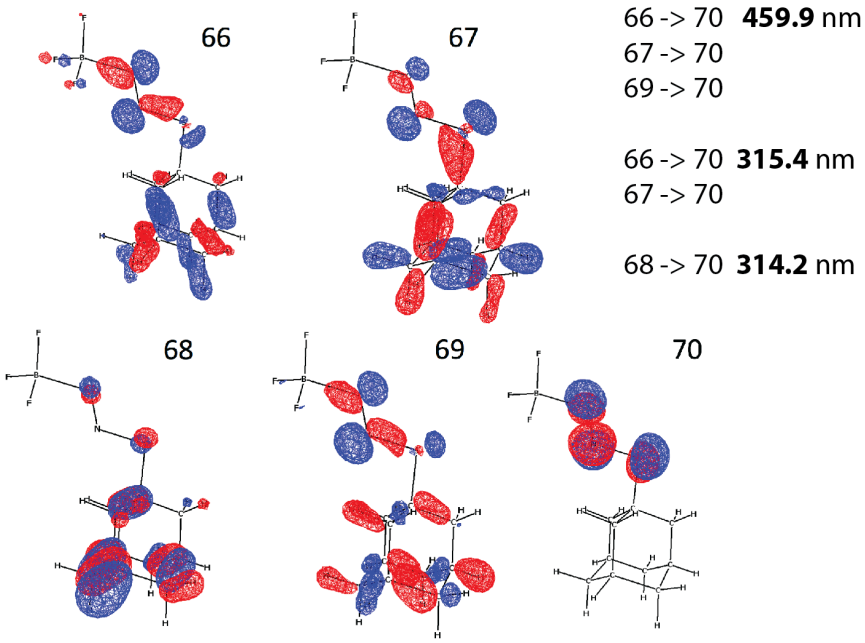

Figure 47. Electronic transitions in O-coordinated AdSNO/BF_3 complex, calculated with TD-PBE0-GD3/def2-TZVPPD, PCM (toluene).

However, similar bleaching of n–>π* transition is also predicted for the N-coordinated structure (Figures 47, 48). Therefore, coexistence of O-coordinated and N-coordinated forms of the AdSNO/BCF complex in solution cannot be completely excluded, although the calculated energy difference, i.e. 6 kcal/mol, suggest that the N-coordinated form is unlikely to have a significant concentration in solution.

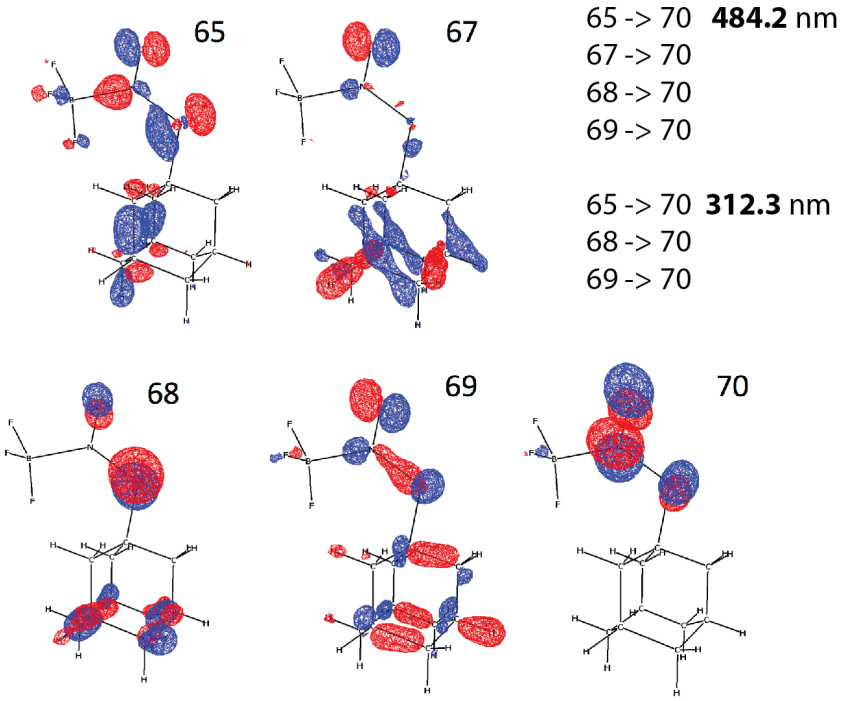

Figure 48. Electronic transitions in N-coordinated AdSNO/BF_3 complex, calculated with TD-PBE0-GD3/def2-TZVPPD, PCM (toluene).

These preliminary experimental results provide a solid validation of our computational approach for the assessment of the energy preference for O vs. N coordination of boron-based Lewis acids. Therefore, although we do not expect that experimentally observed O-coordinated AdSNO/BCF complex would readily

undergo (3+2) cycloaddition reaction, we are reasonably optimistic that the proposed in this work LA-linked norbornadiene reagents would undergo the predicted 1,3-dipolar cycloaddition reaction (Figure 39) since the PBE0 and CBS-QB3 calculations (Table 32, Figure 49), used to model the cycloaddition reaction, and PBE0-GD3 results predict that the N-coordination of reagent 5-BF_2 is by 4-6 kcal/mol more probable than the O-coordination.

Table 32. N vs. O-coordination of 5-BF_2 reagent and CH_3SNO molecule.

Complex	ΔH, kcal/mol	ΔG, kcal/mol
CBS-QB3, PCM (acetonitrile)		
N-coord	-8.7	4.4
O-coord	-4.6 (+4.1)	7.3 (+2.9)
PBE0/def2-SV(P)+d, PCM (acetonitrile)		
N-coord	-8.6	4.3
O-coord	-3.1 (+5.5)	9.4 (+5.1)
PBE0-GD3/def2-SV(P)+d, PCM (acetonitrile)		
N-coord	-12.8	0.7
O-coord	-6.5 (+6.3)	6.3 (+5.6)

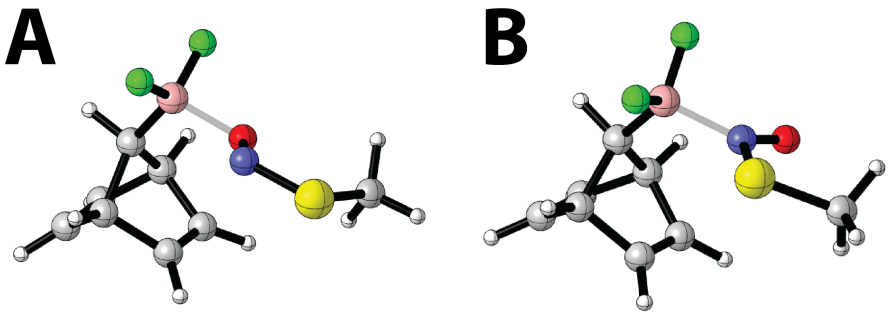

Figure 49. Structures of O-coordinated (A) and N-coordinated (B) CH_3SNO molecule and 5-BF_2 reagent.

D. Conclusions

We demonstrated that the computationally predicted reactivity of RSNOs with alkenes and alkynes is related to the unusual antagonistic nature of the –SNO group electronic structure. However, (3+2) cycloaddition reactions may be useful for RSNO labeling if activated by a LA N-coordination to the RSNO.

In particular, reagents that combine a strain-activated double/triple carbon-carbon bond and a LA moiety in a proper spatial arrangement should be the most efficient in reactions with RSNOs. Development of practical labeling techniques using these principles will undoubtedly require significant experimental and computational effort. Besides efficiency in the reactions with RSNOs, practical considerations such as solubility and stability in water, bioorthogonality, and synthetic feasibility will have to be taken into account.

In this respect, the prototype reagents (5-BF_2, 5-$B(OH)_2$, 5-$B(OR)_2$ and 5-BCF) proposed here might not be immediately useful for labeling of protein RSNOs, although those or similar molecules could be a good model for the first proof-of-concept experiments with simple RSNOs in non-aqueous environment. Nonetheless, we believe that the elegant 'click-like' chemistry of RSNOs, devised from simple chemical ideas and confirmed by computational modeling, will soon find an experimental confirmation that may lead to novel efficient one-step labeling reactions for identification of S-nitrosated cysteine residues in proteins.

Summary

In the present study, we demonstrate that modern computational chemistry tools allow one to accurately predict the structure and properties of the molecules of interest at reasonable computational cost. In particular cases (CH_3SNO molecule), chemical accuracy threshold can be approached with the use of explicitly-correlated coupled cluster theory and carefully tested DFT methods. Furthermore, incorporation of those DFT methods into a multi-scale ONIOM model unlocks the potential to study significantly larger biomolecules, such as proteins.

In the case of theoretical studies of S-nitrosated cysteine (CysNO), it became clear that the underlying complex and flexible electronic structure of the SNO group will determine its observable reactivity and properties. The *ab initio* CH_3SNO model for the first time highlighted that the S–N bond in CysNO, despite the low stretching frequency (398.2 cm^{-1} in cis-CH_3SNO, and 386.1 cm^{-1} in trans-CH_3SNO) and bond dissocaition eenrgy (≈32 kcal/mol in solution) is expected to have a remarkably harmonic character, which makes the further computational studies of CysNO reaction pathways more attainable.

The ONIOM models of CysNO in α-helix and a model protein (DJ-1) pointed out that unique for the protein environment spatial and electrostatic effects can play a significant role in changing the properties of SNO group. Thus, structurally predetermined coordination of the charged residues in the proximity of CysNO affects its structure (S–N bond length increases and decreases in the range from 1.62 to 1.85 Å), as well as the conformational dynamics (activation barriers vary in

the range from 9.6 to 24.2 kcal/mol). The theoretical model of an actual protein, DJ-1, demonstrated that the presence of charged residue in the proximity of CysNO group is likely to affect its properties and reactivity. Those findings can potentially assist both experimental and theoretical studies, aimed to reveal the nature of elegant protein control over the CysNO chemistry, as well as molecular mechanisms of pathological breakdowns of those crucial reactions.

The novel theoretically proposed reaction mechanisms of CysNO labeling revealed that Lewis acid coordination with CysNO and RSNOs in general appears to be a potent mechanism of driving RSNO reactivity in a desired direction, to promote selected chemical mechanisms and avert the others. Inspired by the potential ways to control the CysNO reactivity, we propose that (3+2) cycloaddition reaction can be made possible with carefully designed reagent, combining both the dipolarophile and LA components in one molecule. The emerging experimental evidence of RSNO/LA complexation and subsequent change of RSNO properties makes us believe that theoretical tools can be effectively used in synergy with the experiment, to assist the challenging field of of S-nitrosoproteomics.

BIBLIOGRAPHY

(1) Anand, P.; Stamler, J. S. Enzymatic mechanisms regulating protein S-nitrosylation: implications in health and disease. *Journal of molecular medicine* **2012**, *90*, 233–244.

(2) Smith, B. C.; Marletta, M. A. Mechanisms of S-nitrosothiol formation and selectivity in nitric oxide signaling. *Curr Opin Chem Biol* **2012**, *16*, 498–506.

(3) Raju, K.; Doulias, P. T.; Tenopoulou, M.; Greene, J. L.; Ischiropoulos, H. Strategies and tools to explore protein S-nitrosylation. *Biochim Biophys Acta* **2012**, *1820*, 684–688.

(4) Gaucher, C.; Boudier, A.; Dahboul, F.; Parent, M.; Leroy, P. S-nitrosation/denitrosation in cardiovascular pathologies: facts and concepts for the rational design of S-nitrosothiols. *Curr Pharm Des* **2013**, *19*, 458–472.

(5) Williams, D. L. H. The chemistry of S-nitrosothiols. *Accounts of chemical research* **1999**, *32*, 869–876.

(6) Talipov, M. R.; Timerghazin, Q. K. Protein control of S-nitrosothiol reactivity: interplay of antagonistic resonance structures. *J Phys Chem B* **2013**, *117*, 1827–1837.

(7) Moran, E. E.; Timerghazin, Q. K.; Kwong, E.; English, A. M. Kinetics and mechanism of S-nitrosothiol acid-catalyzed hydrolysis: sulfur activation promotes facile NO+ release. *J Phys Chem B* **2011**, *115*, 3112–3126.

(8) Consortium, U. The universal protein resource (UniProt). *Nucleic acids research* **2008**, *36*, D190–D195.

(9) Pratt, C. W.; Voet, D.; Voet, J. G. Fundamentals of biochemistry: life at the molecular level. *Jonh Wiley and Sons* **2008**, .

(10) Khoury, G. A.; Baliban, R. C.; Floudas, C. A. Proteome-wide post-translational modification statistics: frequency analysis and curation of the swiss-prot database. *Sci Rep* **2011**, *1*, .

(11) Bairoch, A.; Boeckmann, B. The SWISS-PROT protein sequence data bank. *Nucleic Acids Research* **1991**, *19*, 2247.

(12) Blom, N.; Sicheritz-Pontén, T.; Gupta, R.; Gammeltoft, S.; Brunak, S. Prediction of post-translational glycosylation and phosphorylation of proteins from the amino acid sequence. *Proteomics* **2004**, *4*, 1633–1649.

(13) Wiktorowicz, J. E.; Stafford, S. J.; Garg, N. J. Protein Cysteinyl-S-Nitrosylation: Analysis and Quantification. *Methods in Enzymology* **2017**, .

(14) Cieśla, J.; Frączyk, T.; Rode, W. Phosphorylation of basic amino acid residues in proteins: important but easily missed. *Acta Biochim Pol* **2011**, *58*, 137–148.

(15) Cole, P. A.; Shen, K.; Qiao, Y.; Wang, D. Protein tyrosine kinases Src and Csk: a tails tale. *Current opinion in chemical biology* **2003**, *7*, 580–585.

(16) van Weeren, P. C.; de Bruyn, K. M.; de Vries-Smits, A. M.; Van Lint, J.; Boudewijn, M. T. Essential role for protein kinase B (PKB) in insulin-induced glycogen synthase kinase 3 inactivation characterization of dominant-negative mutant of PKB. *Journal of Biological Chemistry* **1998**, *273*, 13150–13156.

(17) Babior, B. M. NADPH oxidase: an update. *Blood* **1999**, *93*, 1464–1476.

(18) Bates, S.; Vousden, K. H. p53 in signaling checkpoint arrest or apoptosis. *Current opinion in genetics & development* **1996**, *6*, 12–18.

(19) Nakamura, T.; Lipton, S. A. Emerging role of protein-protein transnitrosylation in cell signaling pathways. *Antioxid Redox Signal* **2013**, *18*, 239–249.

(20) Stamler, J. S.; Lamas, S.; Fang, F. C. Nitrosylation. the prototypic redox-based signaling mechanism. *Cell* **2001**, *106*, 675–683.

(21) Hess, D. T.; Matsumoto, A.; Kim, S. -O.; Marshall, H. E.; Stamler, J. S. Protein S-nitrosylation: purview and parameters. *Nature Reviews Molecular Cell Biology* **2005**, *6*, 150–166.

(22) Ignarro, L. J.; Buga, G. M.; Wood, K. S.; Byrns, R. E.; Chaudhuri, G. Endothelium-derived relaxing factor produced and released from artery and vein is nitric oxide. *Proceedings of the National Academy of Sciences* **1987**, *84*, 9265–9269.

(23) Palmer, R. M.; Ferrige, A. G.; Moncada, S. Nitric oxide release accounts for the biological activity of endothelium-derived relaxing factor. *Nature* **1987**, *327*, 524–526.

(24) Martínez-Ruiz, A.; Cadenas, S.; Lamas, S. Nitric oxide signaling: classical, less classical, and nonclassical mechanisms. *Free Radic Biol Med* **2011**, *51*, 17–29.

(25) Heinrich, T. A.; daSilva, R. S.; Miranda, K. M.; Switzer, C. H.; Wink, D. A.; Fukuto, J. M. Biological Nitric Oxide Signaling: Chemistry and Terminology (NO Chemical Biology and Terminology). *British journal of pharmacology* **2013**, .

(26) Zaffagnini, M.; De Mia, M.; Morisse, S.; Di Giacinto, N.; Marchand, C. H.; Maes, A.; Lemaire, S. D.; Trost, P. Protein S-nitrosylation in photosynthetic organisms: A comprehensive overview with future perspectives. *Biochim Biophys Acta* **2016**, .

(27) Arasimowicz-Jelonek, M.; Floryszak-Wieczorek, J. Nitric Oxide in the Offensive Strategy of Fungal and Oomycete Plant Pathogens. *Frontiers in Plant Science* **2016**, *7*, 252.

(28) Laver, J. R.; McLean, S.; Bowman, L. A.; Harrison, L. J.; Read, R. C.; Poole, R. K. Nitrosothiols in bacterial pathogens and pathogenesis. *Antioxid Redox Signal* **2013**, *18*, 309–322.

(29) Cutler, M. J.; Plummer, B. N.; Wan, X.; Sun, Q. A.; Hess, D.; Liu, H.; Deschenes, I.; Rosenbaum, D. S.; Stamler, J. S.; Laurita, K. R. Aberrant S-nitrosylation mediates calcium-triggered ventricular arrhythmia in the intact heart. *Proc Natl Acad Sci U S A* **2012**, *109*, 18186–18191.

(30) Honbou, K.; Suzuki, N. N.; Horiuchi, M.; Niki, T.; Taira, T.; Ariga, H.; Inagaki, F. The crystal structure of DJ-1, a protein related to male fertility and Parkinson's disease. *J Biol Chem* **2003**, *278*, 31380–31384.

(31) Tao, X.; Tong, L. Crystal structure of human DJ-1, a protein associated with early onset Parkinson's disease. *J Biol Chem* **2003**, *278*, 31372–31379.

(32) De Lau, L. M.; Breteler, M. M. Epidemiology of Parkinson's disease. *The Lancet Neurology* **2006**, *5*, 525–535.

(33) Choi, M. S.; Nakamura, T.; Cho, S. J.; Han, X.; Holland, E. A.; Qu, J.; Petsko, G. A.; Yates, J. R.; Liddington, R. C.; Lipton, S. A. Transnitrosylation from DJ-1 to PTEN attenuates neuronal cell death in parkinson's disease models. *J Neurosci* **2014**, *34*, 15123–15131.

(34) Nakamura, T.; Tu, S.; Akhtar, M. W.; Sunico, C. R.; Okamoto, S.; Lipton, S. A. Aberrant protein s-nitrosylation in neurodegenerative diseases. *Neuron* **2013**, *78*, 596–614.

(35) Meyer, B.; Genoni, A.; Boudier, A.; Leroy, P.; Ruiz-Lopez, M. Structure and Stability Studies of Pharmacologically Relevant S-nitrosothiols: A Theoretical Approach. *J Phys Chem A* **2016**, .

(36) Bartberger, M. D.; Mannion, J. D.; Powell, S. C.; Stamler, J. S.; Houk, K. N.; Toone, E. J. SN dissociation energies of S-nitrosothiols: on the origins of nitrosothiol decomposition rates. *Journal of the American Chemical Society* **2001**, *123*, 8868–8869.

(37) Stamler, J. S.; Hess, D. T. Nascent nitrosylases. *Nature cell biology* **2010**, *12*, 1024–1026.

(38) Zhang, R.; Hess, D. T.; Reynolds, J. D.; Stamler, J. S. Hemoglobin S-nitrosylation plays an essential role in cardioprotection. *J Clin Invest* **2016**, .

(39) Bach, R. D.; Ayala, P. Y.; Schlegel, H. B. A reassessment of the bond dissociation energies of peroxides. An ab initio study. *Journal of the American Chemical Society* **1996**, *118*, 12758–12765.

(40) Lyn H áWilliams, D. Metal ion catalysis in nitrosothiol (RSNO) decomposition. *Journal of the Chemical Society, Chemical Communications* **1993**, 1758–1759.

(41) JonathanáBarnett, D.; Lyn H áWilliams, D. Catalysis by Cu2+ of nitric oxide release from S-nitrosothiols (RSNO). *Journal of the Chemical Society, Perkin Transactions 2* **1995**, 741–745.

(42) Rose, P. W.; Bi, C.; Bluhm, W. F.; Christie, C. H.; Dimitropoulos, D.; Dutta, S.; Green, R. K.; Goodsell, D. S.; Prlić, A.; Quesada, M. The RCSB Protein Data Bank: new resources for research and education. *Nucleic acids research* **2013**, *41*, D475–D482.

(43) Koo, S. -J.; Spratt, H. M.; Soman, K. V.; Stafford, S.; Gupta, S.; Petersen, J. R.; Zago, M. P.; Kuyumcu-Martinez, M. N.; Brasier, A. R.; Wiktorowicz, J. E. S-Nitrosylation Proteome Profile of Peripheral Blood Mononuclear Cells in Human Heart Failure. *International Journal of Proteomics* **2016**, *2016*, .

(44) Sliwoski, G.; Kothiwale, S.; Meiler, J.; Lowe, E. W. Computational methods in drug discovery. *Pharmacol Rev* **2014**, *66*, 334–395.

(45) Kapetanovic, I. M. Computer-aided drug discovery and development (CADDD): in silico-chemico-biological approach. *Chem Biol Interact* **2008**, *171*, 165–176.

(46) Dixon, D. A.; Feller, D.; Peterson, K. A.; Wheeler, R. A.; Tschumper, G. S. A Practical Guide to Reliable First Principles Computational Thermochemistry Predictions Across the Periodic Table. *Annual Reports in Computational Chemistry* **2012**, *8*, 1-28.

(47) Peterson, K. A.; Feller, D.; Dixon, D. A. Chemical accuracy in ab initio thermochemistry and spectroscopy: current strategies and future challenges. *Theoretical Chemistry Accounts* **2012**, *131*, 1-20.

(48) Talipov, M. R.; Khomyakov, D. G.; Xian, M.; Timerghazin, Q. K. Computational design of S-nitrosothiol "click" reactions. *J Comput Chem* **2013**, *34*, 1527–1530.

(49) Ivanova, L. V.; Anton, B. J.; Timerghazin, Q. K. On the possible biological relevance of HSNO isomers: a computational investigation. *Phys Chem Chem Phys* **2014**, *16*, 8476–8486.

(50) Flister, M.; Timerghazin, Q. K. Structure, Stability, and Substituent Effects in Aromatic S Nitrosothiols: The Crucial Effect of a Cascading Negative Hyperconjugation/Conjugation Interaction. *J Phys Chem A* **2014**, .

(51) Ivanova, L. V.; Cibich, D.; Deye, G.; Talipov, M. R.; Timerghazin, Q. Modeling of S-Nitrosothiol-Thiol Reactions of Biological Significance: HNO Production via S-Thiolation Requires a Proton Shuttle and Stabilization of Polar Intermediates. *Chembiochem* **2017**, .

(52) Jensen, F. *Introduction to computational chemistry*; John Wiley & Sons: 2013.

(53) Cramer, C. J. *Essentials of computational chemistry: theories and models*; John Wiley & Sons: 2013.

(54) Crawford, T. D.; Schaefer, H. F. An introduction to coupled cluster theory for computational chemists. *Reviews in computational chemistry* **2000**, *14*, 33-136.

(55) Raghavachari, K.; Trucks, G. W.; Pople, J. A.; Head-Gordon, M. A fifth-order perturbation comparison of electron correlation theories. *Chemical Physics Letters* **1989**, *157*, 479–483.

(56) Frisch, M.; Trucks, G. W.; Schlegel, H. B.; Scuseria, G. E.; Robb, M. A.; Cheeseman, J. R.; Scalmani, G.; Barone, V.; Mennucci, B.; Petersson, G. A. Gaussian 09, Gaussian. *Inc., Wallingford, CT* **2009**, .

(57) Curtiss, L. A.; Raghavachari, K.; Redfern, P. C.; Rassolov, V.; Pople, J. A. Gaussian-3 (G3) theory for molecules containing first and second-row atoms. *The Journal of chemical physics* **1998**, *109*, 7764–7776.

(58) Adler, T. B.; Knizia, G.; Werner, H. -J. A simple and efficient CCSD (T)-F12 approximation. *The Journal of chemical physics* **2007**, *127*, 221106.

(59) Knizia, G.; Adler, T. B.; Werner, H. -J. Simplified CCSD (T)-F12 methods: Theory and benchmarks. *The Journal of chemical physics* **2009**, *130*, 054104.

(60) Hsu, M. F.; Pan, K. T.; Chang, F. Y.; Khoo, K. H.; Urlaub, H.; Cheng, C. F.; Chang, G. D.; Haj, F. G.; Meng, T. C. S-Nitrosylation of Endogenous Protein Tyrosine Phosphatases in Endothelial Insulin Signaling. *Free Radic Biol Med* **2016**, .

(61) Eichmann, C.; Tzitzilonis, C.; Nakamura, T.; Kwiatkowski, W.; Maslennikov, I.; Choe, S.; Lipton, S. A.; Riek, R. S-Nitrosylation Induces Structural and Dynamical Changes in a Rhodanese Family Protein. *J Mol Biol* **2016**, .

(62) Stamler, J. S.; Jaraki, O.; Osborne, J.; Simon, D. I.; Keaney, J.; Vita, J.; Singel, D.; Valeri, C. R.; Loscalzo, J. Nitric oxide circulates in mammalian plasma primarily as an S-nitroso adduct of serum albumin. *Proceedings of the National Academy of Sciences* **1992**, *89*, 7674–7677.

(63) Stamler, J. S.; Toone, E. J. The decomposition of thionitrites. *Curr Opin Chem Biol* **2002**, *6*, 779–785.

(64) Haldar, S. M.; Stamler, J. S. S-nitrosylation: integrator of cardiovascular performance and oxygen delivery. *J Clin Invest* **2013**, *123*, 101–110.

(65) Cox, A. G.; Saunders, D. C.; Kelsey, P. B.; Conway, A. A.; Tesmenitsky, Y.; Marchini, J. F.; Brown, K. K.; Stamler, J. S.; Colagiovanni, D. B.; Rosenthal, G. J.; Croce, K. J.; North, T. E.; Goessling, W. S-nitrosothiol signaling regulates liver development and improves outcome following toxic liver injury. *Cell Rep* **2014**, *6*, 56–69.

(66) Feechan, A.; Kwon, E.; Yun, B. W.; Wang, Y.; Pallas, J. A.; Loake, G. J. A central role for S-nitrosothiols in plant disease resistance. *Proc Natl Acad Sci U S A* **2005**, *102*, 8054–8059.

(67) Timerghazin, Q. K.; Peslherbe, G. H.; English, A. M. Structure and stability of HSNO, the simplest S-nitrosothiol. *Physical Chemistry Chemical Physics* **2008**, *10*, 1532–1539.

(68) Nagy, B.; Szakács, P.; Csontos, J.; Rolik, Z.; Tasi, G.; Kállay, M. High-accuracy theoretical thermochemistry of atmospherically important sulfur-containing molecules. *J Phys Chem A* **2011**, *115*, 7823–7833.

(69) Hochlaf, M.; Linguerri, R.; Francisco, J. S. On the role of the simplest S-nitrosothiol, HSNO, in atmospheric and biological processes. *J Chem Phys* **2013**, *139*, 234304.

(70) Méndez, M.; Francisco, J. S.; Dixon, D. A. Thermodynamic Properties of the Isomers of [HNOS], [HNO2 S], and [HNOS2] and the Role of the Central Sulfur. *Chemistry* **2014**, .

(71) Khomyakov, D. Towards Reliable Modeling of S-Nitrosothiol Chemistry: Explicitly-Correlated Coupled Cluster and DFT Studies. **2015**, MSc Thesis, Marquette University.

(72) Koppenol, W. H. Nitrosation, thiols, and hemoglobin: energetics and kinetics. *Inorg Chem* **2012**, *51*, 5637–5641.

(73) Fu, Y.; Mou, Y.; Lin, B. -L.; Liu, L.; Guo, Q. -X. Structures of the XY-NO molecules and homolytic dissociation energies of the Y-NO bonds (Y= C, N, O, S). *The Journal of Physical Chemistry A* **2002**, *106*, 12386–12392.

(74) Bharatam, P. V. Negative hyperconjugative interactions in S-nitrosothiols: a theoretical study. *Tetrahedron letters* **2002**, *43*, 8289–8291.

(75) Bharatam, P. V.; Senthilkumar, P. Theoretical investigations on R (O) nS--NO (n= 0, 1, 2) systems. *Tetrahedron* **2004**, *60*, 4801–4805.

(76) Werner, H. -; Knowles, P. J.; Knizia, G.; Manby, F. R.; Schütz, M. Molpro: a general multipurpose quantum chemistry program package. *WIREs Comput Mol Sci* **2012**, *2*, 242–253.

(77) Stanton, J. F.; Gauss, J.; Harding, M. E.; Szalay, P. G.; Auer, A. A.; Bartlett, R. J.; Benedikt, U.; Berger, C.; Bernholdt, D. E.; Bomble, Y. J. CFOUR, a quantum chemical program package. *For the current version, see http://www. cfour. de* **2009**, .

(78) MRCC, a string-based quantum chemical program suite, K´allay, **2014**.

(79) Peterson, K. A.; Adler, T. B.; Werner, H. J. Systematically convergent basis sets for explicitly correlated wavefunctions: the atoms H, He, B-Ne, and Al-Ar. *J Chem Phys* **2008**, *128*, 084102.

(80) Peterson, K. A.; Woon, D. E.; Dunning Jr, T. H. Benchmark calculations with correlated molecular wave functions. IV. The classical barrier height of the H+ H2 H2+ H reaction. *The Journal of chemical physics* **1994**, *100*, 7410–7415.

(81) Easton, R. E.; Giesen, D. J.; Welch, A.; Cramer, C. J.; Truhlar, D. G. The MIDI! basis set for quantum mechanical calculations of molecular geometries and partial charges. *Theoretica chimica acta* **1996**, *93*, 281–301.

(82) Feller, D. The role of databases in support of computational chemistry calculations. *Journal of computational chemistry* **1996**, *17*, 1571–1586.

(83) Hill, J. G.; Mazumder, S.; Peterson, K. A. Correlation consistent basis sets for molecular core-valence effects with explicitly correlated wave functions: the atoms B-Ne and Al-Ar. *J Chem Phys* **2010**, *132*, 054108.

(84) Douglas, M.; Kroll, N. M. Quantum electrodynamical corrections to the fine structure of helium. *Annals of Physics* **1974**, *82*, 89-155.

(85) Jansen, G.; Heß, B. A. Revision of the Douglas-Kroll transformation. *Physical Review A* **1989**, *39*, 6016.

(86) Schwenke, D. W. The extrapolation of one-electron basis sets in electronic structure calculations: how it should work and how it can be made to work. *J Chem Phys* **2005**, *122*, 14107.

(87) Hill, J. G.; Peterson, K. A.; Knizia, G.; Werner, H. -J. Extrapolating MP2 and CCSD explicitly correlated correlation energies to the complete basis set limit with first and second row correlation consistent basis sets. *The Journal of chemical physics* **2009**, *131*, 194105.

(88) Fedorov, D. G.; Koseki, S.; Schmidt, M. W.; Gordon, M. S. Spin-orbit coupling in molecules: chemistry beyond the adiabatic approximation. *International Reviews in Physical Chemistry* **2003**, *22*, 551–592.

(89) Werner, H. -J.; Knowles, P. J. An efficient internally contracted multiconfiguration--reference configuration interaction method. *The Journal of chemical physics* **1988**, *89*, 5803–5814.

(90) Knowles, P. J.; Werner, H. -J. An efficient method for the evaluation of coupling coefficients in configuration interaction calculations. *Chemical Physics Letters* **1988**, *145*, 514–522.

(91) Dunning Jr, T. H. Gaussian basis sets for use in correlated molecular calculations. I. The atoms boron through neon and hydrogen. *The Journal of chemical physics* **1989**, *90*, 1007–1023.

(92) Barone, V. Anharmonic vibrational properties by a fully automated second-order perturbative approach. *J Chem Phys* **2005**, *122*, 14108.

(93) Schwabe, T.; Grimme, S. Towards chemical accuracy for the thermodynamics of large molecules: new hybrid density functionals including non-local correlation effects. *Phys Chem Chem Phys* **2006**, *8*, 4398–4401.

(94) Adamo, C.; Barone, V. Toward reliable density functional methods without adjustable parameters: The PBE0 model. *The Journal of chemical physics* **1999**, *110*, 6158–6170.

(95) Weigend, F.; Ahlrichs, R. Balanced basis sets of split valence, triple zeta valence and quadruple zeta valence quality for H to Rn: design and assessment of accuracy. *Physical Chemistry Chemical Physics* **2005**, *7*, 3297–3305.

(96) Tomasi, J.; Mennucci, B.; Cammi, R. Quantum mechanical continuum solvation models. *Chem Rev* **2005**, *105*, 2999–3093.

(97) Becke, A. D. Density-functional exchange-energy approximation with correct asymptotic behavior. *Phys Rev A* **1988**, *38*, 3098–3100.

(98) Lee, C.; Yang, W.; Parr, R. G. Development of the Colle-Salvetti correlation-energy formula into a functional of the electron density. *Phys Rev B Condens Matter* **1988**, *37*, 785–789.

(99) Grimme, S.; Antony, J.; Ehrlich, S.; Krieg, H. A consistent and accurate ab initio parametrization of density functional dispersion correction (DFT-D) for the 94 elements H-Pu. *The Journal of chemical physics* **2010**, *132*, 154104.

(100) Guido, C. A.; Brémond, E.; Adamo, C.; Cortona, P. Communication: one third: a new recipe for the PBE0 paradigm. *J Chem Phys* **2013**, *138*, 021104.

(101) Chai, J. D.; Head-Gordon, M. Long-range corrected hybrid density functionals with damped atom-atom dispersion corrections. *Phys Chem Chem Phys* **2008**, *10*, 6615–6620.

(102) Grimme, S. Semiempirical hybrid density functional with perturbative second-order correlation. *J Chem Phys* **2006**, *124*, 034108.

(103) Grimme, S.; Antony, J.; Ehrlich, S.; Krieg, H. A consistent and accurate ab initio parametrization of density functional dispersion correction (DFT-D) for the 94 elements H-Pu. *J Chem Phys* **2010**, *132*, 154104.

(104) Kats, D.; Manby, F. R. Communication: The distinguishable cluster approximation. *J Chem Phys* **2013**, *139*, 021102.

(105) Kats, D. Communication: The distinguishable cluster approximation. II. The role of orbital relaxation. *J Chem Phys* **2014**, *141*, 061101.

(106) Baciu, C.; Gauld, J. W. An assessment of theoretical methods for the calculation of accurate structures and SN bond dissociation energies of S-nitrosothiols (RSNOs). *The Journal of Physical Chemistry A* **2003**, *107*, 9946–9952.

(107) Helgaker, T.; Klopper, W.; Koch, H.; Noga, J. Basis-set convergence of correlated calculations on water. *The Journal of chemical physics* **1997**, *106*, 9639–9646.

(108) Feller, D.; Peterson, K. A. Re-examination of atomization energies for the Gaussian-2 set of molecules. *The Journal of chemical physics* **1999**, *110*, 8384–8396.

(109) Field, L.; Dilts, R. V.; Ravichandran, R.; Lenhert, P. G.; Carnahan, G. E. An unusually stable thionitrite from N-acetyl-D, L-penicillamine; X-ray crystal and molecular structure of 2-(acetylamino)-2-carboxy-1, 1-dimethylethyl thionitrite. *Journal of the Chemical Society, Chemical Communications* **1978**, 249–250.

(110) Carnahan, G. E.; Lenhert, P. G.; Ravichandran, R. S-nitroso-N-acetyl-dl-penicillamine. *Acta Crystallographica Section B: Structural Crystallography and Crystal Chemistry* **1978**, *34*, 2645–2648.

(111) Arulsamy, N.; Bohle, D. S.; Butt, J. A.; Irvine, G. J.; Jordan, P. A.; Sagan, E. Interrelationships between conformational dynamics and the redox chemistry of S-nitrosothiols. *Journal of the American Chemical Society* **1999**, *121*, 7115–7123.

(112) Timerghazin, Q. K.; Peslherbe, G. H.; English, A. M. Resonance description of S-nitrosothiols: insights into reactivity. *Org Lett* **2007**, *9*, 3049–3052.

(113) Philippe, R. J. The infrared spectrum of methyl thionitrite. *Journal of Molecular Spectroscopy* **1961**, *6*, 492–496.

(114) Christensen, D. H.; Rastrup-Andersen, N.; Jones, D.; Klabof, P.; Lippincott, E. R. Infrared, Raman and proton magnetic resonance spectra of methylthionitrite. *Spectrochimica Acta Part A: Molecular Spectroscopy* **1968**, *24*, 1581–1589.

(115) Müller, R. P.; Huber, J. R. Two rotational isomers of methyl thionitrite: light-induced, reversible isomerization in an argon matrix. *The Journal of Physical Chemistry* **1984**, *88*, 1605–1608.

(116) Bartberger, M. D.; Houk, K. N.; Powell, S. C.; Mannion, J. D.; Lo, K. Y.; Stamler, J. S.; Toone, E. J. Theory, spectroscopy, and crystallographic analysis of S-nitrosothiols: conformational distribution dictates spectroscopic behavior. *Journal of the American Chemical Society* **2000**, *122*, 5889–5890.

(117) Roy, B.; Du Moulinet d'Hardemare, A.; Fontecave, M. New thionitrites: synthesis, stability, and nitric oxide generation. *The Journal of Organic Chemistry* **1994**, *59*, 7019–7026.

(118) Jahn, A.; Teller, E.; Stability of polyatomic molecules in degenerate electronic states. I. Orbital degeneracy. *Proceedings of the Royal Society of London A: Mathematical, Physical and Engineering Sciences* **1937**, *5*, 220-235.

(119) Montgomery, J. A.; Frisch, M. J.; Ochterski, J. W.; Petersson, G. A. A complete basis set model chemistry. VI. Use of density functional geometries and frequencies. *The Journal of Chemical Physics* **1999**, *110*, 2822.

(120) Hrenar, T.; Werner, H. J.; Rauhut, G. Accurate calculation of anharmonic vibrational frequencies of medium sized molecules using local coupled cluster methods. *J Chem Phys* **2007**, *126*, 134108.

(121) Neff, M.; Rauhut, G. Toward large scale vibrational configuration interaction calculations. *J Chem Phys* **2009**, *131*, 124129.

(122) Kats, D.; Kreplin, D.; Werner, H. J.; Manby, F. R. Accurate thermochemistry from explicitly correlated distinguishable cluster approximation. *J Chem Phys* **2015**, *142*, 064111.

(123) Anand, P.; Hess, D. T.; Stamler, J. S. Identifying single S-nitrosothiol sites with cardioprotection. *Circ Res* **2013**, *113*, 849–851.

(124) Hess, D. T.; Stamler, J. S. Regulation by S-nitrosylation of protein post-translational modification. *Journal of Biological Chemistry* **2012**, *287*, 4411–4418.

(125) Bruce King, S. Potential Biological Chemistry of Hydrogen Sulfide (H< sub> 2</sub> S) with the Nitrogen Oxides. *Free Radical Biology and Medicine* **2012**, .

(126) Filipovic, M. R.; Miljkovic, J. L. j.; Nauser, T.; Royzen, M.; Klos, K.; Shubina, T.; Koppenol, W. H.; Lippard, S. J.; Ivanović-Burmazović, I. Chemical characterization of the smallest S-nitrosothiol, HSNO; cellular cross-talk of H2S and S-nitrosothiols. *J Am Chem Soc* **2012**, *134*, 12016–12027.

(127) Miljkovic, J. L. j.; Kenkel, I.; Ivanović-Burmazović, I.; Filipovic, M. R. Generation of HNO and HSNO from nitrite by heme-iron-catalyzed metabolism with H_2S. *Angew Chem Int Ed Engl* **2013**, *52*, 12061–12064.

(128) Goto, K.; Hino, Y.; Kawashima, T.; Kaminaga, M.; Yano, E.; Yamamoto, G.; Takagi, N.; Nagase, S. Synthesis and crystal structure of a stable S-nitrosothiol bearing a novel steric protection group and of the corresponding S-nitrothiol. *Tetrahedron Letters* **2000**, *41*, 8479–8483.

(129) Goto, K.; Hino, Y.; Takahashi, Y.; Kawashima, T.; Yamamoto, G.; Takagi, N.; Nagase, S. Synthesis, Structure, and Reactions of the First Stable Aromatic S-Nitrosothiol Bearing a Novel Dendrimer-Type Steric Protection Group. *Chemistry Letters* **2001**, 1204–1205.

(130) Lee, J.; Yi, G. -B.; Powell, D. R.; Khan, M. A.; Richter-Addo, G. B. Synthesis, characterization, and protonation of octaethylporphyrin osmium nitrosyl complexes containing axial thiolate ligands-X-ray structures of an alkyl thionitrite (RSNO) and its (OEP) Os (NO)(SR) addition product. *Canadian Journal of Chemistry* **2001**, *79*, 830–840.

(131) Spivey, A. C.; Colley, J.; Sprigens, L.; Hancock, S. M.; Cameron, D. S.; Chigboh, K. I.; Veitch, G.; Frampton, C. S.; Adams, H. The synthesis of water soluble decalin-based thiols and S-nitrosothiols--model systems for studying the reactions of nitric oxide with protein thiols. *Org Biomol Chem* **2005**, *3*, 1942–1952.

(132) Yi, J.; Khan, M. A.; Lee, J.; Richter-Addo, G. B. The solid-state molecular structure of the S-nitroso derivative of L-cysteine ethyl ester hydrochloride. *Nitric Oxide* **2005**, *12*, 261–266.

(133) Chan, N. L.; Rogers, P. H.; Arnone, A. Crystal structure of the S-nitroso form of liganded human hemoglobin. *Biochemistry* **1998**, *37*, 16459–16464.

(134) Frey, D.; Braun, O.; Briand, C.; Vasák, M.; Grütter, M. G. Structure of the mammalian NOS regulator dimethylarginine dimethylaminohydrolase: A basis for the design of specific inhibitors. *Structure* **2006**, *14*, 901–911.

(135) Weichsel, A.; Brailey, J. L.; Montfort, W. R. Buried S-nitrosocysteine revealed in crystal structures of human thioredoxin. *Biochemistry* **2007**, *46*, 1219–1227.

(136) Schreiter, E. R.; Rodríguez, M. M.; Weichsel, A.; Montfort, W. R.; Bonaventura, J. S-nitrosylation-induced conformational change in blackfin tuna myoglobin. *J Biol Chem* **2007**, *282*, 19773–19780.

(137) Chen, Y. Y.; Chu, H. M.; Pan, K. T.; Teng, C. H.; Wang, D. L.; Wang, A. H.; Khoo, K. H.; Meng, T. C. Cysteine S-nitrosylation protects protein-tyrosine phosphatase 1B against oxidation-induced permanent inactivation. *J Biol Chem* **2008**, *283*, 35265–35272.

(138) Chowdhury, R.; Flashman, E.; Mecinović, J.; Kramer, H. B.; Kessler, B. M.; Frapart, Y. M.; Boucher, J. -L.; Clifton, I. J.; McDonough, M. A.; Schofield, C. J. Studies on the reaction of nitric oxide with the hypoxia-inducible factor prolyl hydroxylase domain 2 (EGLN1). *Journal of molecular biology* **2011**, *410*, 268–279.

(139) Skaff, D. A.; Ramyar, K. X.; McWhorter, W. J.; Barta, M. L.; Geisbrecht, B. V.; Miziorko, H. M. Biochemical and structural basis for inhibition of Enterococcus faecalis hydroxymethylglutaryl-CoA synthase, mvaS, by hymeglusin. *Biochemistry* **2012**, *51*, 4713–4722.

(140) Stec, B. Structural mechanism of RuBisCO activation by carbamylation of the active site lysine. *Proc Natl Acad Sci U S A* **2012**, *109*, 18785–18790.

(141) Kumar, V.; Martin, F.; Hahn, M. G.; Schaefer, M.; Stamler, J. S.; Stasch, J. P.; van den Akker, F. Insights into BAY 60-2770 activation and S-nitrosylation-dependent desensitization of soluble guanylyl cyclase via crystal structures of homologous nostoc H-NOX domain complexes. *Biochemistry* **2013**, *52*, 3601–3608.

(142) Perissinotti, L. L.; Estrin, D. A.; Leitus, G.; Doctorovich, F. A surprisingly stable S-nitrosothiol complex. *J Am Chem Soc* **2006**, *128*, 2512–2513.

(143) Timerghazin, Q. K.; Talipov, M. R. Unprecedented External Electric Field Effects on S-Nitrosothiols: Possible Mechanism of Biological Regulation? *The Journal of Physical Chemistry Letters* **2013**, *4*, 1034–1038.

(144) Dapprich, S.; Komáromi, I.; Byun, K. S.; Morokuma, K.; Frisch, M. J. A new ONIOM implementation in Gaussian98. Part I. The calculation of energies,

gradients, vibrational frequencies and electric field derivatives. *Journal of Molecular Structure: THEOCHEM* **1999**, *461*, 1-21.

(145) Chung, L. W.; Sameera, W. M.; Ramozzi, R.; Page, A. J.; Hatanaka, M.; Petrova, G. P.; Harris, T. V.; Li, X.; Ke, Z.; Liu, F.; Li, H. B.; Ding, L.; Morokuma, K. The ONIOM Method and Its Applications. *Chem Rev* **2015**, *115*, 5678–5796.

(146) Vreven, T.; Byun, K. S.; Komáromi, I.; Dapprich, S.; Montgomery, J. A.; Morokuma, K.; Frisch, M. J. Combining Quantum Mechanics Methods with Molecular Mechanics Methods in ONIOM. *J Chem Theory Comput* **2006**, *2*, 815–826.

(147) Vreven, T.; Mennucci, B.; da Silva, C. O.; Morokuma, K.; Tomasi, J. The ONIOM-PCM method: Combining the hybrid molecular orbital method and the polarizable continuum model for solvation. Application to the geometry and properties of a merocyanine in solution. *The Journal of chemical physics* **2001**, *115*, 62–72.

(148) Hinsen, K. The molecular modeling toolkit: a new approach to molecular simulations. *Journal of Computational Chemistry* **2000**, *21*, 79–85.

(149) Rappoport, D.; Furche, F. Property-optimized gaussian basis sets for molecular response calculations. *J Chem Phys* **2010**, *133*, 134105.

(150) Schuchardt, K. L.; Didier, B. T.; Elsethagen, T.; Sun, L.; Gurumoorthi, V.; Chase, J.; Li, J.; Windus, T. L. Basis set exchange: a community database for computational sciences. *J Chem Inf Model* **2007**, *47*, 1045–1052.

(151) Cornell, W. D.; Cieplak, P.; Bayly, C. I.; Gould, I. R.; Merz, K. M.; Ferguson, D. M.; Spellmeyer, D. C.; Fox, T.; Caldwell, J. W.; Kollman, P. A. A second generation force field for the simulation of proteins, nucleic acids, and organic molecules j. am. chem. soc. 1995, 117, 5179-5197. *Journal of the American Chemical Society* **1996**, *118*, 2309–2309.

(152) Roothaan, C. C. J. New developments in molecular orbital theory. *Reviews of modern physics* **1951**, *23*, 69.

(153) Pople, J. A.; Nesbet, R. _. K. Self-consistent orbitals for radicals. *The Journal of Chemical Physics* **1954**, *22*, 571–572.

(154) McWeeny, R.; Diercksen, G. Self-Consistent Perturbation Theory. II. Extension to Open Shells. *The Journal of Chemical Physics* **1968**, *49*, 4852–4856.

(155) Hehre, W. J.; Stewart, R. F.; Pople, J. A. self-consistent molecular-orbital methods. i. use of gaussian expansions of Slater-type atomic orbitals. *The Journal of Chemical Physics* **1969**, *51*, 2657–2664.

(156) Collins, J. B.; Schleyer, P. V. R.; Binkley, J. S.; Pople, J. A. Self-consistent molecular orbital methods. XVII. Geometries and binding energies of second-row molecules. A comparison of three basis sets. *The Journal of Chemical Physics* **1976**, *64*, 5142–5151.

(157) Landis, C. R.; Weinhold, F. The NBO View of Chemical Bonding. In *The Chemical Bond*; ; Wiley-VCH Verlag GmbH & Co. KGaA: Weinheim, Germany, 2014; pp 91-120.

(158) Witt, A. C.; Lakshminarasimhan, M.; Remington, B. C.; Hasim, S.; Pozharski, E.; Wilson, M. A. Cysteine pKa depression by a protonated glutamic acid in human DJ-1. *Biochemistry* **2008**, *47*, 7430–7440.

(159) Zhao, Y. L.; Houk, K. N. Thionitroxides, RSNHO*: the structure of the SNO moiety in "S-Nitrosohemoglobin", a possible NO reservoir and transporter. *J Am Chem Soc* **2006**, *128*, 1422–1423.

(160) Han, S. Force field parameters for S-nitrosocysteine and molecular dynamics simulations of S-nitrosated thioredoxin. *Biochem Biophys Res Commun* **2008**, *377*, 612–616.

(161) Wang, H.; Xian, M. Chemical methods to detect S-nitrosation. *Curr Opin Chem Biol* **2011**, *15*, 32–37.

(162) Bettaieb, A.; Paul, C.; Plenchette, S. Exploration of Fas S-Nitrosylation by the Biotin Switch Assay. *Methods Mol Biol* **2017**, *1557*, 199–206.

(163) Li, R.; Kast, J. Biotin Switch Assays for Quantitation of Reversible Cysteine Oxidation. *Methods in Enzymology* **2016**, .

(164) Martin, B. R. REDOX SIGNALING., .

(165) Bechtold, E.; King, S. B. Chemical methods for the direct detection and labeling of S-nitrosothiols. *Antioxid Redox Signal* **2012**, *17*, 981–991.

(166) Rostovtsev, V. V.; Green, L. G.; Fokin, V. V.; Sharpless, K. B. A stepwise huisgen cycloaddition process: copper(I)-catalyzed regioselective "ligation" of azides and terminal alkynes. *Angew Chem Int Ed Engl* **2002**, *41*, 2596–2599.

(167) Sletten, E. M.; Bertozzi, C. R. From mechanism to mouse: a tale of two bioorthogonal reactions. *Acc Chem Res* **2011**, *44*, 666–676.

(168) Debets, M. F.; van Berkel, S. S.; Dommerholt, J.; Dirks, A. T.; Rutjes, F. P.; van Delft, F. L. Bioconjugation with strained alkenes and alkynes. *Acc Chem Res* **2011**, *44*, 805–815.

(169) Baciu, C.; Cho, K. B.; Gauld, J. W. Influence of Cu+ on the RS-NO bond dissociation energy of S-nitrosothiols. *J Phys Chem B* **2005**, *109*, 1334–1336.

(170) Montgomery, J. A.; Frisch, M. J.; Ochterski, J. W.; Petersson, G. A. A complete basis set model chemistry. VII. Use of the minimum population localization method. *The Journal of Chemical Physics* **2000**, *112*, 6532.

(171) Perdew, J. P.; Burke, K.; Ernzerhof, M. Generalized gradient approximation made simple. *Physical review letters* **1996**, *77*, 3865.

(172) Ribeiro, R. F.; Marenich, A. V.; Cramer, C. J.; Truhlar, D. G. Use of solution-phase vibrational frequencies in continuum models for the free energy of solvation. *J Phys Chem B* **2011**, *115*, 14556–14562.

(173) Glendening, E. D.; Weinhold, F. Natural resonance theory: I. General formalism. *Journal of computational chemistry* **1998**, *19*, 593–609.

(174) Glendening, E. D.; Badenhoop, J. K.; Reed, A. E.; Carpenter, J. E.; Bohmann, J. A.; Morales, C. M.; Weinhold, F. NBO 5.0; Theoretical Chemistry Institute, University of Wisconsin: Madison, WI, 2001. *There is no corresponding record for this reference* **2004**, .

(175) Cavero, M.; Motherwell, W. B.; Potier, P. Studies on the intermolecular free radical addition of thionitrites to alkenes: a convenient method for the preparation of α-tritylthio oximes and related derivatives. *Tetrahedron Letters* **2001**, *42*, 4377–4379.

(176) Lopez, S. A.; Houk, K. N. Alkene distortion energies and torsional effects control reactivities, and stereoselectivities of azide cycloadditions to norbornene and substituted norbornenes. *J Org Chem* **2013**, *78*, 1778–1783.

(177) Gold, B.; Dudley, G. B.; Alabugin, I. V. Moderating strain without sacrificing reactivity: design of fast and tunable noncatalyzed alkyne-azide cycloadditions via stereoelectronically controlled transition state stabilization. *J Am Chem Soc* **2013**, *135*, 1558–1569.

(178) Jewett, J. C.; Sletten, E. M.; Bertozzi, C. R. Rapid Cu-free click chemistry with readily synthesized biarylazacyclooctynones. *J Am Chem Soc* **2010**, *132*, 3688–3690.

(179) Hur, S.; Bruice, T. C. Comparison of formation of reactive conformers (NACs) for the Claisen rearrangement of chorismate to prephenate in water and in the E. coli mutase: the efficiency of the enzyme catalysis. *J Am Chem Soc* **2003**, *125*, 5964–5972.

Appendix A

Computed geometries and energies

cis-MeSNO + Dimethylacetylene

cis-MeSNO

Freq
RB3LYP/6-311G(2d,d,p)
Solvation: PCM(Acetonitrile)
Symmetry: CS
Charge: 0; Mult: 1
E_SCF= -568.079150
T=298.15: H= -568.028705, E+ZPE= -568.034841, G= -568.063109
Freqs: 113.1, 249.9 .. 3150.1

CBS-QB3 Enthalpy= -567.310906 CBS-QB3 Free Energy= -567.345357

XYZ coordinates
C 1.132472 1.193067 0.000000
S 0.755228 -0.572019 0.000000
H 1.695040 1.451401 0.895843
H 0.171452 1.718537 0.000000
N -1.081347 -0.596290 0.000000
O -1.642273 0.445910 0.000000
H 1.695040 1.451401 -0.895843

Dimethylacetylene

Freq
RB3LYP/6-311G(2d,d,p)
Solvation: PCM(Acetonitrile)
Symmetry: D3H
Charge: 0; Mult: 1
E_SCF= -156.027937
T=298.15: H= -155.937564, E+ZPE= -155.944259, G= -155.971157
Freqs: 27.0, 201.1 .. 3081.7

CBS-QB3 Enthalpy= -155.650990 CBS-QB3 Free Energy= -155.684638

XYZ coordinates
C 0.000000 0.000000 2.063530
C 0.000000 0.000000 0.602455
C 0.000000 0.000000 -0.602455
C 0.000000 0.000000 -2.063530
H -0.509871 0.883122 2.458882
H 1.019742 0.000000 2.458882
H -0.509871 -0.883122 2.458882
H 1.019742 0.000000 -2.458882
H -0.509871 0.883122 -2.458882
H -0.509871 -0.883122 -2.458882

(3+2) Transition State: cis-MeSNO + dimethylacetylene

Freq
RB3LYP/6-311G(2d,d,p)
Solvation: PCM(Acetonitrile)
Symmetry: C1
Charge: 0; Mult: 1
E_SCF= -724.052472
T=298.15: H= -723.911054, E+ZPE= -723.922057, G= -723.956817
Freqs: -466.2, 103.5 .. 3154.3

CBS-QB3 Enthalpy= -722.925528 CBS-QB3 Free Energy= -722.971431

XYZ coordinates (Last three columns show the imaginary frequency vector)
C 1.679451 0.051572 1.374489 -0.05 0.00 -0.02
S 1.478998 -0.042374 -0.437888 0.19 -0.03 -0.01
H 1.425451 1.049407 1.728198 -0.13 -0.02 -0.02
H 2.716609 -0.187272 1.607927 -0.06 0.04 0.07
N 0.633590 -1.408293 -0.869214 -0.12 -0.05 0.00
O -0.334121 -1.618926 -0.049789 0.25 -0.29 -0.04
H 0.996977 -0.682274 1.802842 -0.05 -0.04 -0.07
C -2.675547 -0.577677 0.369697 -0.08 -0.09 0.03
C -1.353410 -0.015805 0.049823 -0.33 0.38 0.07
C -0.590951 0.960116 -0.153033 -0.33 0.18 0.04
C -0.442138 2.423716 -0.304381 0.09 0.09 -0.03
H -2.608042 -1.242822 1.235183 0.05 -0.11 0.00
H -3.068110 -1.164049 -0.465118 0.04 -0.13 0.00
H -3.385683 0.220448 0.601916 -0.27 -0.26 0.06
H 0.329289 2.825254 0.359613 0.15 -0.02 -0.03
H -1.382260 2.933191 -0.074294 0.17 0.26 -0.06
H -0.154795 2.684027 -1.326811 0.14 0.01 -0.04

(3+2) Product: cis-MeSNO + dimethylacetylene

Freq
RB3LYP/6-311G(2d,d,p)
Solvation: PCM(Acetonitrile)
Symmetry: C1
Charge: 0; Mult: 1
E_SCF= -724.108378
T=298.15: H= -723.964561, E+ZPE= -723.975126, G= -724.009366
Freqs: 109.1, 112.1 .. 3155.9

CBS-QB3 Enthalpy= -722.985192 CBS-QB3 Free Energy= -723.030134

XYZ coordinates
C 2.005882 0.271537 1.196898
S 1.268919 -0.039145 -0.483540
H 2.138937 1.349140 1.314327
H 2.975550 -0.227131 1.217182
N 0.689994 -1.555440 -0.649228
O -0.631078 -1.555968 0.037878
H 1.339773 -0.125181 1.961862

```
C -2.597034 -0.271980 0.461669
C -1.159017 -0.312406 0.060015
C -0.339225 0.711022 -0.254721
C -0.566355 2.186072 -0.325925
H -2.723380 -0.765994 1.42
H -3.209263 -0.808713 -0.267837
H -2.959895 0.751375 0.543420
H 0.024088 2.730028 0.418504
H -1.617360 2.417687 -0.143889
H -0.304285 2.585438 -1.310005
```

S–N Insertion Transition State: cis-MeSNO + dimethylacetylene

RB3LYP/CBSB7
Solvation: PCM(Acetonitrile)
Symmetry: C1
Charge: 0; Mult: 1
E_SCF= -724.061664
T=298.15: H= -723.920316, E+ZPE= -723.932088, G= -723.968289
Freqs: -375.9, 57.0 .. 3116.0

CBS-QB3 Enthalpy= -722.919366 CBS-QB3 Free Energy= -722.967485

XYZ coordinates

```
C -2.105833 -0.413821 0.972457     0.04 0.01 -0.01
S -1.573760 0.008720 -0.705321     0.09 0.15 0.04
N 0.359240 -1.231077 -0.544282     0.25 0.04 0.02
O 0.284222 -2.031820 0.300750     0.10 -0.02 0.04
H -1.912632 0.390814 1.683365     -0.05 -0.02 0.04
H -1.564253 -1.314835 1.292060     0.06 0.02 -0.03
H -3.171546 -0.645407 0.961121     0.04 0.00 -0.12
C 0.107992 2.509104 0.195325     0.08 -0.03 0.01
C 0.642783 1.166817 -0.010360     -0.37 -0.22 -0.13
C 1.463343 0.231421 -0.047885     -0.33 -0.33 -0.09
C 2.821560 -0.311862 0.131998     -0.11 0.11 0.02
H 3.232390 -0.642171 -0.826315     -0.03 0.13 0.04
H 2.792938 -1.178811 0.799537     0.05 0.14 0.06
H 3.492474 0.433879 0.562610     -0.29 0.28 -0.02
H -0.327324 2.911988 -0.720932     0.11 0.11 0.06
H 0.927928 3.164535 0.514342     0.27 -0.24 -0.02
H -0.657327 2.522643 0.974110     0.13 0.12 0.06
```

S–N Insertion Product: cis-MeSNO + dimethylacetylene

FREQ
RB3LYP/6-311G(2d,d,p)
Solvation: PCM(Acetonitrile)
Symmetry: C1
Charge: 0; Mult: 1
E_SCF= -724.150191
T=298.15: H= -724.005403, E+ZPE= -724.016442, G= -724.052604
Freqs: 26.7 .. 3175.0

CBS-QB3 Enthalpy= -723.012565 CBS-QB3 Free Energy= -723.059905

XYZ coordinates

C	1.86564	-1.66565	0.00028
S	1.86205	0.15005	-0.00012
N	-0.97696	-1.22304	-0.00014
O	-2.10126	-1.75001	-0.00020
H	1.37922	-2.05552	-0.88965
H	1.37931	-2.05511	0.89044
H	2.92764	-1.91976	0.00029
C	0.33201	2.30937	-0.00007
C	0.25039	0.79829	-0.00002
C	-0.97397	0.16375	0.00007
C	-2.29431	0.88536	0.00022
H	-2.87998	0.59103	0.87569
H	-2.87931	0.59287	-0.87634
H	-2.18418	1.96665	0.00137
H	1.36442	2.65951	-0.00043
H	-0.16456	2.71714	0.88375
H	-0.16519	2.71713	-0.88353

cis-MeSNO + Dimethylacetylene + Lewis Acid

BF_3

Freq
RB3LYP/6-311G(2d,d,p)
Solvation: PCM(Acetonitrile)
Symmetry: D3H
Charge: 0; Mult: 1
E_SCF= -324.655652
T=298.15: H= -324.639148, E+ZPE= -324.643626, G= -324.668108
Freqs: 467.7, 467.8 .. 1403.9

CBS-QB3 Enthalpy= -324.265897 CBS-QB3 Free Energy= -324.294878

XYZ coordinates

F	0.000000	0.000000	0.000000
B	0.000000	0.000000	1.317000
F	1.140555	0.000000	1.975500
F	-1.140555	0.000000	1.975500

cis-MeSN(→BF_3)O

Freq
RB3LYP/6-311G(2d,d,p)
Solvation: PCM(Acetonitrile)
Symmetry: CS
Charge: 0; Mult: 1
E_SCF= -892.750980
T=298.15: H= -892.681722, E+ZPE= -892.691741, G= -892.726722
Freqs: 42.0, 110.4 .. 3162.0

CBS-QB3 Enthalpy= -891.598326 CBS-QB3 Free Energy= -891.643442

XYZ coordinates
C -2.969067 -0.406034 0.000000
S -1.550527 0.703368 0.000000
H -2.950893 -1.024112 0.897109
H -2.950893 -1.024112 -0.897109
N -0.284689 -0.442014 0.000000
O -0.504148 -1.624230 0.000000
H -3.843522 0.244290 0.000000
F 1.868779 -0.354316 1.151163
B 1.335391 0.153462 0.000000
F 1.169954 1.518180 0.000000
F 1.868779 -0.354316 -1.151163

(3+2) Transition State: cis-MeSN(→BF_3)O + dimethylacetylene

Freq
RB3LYP/6-311G(2d,d,p)
Solvation: PCM(Acetonitrile)
Symmetry: C1
Charge: 0; Mult: 1
E_SCF= -1048.743849
T=298.15: H= -1048.583476, E+ZPE= -1048.598864, G= -1048.640744
Freqs: -379.1, 26.8 .. 3180.7

CBS-QB3 Enthalpy= -1047.230556 CBS-QB3 Free Energy= -1047.288036

XYZ coordinates (Last three columns show the imaginary frequency vector)
C 1.348223 -1.858549 -1.452950 -0.02 -0.04 -0.01
S 0.283794 -1.485128 -0.035254 0.11 0.14 0.05
H 1.384965 -0.982809 -2.096144 0.02 -0.06 -0.04
H 0.924733 -2.723255 -1.961921 -0.10 -0.03 0.05
N -0.658220 -0.220193 -0.550239 -0.03 -0.06 -0.02
O -0.036421 0.653043 -1.222827 0.26 0.13 0.17
H 2.339678 -2.090780 -1.067611 -0.02 -0.10 -0.03
F -1.721991 1.363521 0.944289 0.00 0.00 0.00
B -2.005135 0.178055 0.289522 0.07 -0.02 -0.03
F -2.214372 -0.880993 1.166581 0.00 -0.01 0.00
F -3.026929 0.315443 -0.630883 0.00 0.01 0.01
C 2.685266 -0.386793 1.680123 -0.02 0.10 -0.07
C 1.861977 0.237579 0.626289 -0.28 -0.26 -0.13
C 1.540363 1.210907 -0.082502 -0.39 -0.20 -0.19
C 1.663292 2.573069 -0.614397 0.03 -0.09 0.08
H 3.161578 -1.308217 1.335689 0.09 0.12 0.02
H 2.081799 -0.630429 2.557445 0.08 0.14 0.01
H 3.473014 0.307001 1.985593 -0.10 0.27 -0.24
H 0.786035 3.170585 -0.358431 0.12 0.04 0.10
H 1.753259 2.555004 -1.703237 0.09 0.02 0.08
H 2.553727 3.052650 -0.199899 0.10 -0.33 0.20

(3+2) Product: cis-MeSN(→BF_3)O + dimethylacetylene

Freq
RB3LYP/6-311G(2d,d,p)
Solvation: PCM(Acetonitrile)

Solvation: PCM(Acetonitrile)
Symmetry: C1
E_SCF= -1048.813320
T=298.15: H= -1048.650367, E+ZPE= -1048.665045, G= -1048.705608
Freqs: 39.2, 61.8 .. 3176.3 SP

CBS-QB3 Enthalpy= -1047.304469 CBS-QB3 Free Energy= -1047.359917

XYZ coordinates

C	1.138131	-2.261594	-1.148956
S	0.379627	-1.263405	0.168915
H	1.447005	-1.610941	-1.963876
H	0.386694	-2.983415	-1.467473
N	-0.689316	-0.248582	-0.645319
O	0.046467	0.940086	-1.042568
H	1.990738	-2.778844	-0.706767
F	-1.616948	0.946989	1.304483
B	-1.978917	0.169377	0.198237
F	-2.546969	-1.043409	0.603970
F	-2.811821	0.881583	-0.655773
C	2.739044	-0.159825	1.356698
C	1.578261	0.031395	0.435198
C	1.191215	1.074591	-0.319192
C	1.859426	2.390230	-0.521053
H	3.398261	-0.965994	1.022982
H	2.405988	-0.394792	2.370902
H	3.330538	0.755131	1.402029
H	1.220107	3.193430	-0.146887
H	2.021345	2.558208	-1.588564
H	2.818634	2.427562	-0.009147

S–N Insertion Transition State: cis-MeSN(→BF_3)O + dimethylacetylene

FREQ
RB3LYP/CBSB7
Solvation: PCM(Acetonitrile)
Symmetry: C1
Charge: 0; Mult: 1
E_SCF= -1048.723751
T=298.15: H= -1048.564548, E+ZPE= -1048.580352, G= -1048.621928
Freqs: -442.4, 44.4 .. 3143.8

CBS-QB3 Enthalpy= -1047.200307 CBS-QB3 Free Energy= -1047.257905

XYZ coordinates

C	-2.127863	-1.639889	1.029001	0.03	0.02	-0.01
S	-1.068659	-1.405251	-0.410598	-0.05	0.13	-0.05
N	0.321450	-0.307419	0.539057	0.02	0.37	0.08
O	0.495189	-0.634310	1.697190	0.04	0.00	0.06
H	-2.891543	-0.867861	1.111717	-0.03	-0.04	0.04
H	-1.476093	-1.626353	1.909926	0.12	0.12	-0.07
H	-2.584821	-2.625913	0.948663	0.11	-0.01	0.01
C	-2.337975	1.461052	-1.433072	0.00	0.06	0.05
C	-1.336110	1.297312	-0.409531	0.01	-0.39	-0.01
C	-0.451220	1.373447	0.469137	0.16	-0.48	0.02

```
C 0.162995 2.232232 1.499603     -0.08 -0.03 -0.11
H 1.134970 2.594656 1.162669     -0.08 0.00 -0.10
H 0.312845 1.633768 2.404103     -0.09 0.11 -0.01
H -0.486043 3.076544 1.731358     -0.19 -0.06 -0.32
H -1.950023 1.188172 -2.416723     -0.05 0.14 0.01
H -2.585275 2.532740 -1.458773     0.19 0.11 0.22
H -3.250045 0.902489 -1.220099     -0.09 0.18 -0.01
F 2.449928 0.831416 0.010977     0.01 0.00 -0.01
B 1.688602 -0.181024 -0.513214     -0.05 -0.02 0.05
F 1.155695 0.087478 -1.747431     0.00 0.00 0.00
F 2.256704 -1.423074 -0.410094     -0.02 -0.01 0.01
```

S–N Insertion Product: cis-MeSN(→BF_3)O + dimethylacetylene

FREQ
RB3LYP/CBSB7
Solvation: PCM(Acetonitrile)
Symmetry: C1
Charge: 0; Mult: 1
E_SCF= -1048.824157
T=298.15: H= -1048.660777, E+ZPE= -1048.675531, G= -1048.715683
Freqs: 63.0 .. 3192.8

CBS-QB3 Enthalpy= -1047.301610 CBS-QB3 Free Energy= -1047.356724

XYZ coordinates

C	0.51728	-1.93481	-1.33661
S	1.68754	-1.45052	-0.03782
N	-0.74544	0.78729	-0.39533
O	-1.45971	1.60087	-1.02004
H	0.36086	-1.10367	-2.02248
H	-0.42307	-2.26602	-0.90909
H	1.01032	-2.75742	-1.85392
C	2.73604	0.73822	1.01773
C	1.54004	0.21355	0.26377
C	0.56575	1.11363	-0.20822
C	0.92772	2.53170	-0.56169
H	0.21044	3.22340	-0.11285
H	0.86272	2.66452	-1.64538
H	1.93413	2.78822	-0.24446
H	3.24107	-0.06681	1.55325
H	2.43803	1.50961	1.72837
H	3.46207	1.16937	0.32185
F	-2.53848	0.50369	1.18836
B	-1.70327	-0.30740	0.44798
F	-0.91103	-1.09603	1.26123
F	-2.37339	-1.04183	-0.51317

cis-MeSNO(→BF_3)

Freq
RB3LYP/6-311G(2d,d,p)
Solvation: PCM(Acetonitrile)
Symmetry: C1
Charge: 0; Mult: 1
E_SCF= -892.748349

T=298.15: H= -892.679604, E+ZPE= -892.689593, G= -892.724794
Freqs: 44.1, 92.2 .. 3170.5

CBS-QB3 Enthalpy= -891.596791 CBS-QB3 Free Energy= -891.642097

XYZ coordinates
C 2.572458 1.164943 -0.000035
S 2.239641 -0.609228 0.000339
H 2.143326 1.610820 0.896746
H 2.143205 1.610450 -0.896941
N 0.622741 -0.757241 0.000347
O -0.058009 0.301573 -0.000099
H 3.657677 1.257809 -0.000126
F -1.957879 -0.635687 1.149487
B -1.698444 0.060902 -0.000036
F -1.957854 -0.636604 -1.149006
F -2.156503 1.349032 -0.000556

(3+2) Transition State: cis-MeSNO(→BF_3) + dimethylacetylene

Freq
RB3LYP/6-311G(2d,d,p)
Solvation: PCM(Acetonitrile)
Symmetry: C1
Charge: 0; Mult: 1
E_SCF= -1048.735625
T=298.15: H= -1048.575738, E+ZPE= -1048.590843, G= -1048.631622
Freqs: -279.5, 50.9 .. 3190.6

CBS-QB3 Enthalpy= -1047.221947 CBS-QB3 Free Energy= -1047.278042

XYZ coordinates (Last three columns show the imaginary frequency vector)
C -1.803314 -1.494655 1.410153 0.04 0.05 -0.01
S -1.527752 -1.274475 -0.382848 0.03 -0.16 -0.02
H -1.010950 -0.994162 1.958942 0.04 0.10 -0.05
H -1.801912 -2.570254 1.586128 0.03 0.07 0.09
N 0.028235 -1.167159 -0.725763 0.03 0.08 0.01
O 0.598423 -0.358177 0.192687 0.09 -0.19 0.03
H -2.778174 -1.073770 1.654174 0.04 0.09 -0.06
F 2.261524 0.645467 -1.219383 -0.02 -0.03 0.01
B 2.136972 -0.115903 -0.068516 0.04 -0.06 0.00
F 2.734720 -1.354329 -0.186749 0.08 -0.03 -0.02
F 2.549928 0.567991 1.063857 0.00 -0.03 -0.01
C 0.184856 2.434193 0.543551 0.09 0.06 0.05
C -0.719346 1.371556 0.132407 -0.22 0.35 0.05
C -1.800898 0.828710 -0.208294 -0.13 0.38 0.02
C -3.206663 1.183324 -0.562682 -0.17 -0.05 -0.07
H -0.399862 3.354575 0.654759 0.33 0.20 0.12
H 0.970580 2.593449 -0.195938 0.09 -0.10 0.02
H 0.654665 2.202579 1.500700 0.10 -0.08 0.02
H -3.432495 0.877900 -1.586799 -0.08 -0.18 -0.05
H -3.353109 2.260478 -0.475741 -0.41 -0.07 -0.17
H -3.917949 0.684914 0.100436 -0.09 -0.13 -0.05

(3+2) Product: cis-MeSNO(→BF_3) + dimethylacetylene

Freq
RB3LYP/6-311G(2d,d,p)
Solvation: PCM(Acetonitrile)
Symmetry: C1
Charge: 0; Mult: 1
E_SCF= -1048.775805
T=298.15: H= -1048.613885, E+ZPE= -1048.628943, G= -1048.670015
Freqs: 39.0, 46.9 .. 3167.3

CBS-QB3 Enthalpy= -1047.267863 CBS-QB3 Free Energy= -1047.324206

XYZ coordinates
C -2.359124 -1.486972 1.210712
S -1.726546 -1.034100 -0.457908
H -1.693730 -1.092377 1.976286
H -2.400631 -2.575632 1.240497
N -0.138556 -1.341957 -0.617564
O 0.517833 -0.191227 0.174524
H -3.364553 -1.074032 1.310675
F 2.408418 0.466483 -1.212814
B 2.207127 -0.192334 -0.032116
F 2.522278 -1.512580 -0.045478
F 2.648973 0.483146 1.072421
C 0.378710 2.242714 0.498318
C -0.275432 0.963040 0.107286
C -1.545655 0.743224 -0.246499
C -2.702237 1.675348 -0.392773
H -0.353362 3.047656 0.501091
H 1.180812 2.491284 -0.198929
H 0.815009 2.153993 1.494218
H -3.140332 1.597569 -1.390958
H -2.384941 2.707539 -0.242546
H -3.488930 1.458166 0.335346

cis-MeS(→BF_3)NO

FREQ
RB3LYP/CBSB7
Solvation: PCM(Acetonitrile)
Symmetry: C1
Charge: 0; Mult: 1
E_SCF= -892.735625
T=298.15: H= -892.667306, E+ZPE= -892.678510, G= -892.715792
Freqs: 20.4 .. 3165.9

CBS-QB3 Enthalpy= -891.580366 CBS-QB3 Free Energy= -891.628979

XYZ coordinates

C	1.16842	1.67987	0.42728
S	0.50482	0.59157	-0.84647
H	1.78936	2.44332	-0.03605

H	1.77577	1.07768	1.11319
N	1.55292	-1.12971	-0.37467
O	2.28863	-1.00133	0.48640
H	0.34274	2.13007	0.97551
F	-2.03237	0.92728	0.33758
B	-1.30185	-0.20156	0.12918
F	-0.82084	-0.79311	1.26036
F	-1.77630	-1.05295	-0.81874

S–N Insertion Transition State: cis-MeS(→BF_3)NO + dimethylacetylene

FREQ
RB3LYP/CBSB7
Solvation: PCM(Acetonitrile)
Symmetry: C1
Charge: 0; Mult: 1
E_SCF= -1048.737024
T=298.15: H= -1048.577794, E+ZPE= -1048.594110, G= -1048.637194
Freqs: -291.1, 31.6 .. 3155.0

CBS-QB3 Enthalpy= -1047.208552 CBS-QB3 Free Energy= -1047.268173

XYZ coordinates

C	-0.715914	0.810635	1.964195	-0.08 0.00 0.03
S	-0.503905	0.914065	0.168365	-0.09 -0.09 0.03
N	0.786368	-1.139763	0.153671	-0.15 0.05 0.06
O	0.860559	-1.669604	1.184978	-0.12 0.08 0.00
H	-0.079082	1.547515	2.449362	-0.06 0.03 -0.03
H	-0.463895	-0.195628	2.312312	-0.03 0.02 0.07
H	-1.762640	1.013623	2.189421	-0.07 -0.02 0.09
C	2.190878	2.319681	-0.423473	-0.04 0.09 0.01
C	2.008348	0.879738	-0.340308	0.43 0.05 -0.08
C	2.279798	-0.345034	-0.321644	0.39 0.13 -0.15
C	3.345956	-1.357445	-0.501383	0.06 -0.17 -0.03
H	3.436928	-1.962078	0.405486	-0.10 -0.15 0.00
H	1.535932	2.771723	-1.170314	-0.16 -0.05 0.03
H	3.233986	2.504160	-0.710541	-0.09 0.39 0.00
H	2.017239	2.802900	0.540461	-0.15 0.01 0.03
F	-2.093012	-1.403933	0.227875	-0.02 -0.01 0.00
B	-2.074833	-0.231936	-0.501553	-0.01 0.04 0.04
F	-1.812323	-0.424657	-1.843187	0.00 0.01 0.02
F	-3.197866	0.544646	-0.272251	-0.06 -0.02 -0.01
H	4.304238	-0.878490	-0.701844	0.18 -0.40 -0.01
H	3.099299	-2.023847	-1.332195	-0.05 -0.16 -0.01

S–N Insertion Product: cis-MeS(→BF_3)NO + dimethylacetylene

FREQ
RB3LYP/CBSB7
Solvation: PCM(Acetonitrile)
Symmetry: C1
Charge: 0; Mult: 1
E_SCF= -1048.809474
T=298.15: H= -1048.646425, E+ZPE= -1048.663018, G= -1048.709654
Freqs: 17.3 .. 3181.8

CBS-QB3 Enthalpy= -1047.283739 CBS-QB3 Free Energy= -1047.347183

XYZ coordinates

C	0.05951	-2.21484	-0.78101
S	0.35814	-0.49335	-1.27710
N	-2.25662	-0.98759	0.41830
O	-3.27921	-1.20064	1.08073
H	-0.87411	-2.58046	-1.19828
H	0.05049	-2.30913	0.30106
H	0.90867	-2.75381	-1.20580
C	-0.52918	2.00397	-1.05272
C	-0.85844	0.58675	-0.65195
C	-1.98766	0.33995	0.09537
C	-2.90856	1.44413	0.54190
H	-3.69029	1.01112	1.16380
H	0.35695	2.05948	-1.68478
H	-0.35212	2.61248	-0.16164
H	-1.36853	2.44773	-1.59420
F	3.53826	0.19847	-0.22804
B	2.61427	0.20663	0.71324
F	2.34952	-0.89796	1.38661
F	2.03468	1.34197	1.05831
H	-3.38053	1.94457	-0.30853
H	-2.37821	2.20457	1.12042

Norbornadiene and LA-linked Norbornadiene

Norbornadiene

Freq
RB3LYP/6-311G(2d,d,p)
Solvation: PCM(Acetonitrile)
Symmetry: C2V
Charge: 0; Mult: 1
E_SCF= -271.549277
T=298.15: H= -271.415630, E+ZPE= -271.421467, G= -271.448942
Freqs: 423.7, 455.5 .. 3220.2

CBS-QB3 Enthalpy= -270.942545 CBS-QB3 Free Energy= -270.975931

XYZ coordinates

C 0.000000 1.123106 0.285453
C 1.242612 0.666791 -0.509843
C 1.242612 -0.666791 -0.509843
C 0.000000 -1.123106 0.285453
C -1.242612 0.666791 -0.509843
H 0.000000 -2.158144 0.622105
C -1.242612 -0.666791 -0.509843
C 0.000000 0.000000 1.368554
H 1.930245 -1.336585 -1.008867
H 1.930245 1.336585 -1.008867
H 0.897769 0.000000 1.990460
H 0.000000 2.158144 0.622105

H -0.897769 0.000000 1.990460
H -1.930245 -1.336585 -1.008867
H -1.930245 1.336585 -1.008867

(3+2) Transition State: cis-MeSNO + norbornadiene

Freq
RB3LYP/6-311G(2d,d,p)
Solvation: PCM(Acetonitrile)
Symmetry: C1
Charge: 0; Mult: 1
E_SCF= -839.586134
T=298.15: H= -839.400625, E+ZPE= -839.411187, G= -839.445886
Freqs: -406.7, 99.8 .. 3218.6

CBS-QB3 Enthalpy= -838.229813 CBS-QB3 Free Energy= -838.275232

XYZ coordinates (Last three columns show the imaginary frequency vector)
C 2.701037 -0.856342 -0.946191 -0.02 0.03 0.01
S 1.908534 -0.455677 0.648370 0.23 -0.03 0.11
H 2.332965 -1.812510 -1.315092 -0.12 0.08 -0.02
H 3.775967 -0.904711 -0.776824 -0.01 -0.04 -0.14
N 1.545482 1.176024 0.696728 -0.04 0.12 -0.04
O 1.088163 1.576605 -0.444879 0.41 0.22 0.17
H 2.451109 -0.055368 -1.641549 -0.06 0.08 0.07
C -1.661199 1.023122 -0.253763 -0.08 -0.04 -0.05
C -0.416747 0.452654 -0.957063 -0.34 -0.30 -0.21
C -0.177737 -0.810044 -0.354260 -0.30 -0.02 -0.24
C -1.280515 -0.973681 0.714951 -0.07 -0.02 -0.05
C -2.822952 0.090147 -0.654343 -0.15 -0.01 0.06
H -1.101733 -1.738260 1.468586 0.01 -0.02 -0.06
C -2.596968 -1.093914 -0.078877 -0.14 0.00 0.06
C -1.413523 0.498590 1.184954 0.00 -0.02 -0.05
H 0.137490 -1.666494 -0.935654 0.18 -0.06 0.10
H -0.238778 0.643540 -2.005438 0.09 0.09 -0.05
H -0.509469 0.899515 1.645016 0.02 -0.03 -0.08
H -1.828897 2.089171 -0.390185 -0.02 -0.03 -0.07
H -2.272693 0.652479 1.838882 0.04 0.02 0.00
H -3.170370 -2.005700 -0.182919 -0.15 0.01 0.10
H -3.624188 0.360964 -1.329258 -0.17 0.00 0.09

(3+2) Product: cis-MeSNO + norbornadiene

Freq
RB3LYP/6-311G(2d,d,p)
Solvation: PCM(Acetonitrile)
Symmetry: C1
Charge: 0; Mult: 1
E_SCF= -839.622797
T=298.15: H= -839.434397, E+ZPE= -839.444537, G= -839.478576
Freqs: 97.2, 160.5 .. 3212.8
CBS-QB3 Enthalpy= -838.271771 CBS-QB3 Free Energy= -838.316105

XYZ coordinates
C 2.688442 -1.009881 -0.914260
S 1.644197 -0.482395 0.515626
H 2.528741 -2.073779 -1.094449
H 3.722173 -0.829012 -0.621942
N 1.532454 1.132421 0.628233
O 0.823866 1.537807 -0.607638
H 2.424151 -0.417912 -1.788838
C -1.628239 1.056365 -0.116853
C -0.295776 0.678472 -0.851964
C -0.001966 -0.752036 -0.277188
C -1.182300 -0.992332 0.716567
C -2.670813 0.096360 -0.682332
H -1.018168 -1.803881 1.422907
C -2.406151 -1.119465 -0.192889
C -1.417051 0.430154 1.281452
H 0.099383 -1.538616 -1.021189
H -0.421503 0.676310 -1.934932
H -0.563463 0.843795 1.815968
H -1.856893 2.119101 -0.173328
H -2.316567 0.477987 1.897611
H -2.883722 -2.056055 -0.450760
H -3.415149 0.357018 -1.424025

Norbornadiene-BF_2

Freq
RB3LYP/6-311G(2d,d,p)
Solvation: PCM(Acetonitrile)
Symmetry: CS
Charge: 0; Mult: 1
E_SCF= -495.678761
T=298.15: H= -495.542712, E+ZPE= -495.551632, G= -495.585246
Freqs: 40.6, 114.5 .. 3224.8 SP

CBS-QB3 Enthalpy= -494.805095 CBS-QB3 Free Energy= -494.847750

XYZ coordinates
C -0.847361 0.176025 -1.124694
C -0.864642 -1.301488 -0.667676
C -0.864642 -1.301488 0.667676
C -0.847361 0.176025 1.124694
C -2.177977 0.808766 -0.666304
H -0.559651 0.351668 2.158909
C -2.177977 0.808766 0.666304
C 0.090853 0.736162 0.000000
H -0.932700 -2.148497 1.336873
H -0.932700 -2.148497 -1.336873
B 1.539817 0.151445 0.000000
F 2.214650 -0.090696 1.124717
F 2.214650 -0.090696 -1.124717
H -0.559651 0.351668 -2.158909
H 0.114107 1.832805 0.000000
H -2.965260 1.124508 1.337492
H -2.965260 1.124508 -1.337492

(3+2) Pre-reactive complex: cis-MeSNO + norbornadiene-BF_2

Freq
RB3LYP/6-311G(2d,d,p)
Solvation: PCM(Acetonitrile)
Symmetry: C1
Charge: 0; Mult: 1
E_SCF= -1063.760312
T=298.15: H= -1063.571548, E+ZPE= -1063.586123, G= -1063.627562
Freqs: 18.9, 51.8 .. 3218.9 SP

CBS-QB3 Enthalpy= -1062.129817 CBS-QB3 Free Energy= -1062.186050

XYZ coordinates
C -3.472489 -1.506521 0.315490
S -2.489773 -0.425466 -0.737766
H -4.218187 -1.951271 -0.343041
H -3.954995 -0.922089 1.098000
N -1.402593 0.205136 0.429859
O -1.490286 -0.103593 1.587369
H -2.836488 -2.278926 0.747280
C 1.820180 -0.157746 1.066284
C 1.116834 -1.481078 0.697283
C 1.081195 -1.551362 -0.633384
C 1.769711 -0.280651 -1.173471
C 3.283859 -0.295489 0.583994
H 1.585733 -0.044459 -2.219876
C 3.253101 -0.370259 -0.746900
C 1.278754 0.748241 -0.095977
H 0.714717 -2.360611 -1.250980
H 0.782586 -2.217615 1.415758
B -0.218262 1.319916 -0.128896
F -0.698003 1.598930 -1.414307
F -0.432002 2.384645 0.741432
H 1.685228 0.185750 2.090456
H 1.892588 1.657438 -0.159478
H 4.079111 -0.521003 -1.429534
H 4.139822 -0.372165 1.241573

(3+2) Transition State: cis-MeSNO + norbornadiene-BF_2

Freq
RB3LYP/6-311G(2d,d,p)
Solvation: PCM(Acetonitrile)
Symmetry: C1
Charge: 0; Mult: 1
E_SCF= -1063.741009
T=298.15: H= -1063.553163, E+ZPE= -1063.566059, G= -1063.603479
Freqs: -295.6, 100.6 .. 3232.4

CBS-QB3 Enthalpy= -1062.121133 CBS-QB3 Free Energy= -1062.171652

XYZ coordinates (Last three columns show the imaginary frequency vector)

C -2.696474 -1.811177 0.219403 0.00 0.01 -0.02
S -1.863487 -0.505250 -0.708242 0.25 -0.10 0.04
H -2.677817 -2.695948 -0.416663 -0.03 -0.01 0.00
H -3.725281 -1.503043 0.402885 0.02 0.13 -0.15
N -1.295071 0.535180 0.504326 -0.05 0.06 0.02
O -0.947985 -0.047642 1.575206 0.40 -0.26 -0.08
H -2.164871 -1.991069 1.149920 -0.12 -0.03 0.04
C 1.730027 -0.021556 0.987075 -0.07 0.07 -0.01
C 0.710404 -1.174219 0.994447 -0.34 0.32 0.08
C 0.470565 -1.486448 -0.345543 -0.30 0.21 -0.10
C 1.297804 -0.486982 -1.171529 -0.06 0.07 -0.02
C 3.016671 -0.608970 0.379169 -0.13 -0.11 0.04
H 1.012309 -0.383543 -2.215988 0.01 0.09 -0.04
C 2.759655 -0.886947 -0.902426 -0.13 -0.11 0.04
C 1.188378 0.771476 -0.243606 0.01 0.08 -0.03
H 0.161316 -2.456720 -0.708692 0.10 0.02 0.05
H 0.581231 -1.858089 1.820154 -0.03 0.07 -0.07
B -0.206159 1.592938 -0.092183 -0.05 -0.03 0.02
F -0.732685 2.022285 -1.324449 -0.02 0.01 -0.01
F -0.117785 2.646025 0.818760 -0.01 0.01 0.00
H 1.836890 0.508872 1.929981 -0.02 0.09 -0.03
H 1.931484 1.513846 -0.559595 0.04 0.03 -0.03
H 3.405705 -1.368384 -1.624544 -0.16 -0.20 0.07
H 3.927051 -0.797580 0.932650 -0.15 -0.17 0.06

(3+2) Product: cis-MeSNO + norbornadiene-BF_2

Freq
RB3LYP/6-311G(2d,d,p)
Solvation: PCM(Acetonitrile)
Symmetry: C1
Charge: 0; Mult: 1
E_SCF= -1063.791650
T=298.15: H= -1063.600674, E+ZPE= -1063.612911, G= -1063.649312
Freqs: 109.4, 134.1 .. 3212.8

CBS-QB3 Enthalpy= -1062.179339 CBS-QB3 Free Energy= -1062.228176
XYZ coordinates

C -2.578376 -1.924899 0.195211
S -1.555174 -0.700085 -0.650690
H -2.495569 -2.853093 -0.369897
H -3.601337 -1.553171 0.157934
N -1.380964 0.551983 0.507828
O -0.740552 -0.115163 1.610313
H -2.234916 -2.044728 1.219094
C 1.619486 0.198267 0.936004
C 0.441672 -0.799744 1.128905
C 0.159657 -1.282302 -0.342502
C 1.139311 -0.390945 -1.182463
C 2.799255 -0.600929 0.407608
H 0.884349 -0.329982 -2.238978
C 2.519072 -0.947412 -0.852099

```
C 1.103293 0.922950 -0.339252
H 0.224992 -2.352209 -0.521581
H 0.624278 -1.605865 1.836046
B -0.342457 1.627010 -0.134581
F -0.948546 2.031805 -1.351143
F -0.296526 2.702694 0.769456
H 1.791596 0.800569 1.826178
H 1.848765 1.632017 -0.713682
H 3.090341 -1.594553 -1.505397
H 3.657870 -0.900056 0.995328
```

Performance of CCSD(T)-F12a/VDZ-F12, CBS-QB3 and DFT Methods

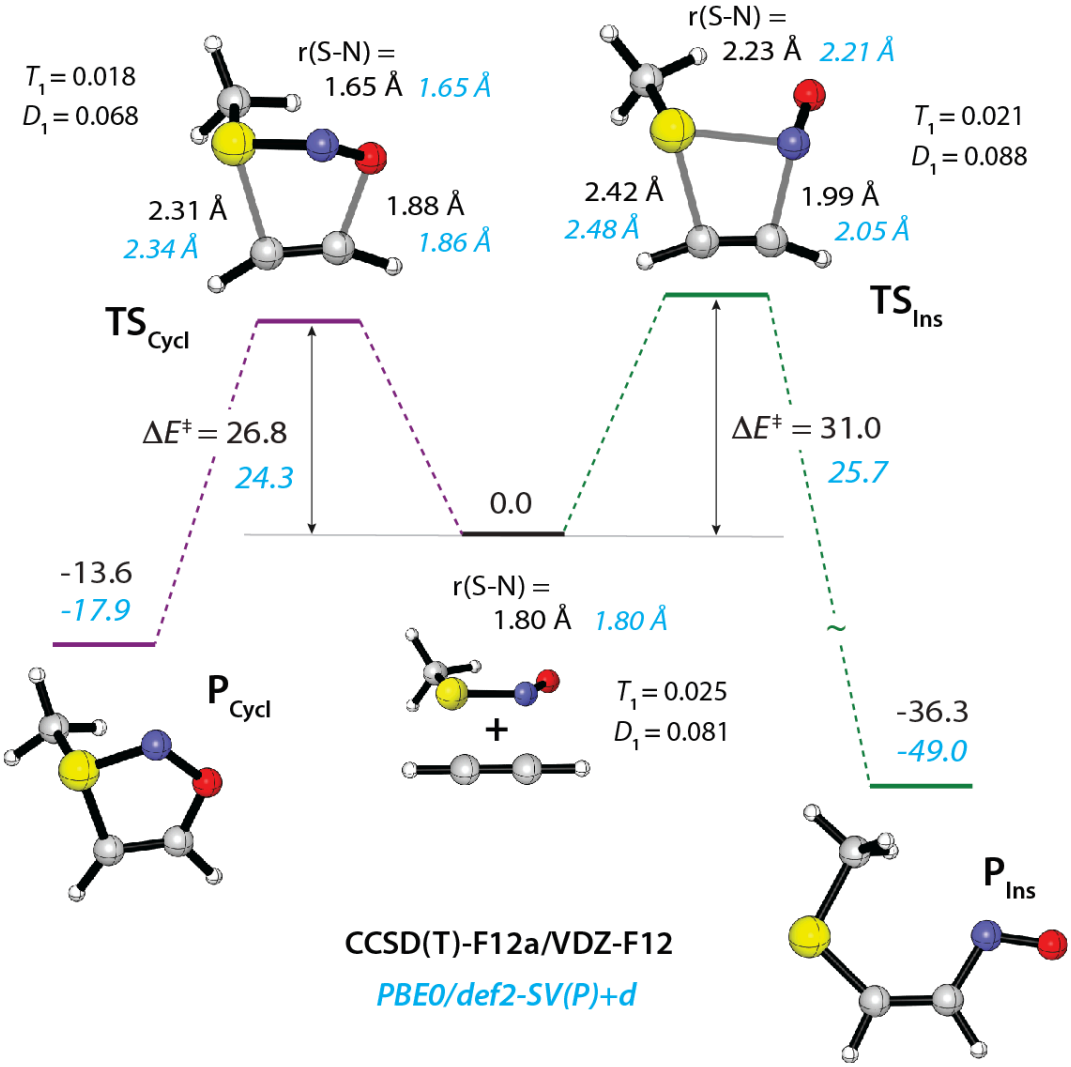

Figure A1. (3+2) Cycloaddition (left) and S–N bond insertion reaction (right) pathways, calculated for cis-CH_3SNO and C_2H_2 reactants at the CCSD(T)-F12a/VDZ-F12 and PBE0/def2-SV(P)+d levels of theory (in the gas phase). T_1 and D_1 coupled cluster diagnostic values are listed for the cis-CH_3SNO molecule and the transition states TS_{cycl} and TS_{Ins}.

Table A1. Transition state of cis-CH_3SNO and C_2H_2 (3+2) cycloaddition reaction, ab initio and DFT parameters (in the gas phase).

Method	r(S–N), Å	r(C–C), Å	r(S–C), Å	r(O–C), Å	$E^{\neq}$, kcal/mol
CCSD(T)-F12a/ VDZ-F12	1.647	1.252	2.307	1.881	26.8
CBS-QB3	1.662	1.250	2.318	1.831	23.8
DFT methods with def2-TZVPPD basis set					
B3LYP	1.648	1.245	2.327	1.854	31.8
PBE0	1.643	1.241	2.311	1.895	25.5
PBE0-1/3	1.629	1.237	2.313	1.890	26.8
PBE0-GD3	1.642	1.242	2.308	1.891	23.7
ωB97XD	1.629	1.240	2.306	1.879	30.0
B2PLYPD	1.660	1.252	2.297	1.842	25.4
MPW2PLYPD	1.649	1.249	2.302	1.847	26.1
DFT methods with def2-SV(P)+d basis set					
B3LYP	1.652	1.259	2.360	1.822	29.8
PBE0	1.645	1.254	2.337	1.861	24.3
PBE0-1/3	1.631	1.250	2.338	1.857	25.7
PBE0-GD3	1.644	1.255	2.335	1.856	22.6
ωB97XD	1.632	1.254	2.338	1.844	28.4
B2PLYPD	1.659	1.267	2.333	1.795	26.9
MPW2PLYPD	1.649	1.263	2.337	1.802	27.2

Table A2. Transition state of cis-CH_3SNO and C_2H_4 (3+2) cycloaddition reaction, ab initio and DFT parameters (in the gas phase).

Method	*r*(S–N), Å	*r*(C–C), Å	*r*(S–C), Å	*r*(O–C), Å	$E^{\neq}$, kcal/mol
CCSD(T)-F12a/ VDZ-F12	1.642	1.412	2.265	1.885	26.6
CBS-QB3	1.656	1.424	2.264	1.820	24.5
DFT methods with def2-TZVPPD basis set					
B3LYP	1.640	1.416	2.273	1.842	33.3
PBE0	1.637	1.402	2.264	1.888	26.3
PBE0-1/3	1.625	1.396	2.274	1.891	27.4
PBE0-GD3	1.636	1.404	2.258	1.884	23.9
ωB97XD	1.624	1.402	2.266	1.883	30.1
B2PLYPD	1.647	1.421	2.234	1.827	24.9
MPW2PLYPD	1.640	1.415	2.249	1.839	25.6
DFT methods with def2-SV(P)+d basis set					
B3LYP	1.645	1.428	2.286	1.803	32.1
PBE0	1.640	1.415	2.272	1.845	25.8
PBE0-1/3	1.627	1.409	2.284	1.851	26.8
PBE0-GD3	1.638	1.417	2.269	1.840	23.4
ωB97XD	1.628	1.415	2.280	1.844	29.1
B2PLYPD	1.646	1.434	2.254	1.776	27.6
MPW2PLYPD	1.639	1.428	2.267	1.790	27.7

Table A3. Product of cis-CH_3SNO and C_2H_2 (3+2) cycloaddition reaction, ab initio and DFT parameters (in the gas phase).

Method	*r*(S–N), Å	*r*(C–C), Å	*r*(S–C), Å	*r*(O–C), Å	*ΔE*, kcal/mol*	S–C BDE, kcal/mol
CCSD(T)-F12a/ VDZ-F12	1.613	1.346	1.760	1.332	-13.6	36.2
CBS-QB3	1.631	1.345	1.775	1.328	-13.0	34.9
DFT methods with def2-TZVPPD basis set						
B3LYP	1.623	1.342	1.765	1.325	-6.1	27.1
PBE0	1.611	1.341	1.751	1.319	-18.5	31.8
PBE0-1/3	1.604	1.338	1.747	1.315	-20.4	31.1
PBE0-GD3	1.610	1.341	1.752	1.320	-19.6	33.2
ωB97XD	1.609	1.339	1.755	1.319	-14.3	32.3
B2PLYPD	1.619	1.345	1.762	1.329	-9.5	32.2
MPW2PLYPD	1.615	1.343	1.759	1.326	-11.2	32.0
DFT methods with def2-SV(P)+d basis set						
B3LYP	1.621	1.355	1.767	1.323	-7.1	27.0
PBE0	1.609	1.352	1.754	1.317	-17.9	31.5
PBE0-1/3	1.602	1.349	1.750	1.312	-19.6	30.5
PBE0-GD3	1.609	1.352	1.754	1.317	-19.1	32.8
ωB97XD	1.608	1.351	1.757	1.317	-14.4	31.4
B2PLYPD	1.616	1.356	1.763	1.325	-6.6	29.6
MPW2PLYPD	1.612	1.354	1.761	1.322	-8.6	29.5

* calculated with respect to the separated reagents (cis-CH_3SNO and C_2H_2).

Table A4. Product of cis-CH_3SNO and C_2H_4 (3+2) cycloaddition reaction, ab initio and DFT parameters (in the gas phase).

Method	*r*(S–N), Å	*r*(C–C), Å	*r*(S–C), Å	*r*(O–C), Å	ΔE^*, kcal/mol	S–C BDE, kcal/mol
CCSD(T)-F12a/ VDZ-F12	1.608	1.543	1.821	1.420	3.9	39.8
CBS-QB3	1.622	1.546	1.862	1.424	4.0	39.5
DFT methods with def2-TZVPPD basis set						
B3LYP	1.612	1.543	1.850	1.421	15.5	29.4
PBE0	1.602	1.537	1.828	1.410	3.2	34.2
PBE0-1/3	1.596	1.534	1.819	1.404	0.9	33.3
PBE0-GD3	1.602	1.537	1.828	1.411	1.3	35.7
ωB97XD	1.601	1.541	1.829	1.410	5.7	35.0
B2PLYPD	1.612	1.542	1.843	1.423	8.6	35.9
MPW2PLYPD	1.608	1.540	1.838	1.418	7.1	35.4
DFT methods with def2-SV(P)+d basis set						
B3LYP	1.610	1.551	1.861	1.415	16.0	28.6
PBE0	1.600	1.544	1.838	1.405	5.5	32.9
PBE0-1/3	1.594	1.541	1.830	1.400	3.3	31.8
PBE0-GD3	1.600	1.545	1.839	1.406	3.6	34.5
ωB97XD	1.598	1.549	1.839	1.406	7.3	33.2
B2PLYPD	1.608	1.549	1.853	1.416	12.9	32.2
MPW2PLYPD	1.604	1.548	1.848	1.412	11.0	31.9

* calculated with respect to the separated reagents (cis-CH_3SNO and C_2H_4)

Table A5. Complexes of cis-CH_3SNO and BH_3, ab initio and DFT parameters (in the gas phase).

	N-coordinated BH_3*		O-coordinated BH_3*		S-coordinated BH_3*	
Method	r(S–N), Å (Δr(S–N), Å)	ΔE, kcal/mol	r(S–N), Å (Δr(S–N), Å)	ΔE, kcal/mol	r(S–N), Å (Δr(S–N), Å)	ΔE, kcal/mol
CCSD(T)-F12a/ VDZ-F12	1.714 (-0.083)	-24.7	1.670 (-0.127)	-12.8	1.981 (+0.184)	-17.8
CBS-QB3	1.753 (-0.119)	-25.4	1.679 (-0.193)	-12.6	2.032 (+0.160)	-17.5
DFT methods with def2-TZVPPD basis set						
B3LYP	1.736 (-0.080)	-23.2	1.669 (-0.147)	-10.9	1.985 (+0.169)	-12.8
PBE0	1.714 (-0.065)	-29.5	1.654 (-0.124)	-15.2	1.937 (+0.158)	-19.2
PBE0-1/3	1.703 (-0.057)	-29.1	1.647 (-0.112)	-15.0	1.905 (+0.145)	-18.7
PBE0-GD3	1.715 (-0.065)	-30.6	1.654 (-0.125)	-16.3	1.941 (+0.161)	-20.6
ωB97XD	1.711 (-0.056)	-25.3	1.655 (-0.112)	-12.3	1.914 (+0.147)	-16.2
B2PLYPD	1.723 (-0.089)	-25.0	1.667 (-0.144)	-12.6	2.014 (+0.203)	-16.3
MPW2PLYPD	1.717 (-0.078)	-25.5	1.662 (-0.133)	-13.2	1.986 (+0.191)	-16.2
DFT methods with def2-SV(P)+d basis set						
B3LYP	1.742 (-0.088)	-27.9	1.666 (-0.164)	-14.2	2.026 (+0.197)	-15.2
PBE0	1.721 (-0.073)	-33.5	1.652 (-0.143)	-17.5	1.983 (+0.188)	-20.9
PBE0-1/3	1.709 (-0.060)	-32.9	1.645 (-0.124)	-17.2	1.948 (+0.179)	-20.2
PBE0-GD3	1.722 (-0.073)	-34.6	1.652 (-0.143)	-18.6	1.987 (+0.193)	-22.4
ωB97XD	1.716 (-0.058)	-29.0	1.653 (-0.121)	-14.6	1.953 (+0.179)	-16.9
B2PLYPD	1.730 (-0.096)	-28.7	1.664 (-0.162)	-14.7	2.071 (+0.245)	-18.2
MPW2PLYPD	1.723 (-0.085)	-29.4	1.659 (-0.149)	-15.5	2.041 (+0.234)	-18.1

* Δr(S–N) indicates the difference in bond length between the corresponding cis-CH_3SNO/BH_3 complex and the isolated cis-CH_3SNO molecule

Table A6. The results of fitting the S–N bond energy profiles in CH_3SNO to the harmonic potential, $E=k\Delta x^2$.

Method/Basis set	k, mDyne/Å	R^2
cis-CH_3SNO		
CCSD/cc-pV(D+d)Z	0.78313	0.9683
DCSD/cc-pV(D+d)Z	0.67259	0.9976
CCSD(T)/cc-pV(D+d)Z	0.65873	0.8909
CCSDT/cc-pV(D+d)Z	0.62930	0.9787
CCSDT(Q)/cc-pV(D+d)Z	0.55738	0.9603
FPD	0.84089	0.9591
PBE0/def2-TZVPPD	1.05325	0.8953
PBE0-GD3/def2-TZVPPD	1.05528	0.8266
MPW2PLYP/def2-TZVPPD	0.87296	0.9599
MPW2PLYPD/def2-TZVPPD	0.87623	0.9930
trans-CH_3SNO		
CCSD/cc-pV(D+d)Z	0.76367	0.9809
DCSD/cc-pV(D+d)Z	0.62744	0.9611
CCSD(T)/cc-pV(D+d)Z	0.61327	0.8696
CCSDT/cc-pV(D+d)Z	0.58587	0.9312
CCSDT(Q)/cc-pV(D+d)Z	0.52063	0.9907
cis-trans isomerization TS		
CCSD/cc-pV(D+d)Z	0.53636	0.9931
DCSD/cc-pV(D+d)Z	0.43438	0.9813
CCSD(T)/cc-pV(D+d)Z	0.37117	0.9279
CCSDT/cc-pV(D+d)Z	0.36307	0.9474
CCSDT(Q)/cc-pV(D+d)Z	0.33084	0.9771